(2)

TECHNICAL REPORT SL-92-21

GROUT FOR CLOSURE OF THE DEMONSTRATION VAULT AT THE US DOE HANFORD FACILITY

by

Lillian D. Wakeley, James J. Ernzen

Structures Laboratory

DEPARTMENT OF THE ARMY
Waterways Experiment Station, Corps of Engineers
3909 Halls Ferry Road, Vicksburg, Mississippi 39180-6199

August 1992
Final Report

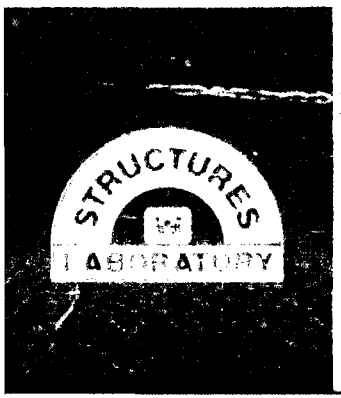

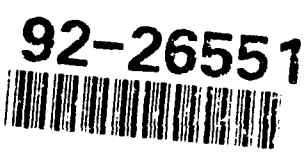

Prepared for US DEPARTMENT OF ENERGY
Oak Ridge Operations, PO Box 2001
[illegible] 37831-8614

TECHNICAL REPORT SL-92-21

(2)

US Army Corps of Engineers

GROUT FOR CLOSURE OF THE DEMONSTRATION VAULT AT THE US DOE HANFORD FACILITY

by

Lillian D. Wakeley, James J. Ernzen

Structures Laboratory

DEPARTMENT OF THE ARMY
Waterways Experiment Station, Corps of Engineers
3909 Halls Ferry Road, Vicksburg, Mississippi 39180-6199

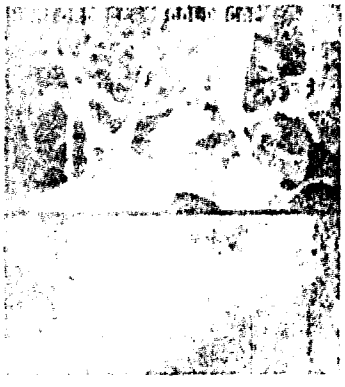

August 1992
Final Report

STRUCTURES LABORATORY

Prepared for US DEPARTMENT OF ENERGY
Oak Ridge Operations, PO Box 2001
Oak Ridge, Tennessee 37831-8614

When this report is no longer needed return it to the originator.

The findings in this report are not to be construed as an official Department of the Army position unless so designated by other authorized documents.

The contents of this report are not to be used for advertising, publication, or promotional purposes. Citation of trade names does not constitute an official endorsement or approval of the use of such commercial products.

REPORT DOCUMENTATION PAGE

Form Approved
OMB No. 0704-0188

1. AGENCY USE ONLY *(Leave blank)*	2. REPORT DATE	3. REPORT TYPE AND DATES COVERED
	August 1992	Final report

4. TITLE AND SUBTITLE

Grout for Closure of the Demonstration Vault at the US DOE Hanford Facility

5. FUNDING NUMBERS

6. AUTHOR(S)

Lillian D. Wakeley
James J. Ernzen

7. PERFORMING ORGANIZATION NAME(S) AND ADDRESS(ES)

U.S. Army Engineer Waterways Experiment Station
Structures Laboratory
3909 Halls Ferry Road
Vicksburg, MS 39180-6199

8. PERFORMING ORGANIZATION REPORT NUMBER

Technical Report
SL-92-21

9. SPONSORING/MONITORING AGENCY NAME(S) AND ADDRESS(ES)

U.S. Department of Energy
Oak Ridge Operations
P.O. Box 2001
Oak Ridge, TN 37831-8614

10. SPONSORING/MONITORING AGENCY REPORT NUMBER

11. SUPPLEMENTARY NOTES

Available from National Technical Information Service, 5285 Port Royal Road, Springfield, VA 22161

12a. DISTRIBUTION/AVAILABILITY STATEMENT

Approved for public release; distribution is unlimited.

12b. DISTRIBUTION CODE

13. ABSTRACT *(Maximum 200 words)*

The Waterways Experiment Station (WES) developed a grout to be used as a cold- (nonradioactive) cap or void-fill grout between the solidified low-level waste and the cover blocks of a demonstration vault for disposal of phosphate-sulfate waste (PSW) at the U.S. Department of Energy (DOE) Hanford Facility. The project consisted of formulation and evaluation of candidate grouts and selection of the best candidate grout, followed by a physical scale-model test to verify grout performance under project-specific conditions. Further, the project provided data to verify numerical models (accomplished elsewhere) of stresses and isotherms inside the Hanford demonstration vault. Evaluation of unhardened grout included obtaining data on segregation, bleeding, flow, and working time. For hardened grout, strength, volume stability, temperature rise, and chemical compatibility with surrogate wasteform grout were examined.

(Continued)

14. SUBJECT TERMS

Grout
Waste disposal
Hanford

15. NUMBER OF PAGES

156

16. PRICE CODE

17. SECURITY CLASSIFICATION OF REPORT	18. SECURITY CLASSIFICATION OF THIS PAGE	19. SECURITY CLASSIFICATION OF ABSTRACT	20. LIMITATION OF ABSTRACT
UNCLASSIFIED	UNCLASSIFIED		

NSN 7540-01-280-5500

Standard Form 298 (Rev 2-89)
Prescribed by ANSI Std 239-18
298-102

13. ABSTRACT (Continued).

The grout was formulated to accommodate unique environmental boundary conditions (vault temperature = 45 °C) and exacting regulatory requirements (mandating less than 0.1 percent shrinkage with no expansion and no bleeding); and to remain pumpable for a minimum of 2 hr. A grout consisting of API Class H oil-well cement, an ASTM C 618 Class F fly ash, sodium bentonite clay, and a natural sand from the Hanford area met performance requirements in laboratory studies. It is recommended for use in the DOE Hanford demonstration PSW vault.

PREFACE

The work described in this report is part of an ongoing research effort accomplished in the Concrete Technology Division (CTD), Structures Laboratory (SL), U.S. Army Engineer Waterways Experiment Station (WES), under an Interagency Agreement with the U.S. Department of Energy, Oak Ridge Office via Oak Ridge National Laboratory (ORNL), Oak Ridge, TN, for support to the DOE Hanford, WA, Facility. Mr. Earl W. McDaniel, ORNL, was the technical monitor for this research.

Drs. Lillian D. Wakeley and James J. Ernzen directed the laboratory studies in CTD and prepared this report under the general supervision of Mr. Bryant Mather, Director, SL, and Mr. Kenneth L. Saucier, Chief, CTD. The authors acknowledge Messrs. Billy Neeley, L. W. Mason, Charles White, Dennis Bean, Mike Hammons, Anthony Bombich, Dan Wilson, Cliff Gill, Brent Lamb, Michel Alexander, Mike Lloyd, and Percy Collins and Mses. Linda Mayfield and Judy Tom for their assistance during this investigation. The authors also acknowledge the support of Drs. Toy Poole and Charles Weiss, Jr., and Messrs. J. Pete Burkes, John Boa, Jr., Hugh Wilson, Ken Loyd, Don Walley, Melvin Sykes, and John Cook and Ms. Estelle Stegall.

Westinghouse Hanford Corporation (WHC) is responsible for the Hanford Grout Vault Program. Messrs. Jeff Voogd and Kenneth Bledsoe, WHC, reviewed and commented on this document during its preparation.

At the time of publication of this report, Director of WES was Dr. Robert W. Whalin. Commander and Deputy Director was COL Leonard G. Hassell, EN.

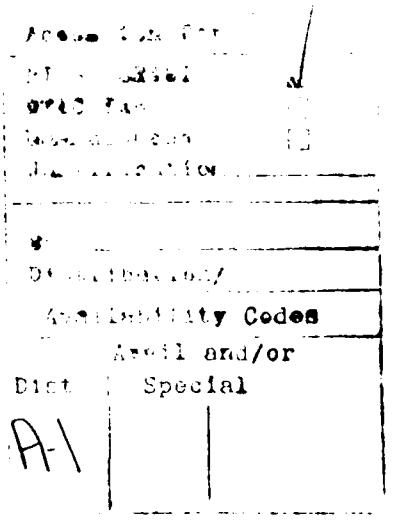

CONTENTS

CONVERSION FACTORS, NON-SI TO SI (METRIC)
UNITS OF MEASUREMENT

Non-SI units of measurement used in this report can be converted to SI (metric) units as follows:

Multiply	By	To Obtain
Btu (International Table) per pound (mass) · degree Fahrenheit	4,186.800	joules per kilogram kelvin
Fahrenheit degrees	5/9	Celsius degrees or kelvins*
feet	0.3048000	metres
fluid ounces	29.5625	millilitres
inches	25.40000	millimetres
pounds (force) per square inch	0.006894757	megapascals
pounds (mass)	0.4535924	kilograms
pounds (mass) per cubic foot	16.01846	kilograms per cubic metre
pounds (mass) per cubic yard	1.6875	kilograms per cubic metre

* To obtain Celsius (C) temperature readings from Fahrenheit (F) readings, use the following formula: $C = (5/9)(F - 32)$. To obtain Kelvin (K) readings, use: $K = (5/9)(F - 32) + 273.15$.

GROUT FOR CLOSURE OF THE DEMONSTRATION VAULT AT THE US DOE HANFORD FACILITY

PART I: INTRODUCTION

Executive Summary

1. The US Army Engineer Waterways Experiment Station (WES) recommends the following formulation for the cold-cap grout to serve as a void-fill material between the waste-form grout and the cover blocks in the phosphate-sulfate waste (PSW) demonstration vault at Hanford, WA. This grout mixture was designated CC-20 in our experiments.

Material	Lb Per Cubic Yard*
API Class H Cement	300
ASTM Class F Fly Ash	1,112
Natural Fine Aggregate (all passing the 2.36-mm [No. 8] sieve)	1,314
Sodium Bentonite Clay	38
Water	564
High-Range Water-Reducing Admixture	4.5
Set-Retarding Admixture	4.56 fluid oz

2. Materials selection and experimental design focused on meeting the grout requirements provided by Westinghouse Hanford Corporation (WHC), dated October 25, 1990, which had been revised following our written comments of October 17, 1990. These requirements are summarized here. The grout was required to have a compressive strength of 400 psi or greater at 28 days of age. Shrinkage was to be no more than 0.1 percent in the lower lifts and not more than 0.01 percent in the top lift, and the grout was to be nonexpansive. It was to be chemically stable in contact with the wasteform grout at

---

* A table of factors for converting non-SI units of measurement to SI (metric) units is presented on page 3.

temperature up to 70 °C and should not bleed. The grout must generate as little heat as possible. It must be pumpable and be capable of flowing approximately 14 ft horizontally without segregating after a placement drop of 4 ft. Although not stated originally, subsequent conversations revealed that the grout probably would be mixed offsite by a supplier of ready-mixed concrete. This would require approximately an hour of transport time, in addition to anticipated mixing and pumping time.

3. Materials were selected and proportioned based on those requirements. API Class H oil-well cement was chosen because of its coarse particle size and resulting slow heat evolution. Class F fly ash was chosen over Class C because of its demonstrated ability to reduce permeability over time and because mixtures containing Class F fly ash commonly generate less heat and are less subject to sulfate attack. An appropriate Class F fly ash was available near the Hanford site. Two fine aggregates with differing thermal expansion characteristics were tested: a crushed limestone sand available at WES and a natural sand from a supplier close to Hanford. The latter was selected for this grout. Sodium bentonite was chosen for its ability to hold water, aid in pumpability, and reduce bleeding. The high-range water-reducing and set-retarding admixtures were chosen because of their demonstrated performance in WES experience with mixtures containing similar materials.

4. In proportioning this mixture, we used a low cement content to minimize the heat rise and still meet the specified unhardened and hardened properties. The ratio of cement to fly ash (c/fa) was held between 1:2 and 1:3 to obtain a low cement content. The ratio of cement + fly ash to fine aggregate was initially varied between 1:1 and 2:1 to investigate how the aggregate content would affect the volume stability of the grout at the elevated temperatures in the vault. The ratio of water to cement + fly ash (w/c+fa) was held low at 0.4 by mass to obtain a high quality microstructure and still deliver pumpable grout of the required properties during the transit times expected. The dosages of high-range water reducer and set retarder were adjusted to aid in maintaining these properties until the grout was in place.

5. Over 20 different mixtures were proportioned, cast, and tested in the early phase of the research effort. Proportions for these mixtures are presented in Appendix A. These mixtures were prepared in Hobart mixers

(described in ASTM 305) as 0.1-cu-ft batches, mixed for 2 hr, and tested for flow, segregation, bleeding, and compressive strength. Grout flow was measured according to ASTM C 939, bleeding according to ASTM C 940, and strength according to ASTM C 109. Occurrence or nonoccurrence of mixture segregation was determined by visual inspection. Four of the mixtures, after passing these requirements, were then cast in larger batches and tested additionally for time of setting (ASTM C 191), chemical interaction with simulated PSW waste grout (by phase composition using X-ray diffraction [XRD] and chemical composition by energy dispersive X-ray analysis [EDX]), semiadiabatic heat rise (using a CIMS HayBox Calorimeter), and volume stability.

6. The volume-stability measurements involved measuring the length changes of 1- by 1- by 11-in. prisms that were cured and stored at 45 °C and 100 percent relative humidity. The temperature of 45 °C was provided to the WES from WHC Process Engineering Office as the current vault temperature as of 1991. Relative humidity of 100 percent was chosen as a reasonable approximation of probable vault conditions. Molds and comparator were as described in ASTM C 157, as was the method of calculating length change. Measurements of heat rise were obtained by measuring the thermal loss from a 6- by 12-in. grout cylinder, in a calibrated environment (inside the CIMS calorimeter), and then calculating the adiabatic heat rise this mixture would exhibit inside the vault (assuming the vault will remain at a temperature of 45 °C).

7. Test results showed that all mixtures, when prepared as described, met the specifications with regard to strength and flow, and with adjustments to the admixtures or the clay content or both, could meet the segregation and bleeding requirements. The deciding factors on choice of materials and proportions hinged upon the issues of volume stability and heat rise. The mixtures with higher sand contents clearly showed lower temperatures than identical mixtures with less sand and more fly ash in them. This factor eliminated the low-sand mixtures.

8. At 60 days, expansion prisms of the grout made with 480 lb of cement and natural sand showed an average positive expansion of 0.003 percent. Data from tests at 120 days age show that the prisms of the grout made with natural sand have an average expansion of +0.002 percent. These values represent

extremely small changes (they are close to the limit of measuring error) and excellent volume stability. The small positive expansions observed are not a serious concern and are probably beneficial. With time the vault will begin to cool, and some thermal contraction will result. The natural sand was selected for the final phase of testing, the proximity of its source to Hanford being an important factor.

9. A mixture with natural sand and 480 lb of cement was chosen for full-scale adiabatic tests. For these tests, batches of 0.5 cu yd were mixed for 2 hr in a revolving drum mixer. The results of the initial large-scale adiabatic test showed this mixture to be much hotter (temperature rise >57 °C in 4 days) than was estimated from the smaller CIMS calorimeter tests. It was unclear whether this mixture would overheat inside the vault environment.

10. For this reason, a new mixture containing 300 lb of cement was proportioned and tested by the previously described regimen. This mixture, CC-20, is the one recommended by WES, and meets all the specifications for the grout in the unhardened and hardened state except for shrinkage where its volume change is -0.02 percent. This value easily meets the requirement for the lower lifts but misses the specification for less than 0.01 percent shrinkage in the top lift. As we stated in letters exchanged before the research effort began at WES, we have come as close as we could to the specifications in the time and with the resources given. This is an extremely small volume change. It seems unlikely that shrinkage between 0.02 and 0.05 percent in the top lift will compromise the integrity of the cover blocks above it.

11. The final phase of the research was to cast large-scale batches, 1.5 cu yd in size, and place them in a fully instrumented, full-depth physical model. This model is a cube, 5 ft on each side, heated to 45 °C to simulate the vault environment and the thickness between the PSW waste grout and the cover blocks. Materials were batched and mixed in a computer-controlled automated batch plant using a pug-mill mixer and a mixing time of 2 hr. Three 16-in. lifts were placed on top of a 6-in. layer of simulated waste grout.

12. The highest temperature attained in the WES physical model was approximately 60 °C, and no significant problems were encountered. The final lift was instrumented with six dial gages to measure the movement of the grout relative to the bottom of the cover blocks. Analyses of interfaces between

simulated wasteform grout and WES cold-cap grout indicated virtually no bonding and minimal potential for chemical interaction.

The Grout Vault Program

13. The Hanford Grout Vault Program was developed to reduce the need for temporary storage capacity for soluble radioactive waste and provide permanent disposal of defense low-level wastes at the Department of Energy facility at Hanford, WA. These wastes include chemically toxic and radioactive salts created during more than 40 years of processing nuclear weapons materials. The wastes have been dewatered to varying extents and stored in "temporary" underground steel tanks. For permanent disposal, the waste is removed from its temporary tank, mixed with the dry-blended components of the wasteform grout, and then pumped into underground concrete vaults. Being solidified in wasteform grout makes the radioactive waste components less soluble and less likely to be leached or otherwise transported into the biosphere (Hanford Support Team, 1990). The PSW grout campaign, during which the demonstration vault was filled with its wasteform grout, is described elsewhere (Cline et al., 1990).

14. For the demonstration vault, the cold-cap grout will be placed on top of the wasteform grout in at least three layers, filling the vault to the underside of its cover blocks to form a load-bearing barrier between the covering layers and the hazardous materials contained below them. The vault measures 15.2 m by 38.1 m by 10.4 m and is filled to a height of 9.2 m with wasteform grout and later covered with 1.2 m of cold-cap grout (Cline et al., 1990). Figure 1 shows a section view of the first concrete vault at Hanford which is filled with wasteform grout. WES developed the cold-cap grout for this vault.

Performance Requirements for Cold-Cap Grout

15. There are three categories of performance requirements: (1) pumping and placement properties, (2) properties of unhardened grout after placement, and (3) properties of hardened grout.

Pumping and placement

16. The location of existing ports in the cover blocks dictates that the grout will drop 4 ft vertically when pumped into the vault and must flow at least 14 ft horizontally from each entry point to cover the wasteform and fill the void space. For this the grout must be self-levelling and non-segregating. From WES grouting experience, we determined that a flow time of 15 to 18 sec (ASTM C 939) was an appropriate measure of this property. Batching may be accomplished at a concrete plant, requiring a minimum 1 hr travel time; the grout will need to be pumpable for 2 hr after mixing begins.

Unhardened grout

17. Avoiding evolution of free liquid, or bleeding, is the most critical property after placement and before final set. We anticipated that free liquid on the upper surface of the wasteform might have left a layer of soft and possibly soluble radioactive mineral matter. Avoiding free liquid from the cold cap will reduce the likelihood of (1) chemical interaction between the two grouts, (2) physical disturbance and remobilization of radioactive or hazardous components to contaminate the cold cap and violate the multiple-barrier system.

Hardened grout

18. The grout was required to attain an unconfined compressive strength of 400 psi (3.0 MPa) at 28 days. Volume stability is critical for maintaining the integrity of the cap, so shrinkage is limited to 0.1 percent in the lower lifts and 0.01 percent in the top lift, and no expansion is permitted. The grout must be geochemically stable in contact with the wasteform grout at temperatures estimated to reach 70 °C or more and contribute as little heat as possible to the vault itself. The current demonstration vault temperature is 45 °C; a maximum temperature rise of 50 °C was chosen as a requirement to avoid overheating.

PART II: MATERIALS SELECTION AND CHARACTERIZATION

Criteria

19. Three groups of criteria were considered in selection of component materials for the grout. The first group was the performance demands of chemical and mechanical stability, heat generation, durability, and placability. The second group was economic, including availability of materials near the site locations, likelihood of continued availability, and shipping costs. The third group of selection criteria included WES experience with comparable materials and an acceptable performance record in comparable grout operations.

Cement and Fly Ash

20. The two main considerations in cement choice were low heat generation and resistance to sulfate attack. API Class H oil-well cement was chosen because of its coarse particle size and resultant reduced rate of heat evolution, expected to reduce cracking due to thermal strains. The low alumina content of the cement was also expected to provide excellent resistance to sulfates (Mindess and Young, 1981) which are known to be present in the liquid waste. The chemical and physical properties of the cement selected are shown in Table 1.

21. A low-calcium ASTM Class F fly ash was chosen over a Class C ash because of the demonstrated ability of the former to provide added resistance to sulfate attack and lower early-age heat generation (Barrow et al., 1988, 1989). This fly ash also had a positive effect on workability and was expected to contribute to the cementitious microstructure with time to enhance chemical stability and leach resistance. The chemical and physical characteristics of the fly ash are shown in Table 2.

Aggregates

22. Two different fine aggregates were tested during the project. The first was a natural, well-rounded sand from a source near the Hanford site,

and the second was a crushed limestone sand available at WES. The two aggregates were chosen specifically for their different physical and mineralogical makeup and differing linear coefficients of thermal expansion (CTE). Since aggregate makes up a significant proportion of the grout volume, the volume stability of the grout at elevated temperature is heavily dependent upon the coefficient of thermal expansion of the aggregate which is counteracting drying shrinkage of the paste. For this reason, the limestone aggregate with a CTE of 3.3 microstrains/°F was compared with the silica-rich Hanford sand which has a CTE of 4.4 microstrains/°F. This allowed us to measure the effect of the CTE of the aggregate on the volume stability of the grout. The characterization tests performed on the fine aggregates included grading, bulk specific gravity, absorption, and mineralogical analysis by XRD. Data from the natural aggregate used in CC-20 are presented in Appendix A. The grading was determined according to ASTM C 136, while the specific gravity and absorption were determined in accordance with ASTM C 127 and ASTM C 128, respectively. These results are shown in Table 3. The fractions larger than the 2.36-mm (No. 8) sieve size were sieved out to reduce segregation in the mixcure and improve flow properties of the grout.

Other Components

23. Approximately 22.5 kg of sodium bentonite were used per cubic yard of grout to aid in pumpability, reduce segregation, and eliminate bleeding. A commercial brand of clay familiar to WES researchers and used extensively in the grouting industry was chosen and tested for mineralogical composition by XRD and for pozzolanic activity according to ASTM C 618. The results are shown in Table 4.

24. To produce as durable a product as possible, the ratio of water to cementitious materials was held at 0.40 by mass. This necessitated the use of a high-range water-reducing admixture (HRWRA) and a set retarder to obtain the required flow properties for the 2-hr time period needed between mixing and pumping. The HRWRA used was DAXAD19®, a naphthalene-based product marketed by W. R. Grace. The set-retarding admixture was a salt of hydroxylated carboxylic acid marketed by Sika Corporation as Plastiment®.

PART III: EXPERIMENTAL PROCEDURES

25. The experimental testing program was accomplished in three phases: (a) mixture proportioning and unhardened properties testing, (b) hardened properties testing, and (c) full-depth physical model.

Mixture Proportioning and Unhardened Properties Testing

26. The cold-cap grout will be pumped into an opening that is the upper 1.2-m depth of the entire vault, above the wasteform grout. WHC has monitored the temperature of the demonstration vault since placement of the wasteform grout. The working temperature they provided to WES for our testing and physical modelling was 45 °C. It was desirable to proportion the mixture with a minimum cement content and still meet the unhardened and hardened grout properties specified. For this reason, fly ash amounts of 67 to 80 percent of the cementitious medium were used. The ratio of cementitious materials to sand (C+FA/S) was varied between 1:1 and 2:1 initially, when we had not yet determined how the aggregate content would affect the volume stability of the grout at the elevated vault temperature. Initial mixtures were proportioned in 0.003-m^3 batches in a laboratory bench-top mixer meeting the requirements of ASTM C 305 and were tested for flow, segregation, bleeding, shrinkage, and compressive strength. Quantities of all component materials were measured on mass balances certified as accurate within 0.1 percent. Balance verification records are on file at the WES.

27. Grout flow was tested using the flow cone procedure in ASTM C 939 at intervals of 15, 30, 60, 90, and 120 minutes after starting mixing. From WES experience with grouting operations, we judged that a grout with a flow time of 15 to 18 sec would meet the flow requirements. Bleeding and shrinkage were estimated by measuring the space left at the top of the cylinder after final set. Compressive strength was measured using 3- by 6-in. (76- by 152-mm) cylinders at 7 days, according to ASTM C 39. Mixture segregation was checked by physical inspection prior to each flow test. A total of 20 mixtures was proportioned from the materials listed and tested in the laboratory during this phase of the research. At the completion of Phase I, the four best candidate mixtures (CC-10, CC-11, CC-13, CC-16) were selected to

continue to Phase II. Table 5 shows the mixture proportions for these mixtures which were chosen to proceed with hardened properties testing. Table 5 also shows proportions for mixture CC-20, the recommended candidate mixture, which was developed as a result of Phase II testing.

Hardened Properties Testing

28. The five mixtures shown in Table 5 were proportioned in 0.008-m^3 batches and tested for flow, segregation, bleeding, and time of setting. Also from these batches, specimens were cast for measurements of volume stability, chemical interaction with simulated wasteform grout, compressive strength, and semiadiabatic temperature rise. Duplicate batches were cast of each of these mixtures to attain statistically credible values and to minimize possible proportioning errors. Bleeding was measured, after 2 hr of mixing time, at appropriate intervals for 3 hr after casting in a 500-mL graduated cylinder, as described in ASTM C 940. The time of setting was measured using a Vicat apparatus according to ASTM C 953. Compressive strength was obtained by testing 2-in. (50.8-mm) cubes according to ASTM C 109 at 7, 14, and 28 days. Strength after aging at elevated temperature also was measured on companion cubes cast in each batch and cured at 38 °C and 40 percent RH. The results of the strength tests are summarized in Table 6.

29. The volume stability measurements were made on 1- by 1- by 11-1/4-in. (25.4- by 25.4- by 287-mm) prisms which were cured and stored in environmental conditions of 45 °C and 100 percent relative humidity to simulate conditions inside the vault. Since the exact relative humidity inside the vault was not known, companion prisms from each mixture were cast and stored at 38 °C and 40 percent relative humidity to bracket plausible conditions. All batches were mixed at 23 °C for 2 hr, after which the molds were filled and immediately placed in the elevated temperature chamber. The specimens were removed at 24 hr, demolded, and returned to the chamber. Measurements were taken daily through 7 days, weekly through 28 days, then monthly to 150 days. Figures 2 through 6 plot the volume stability versus time for the five mixtures at each temperature and relative humidity through 150 days of age.

30. As we anticipated, the specimens stored in the higher humidity environment exhibited much better volume stability than their companion prisms in the lower humidity. Table 7 summarizes prism expansion measured at 150 days. In each case involving both aggregates the mixture with moist curing exhibited shrinkage of 0.03 percent or less, while those mixtures subjected to lower humidity showed shrinkage values consistently near 0.1 percent with one as high as 0.23 percent. It is clear from these data that, at constant cement levels, varying the fine aggregate type or content did not have a large effect on the volume stability of the grout. It is also clear that lowering the cement content of the mixture caused a slight increase in the amount of shrinkage measured. Since the fine aggregate type had minimal effect on volume stability, mixtures made with limestone fine aggregate were deleted from the test matrix, and the remainder of the investigation centered on mixtures containing the natural sand fine aggregate local to the Hanford area.

31. At this point in the investigation, we decided to continue thermal investigative work with mixtures CC-10, CC-16, and CC-20. Initial thermal screening of each candidate mixture was performed using CIMS, which measures the heat signature from a 152- by 305-mm cylinder specimen in a calibrated calorimeter. The CIMS coupled this heat signature with heat capacity information entered for the individual materials and calculated an adiabatic temperature rise for the mixture. This test assumed the vault would respond like an adiabatic environment at 45 °C. This test was used to screen the three remaining candidate mixtures to select the best mixture for full-scale adiabatic testing. Figure 7 shows the adiabatic temperature rise calculated by the CIMS system for these three mixtures.

32. Since the grout would be placed into an environment at 45 °C, an adiabatic temperature rise limit of 50 °C was placed on the cold-cap mixture to ensure it did not overheat in the vault. The data shown in Figure 7 indicate that mixtures CC-10 and CC-16 exhibited peak temperature rise values greater than 50 °C with mixture CC-16 with its higher sand content being slightly cooler. Mixture CC-20, with its lower cement content, recorded a calculated adiabatic heat rise of 41 °C. For this reason, mixtures CC-16 and CC 20 were chosen to perform full adiabatic temperature rise tests.

33. Adiabatic temperature rise of candidate grout was determined by the method given in CRD-C 38 (Corps of Engineers, 1949). For this test, a 0.40-m^3 sample was mixed in a rotary drum mixer for 2 hr and placed in an environmentally controlled room where the temperature of the room was matched to the heat generation of the sample. Figure 8 shows the adiabatic temperature rise measured on mixtures CC-16 and CC-20. Mixture CC-16 exceeded the 50 °C limit almost immediately, and the test was terminated after 2 days. The temperature of mixture CC-20 rose more slowly and stayed below the 50 °C limit. Based upon these data and data generated from the volume stability measurements of prisms, we decided to use mixture CC-20 in the full-depth physical model phase of the test program. The mixture proportions for CC-20 are shown in Table 5.

Interface With Wasteform Grout

34. As part of the laboratory experiments that led to mixture selection, we prepared 2- by 2-in. (50.8- by 50.8-mm) cylinders of simulated wasteform grout (based on different cement and fly ash, and two clays; formulation given in Lokken et al., 1988) in plastic molds 4 in. high. We then cast candidate cold-cap grouts (CC-9 through CC-16, Table 5) in the upper half of each mold when the simulated wasteform in the bottom half was 2 to 3 weeks old. The interfaces were studied at ages between 4 and 9 weeks, by visual and petrographic observations, XRD, and chemical composition by EDX in appropriate profiles. Observations included aggregate distribution, evidence of fluid movement, and description of interface surface textures. A typical petrographic report from these studies is included in Appendix B. As anticipated, there was virtually no bonding between candidate cold-cap grouts and simulated waste grout. The lower surface of each cold-cap grout appeared frothy, covered by a 1-mm-thick layer of uniformly sized thin-walled voids, while the upper surface of the simulated waste grout was smooth.

Analyses of Small Interface Samples

35. Phases identified by XRD are consistent with partial hydration of cementitious components both in the cold cap and in the simulated wasteform

grout (calcium hydroxide, calcium silicate hydrate, dicalcium silicate, and mineral constituents of the aggregate). Calcite is most abundant in the froth, and ettringite is present only in the froth and not within the grouts. EDX elemental analysis revealed Na, Al, Ti, and S more abundant in froth than grouts, and Ca more abundant in grouts than in froth. kesults of XRD and EDX analysis are summarized in Appendix B.

PART IV: PHYSICAL MODEL TEST

36. In the final phase of this research, we constructed an insulated and heated cube proportioned to represent the full depth of one corner of the cold-cap grout layer of the Hanford demonstration vault and cast a large-scale physical model of the cold cap. This endeavor incorporated measuring all of the grout properties tested separately in the previous phases and included extensive instrumentation and data acquisition. The concept was to simulate on an engineering scale the environmental conditions in the vault and the mixing and placement operations as they might occur at the site. Figure 9 is a photograph of the interior of the cube immediately after placement of first grout lift. This physical model was maintained at 45 °C to simulate the vault environment and was instrumented for strain, temperature, and volume change. Model dimensions were chosen to reflect the actual depth being placed in the vault, to eliminate the size effects inherent in small specimens, and to give realistic temperature and strain profiles and volume changes. Long-term data from this model were intended to validate the measurements made on previously cast laboratory specimens and provide more complete data for thermal modelling efforts to follow.

Mixing and Placement

37. At the base of the cube, we placed a 150-mm lift of surrogate PSW wasteform grout, using the formula provided by Lokken et al. (1988). When the simulated wasteform grout layer had been in place and at temperature in the model for several weeks, we then placed the first of three 410-mm lifts of cold-cap grout. Two more lifts followed after one week and four weeks, respectively. The cap was cast in separate lifts since the vault will be filled in this manner to decrease the likelihood of continuous crack propagation. One quarter of the cube was instrumented with 18 Carlson strain meters and 19 separate thermocouples, to measure changes in both strain and temperature from the block centerline to the outside wall as each lift was added to the cube. Figure 10 shows a 3-D view of the cube with the location of the 18 strain meters. Six meters were placed in each lift with one at the cube centerline and the remaining meters placed in a rectangular pattern to measure changes in the material as the grout approaches the corner of the

model. Figures 11 through 13 show the meter trees and the numbered meters showing their location in the cube. Each cold-cap lift also was instrumented at the cube centerline with four thermocouples, plus one in the wasteform grout, to record a continuous profile of temperature data. This thermocouple tree is shown in Figure 14, with the centerline marked "CL."

38. Each lift of cap grout was batched in a fully automated, computer-controlled batch plant and mixed for 2 hr in a pug mill prior to being placed in the cube by concrete bucket. Figure 15 shows the pug mill mixing the grout for the first lift. Flow and segregation were measured at 30-min intervals during the 2-hr mixing period, and nine 152- by 305-mm cylinders were cast and tested for compressive strength in groups of three at 7, 14, and 28 days. Figure 16 depicts the strength gain with time for two of the three lifts placed in the physical model compared to the strength figures obtained from the 2-in. cubes cast for the same mixture in the earlier phase of the project. The average 28-day compressive strength of the grout placed in the physical model was approximately 10.7 MPa. None of the lifts exhibited any bleed water.

Strain and Temperature Measurements

39. Each grout lift was batched at approximately 27 °C and placed immediately into the physical model which was kept at 45 °C. The highest temperature attained by any of the three lifts was 61 °C which equated to a 41 °C rise in the grout itself. Figure 17 plots the grout strain versus time at the centerline of each lift at the center of the cube. The maximum strain recorded at the block centerline in the first lift was over 2000 microstrains, which is well above the strain limit expected for cementitious grout. Visual inspection of the surface revealed several cracks, but it was not obvious whether they were due to thermal effects or to drying shrinkage, since they propagated from the instrumentation tree. Figure 18 is a photograph of the cracks propagating from around the instrumentation supports. While crack elimination was not a performance requirement, WES did try to prevent cracking and to determine its cause when it was observed.

40. The second lift of cold-cap grout was placed six days after the first. In an attempt to remedy the cracking problem, this lift was moist

cured by ponding a thin layer of water on the surface each day. Most of this water was lost each day by a combination of absorption and evaporation, but it served to keep the surface from drying out and no cracking was observed during the 30-day period in between lifts 2 and 3. Measurements made on specimens placed on the grout surface and ponded with the same thickness of water each day showed that 70 percent of the ponded water was evaporated by the heat from the model, and we assume that the remaining 30 percent was absorbed or otherwise incorporated into the grout.

41. The maximum strain measured at the cube centerline in the second lift was 1550 microstrains. This is also many times the strain limit typically associated with hardened grout yet this lift showed no visible signs of cracking. We postulate that the cracking observed in the first lift was due to drying shrinkage coupled with the restraint imposed by the instrumentation. The model was not actually a sealed system, but it is possible that enough water was evaporated from the surface of the grout to saturate the air above the surface on which cracking was observed. This situation may have been exacerbated by the failure to seal the plywood ceiling of the block. This ceiling undoubtedly absorbed water from the air above the grout surface, which would then continue to draw water from the grout. The daily wet curing of the second lift surface by ponding apparently prevented the heat from evaporating enough water away from the surface to cause it to crack. It is also possible that the elastic modulus of the grout may be low enough at early ages that the material can accommodate these large strains without macroscopic damage.

42. The third lift was placed 30 days after the second (during which we awaited arrival of additional materials). The cube was filled to within 150 mm of the underside of the roof to allow room for surface measurements and was not cured by ponding with water. The maximum strain in lift three was attained by the centerline meter and totaled 1300 microstrains. Several lifting shackles were inserted into the top lift which served as starting points for cracks as the grout stiffened. A complete listing of the strain vs time and temperature vs time plots for each meter is presented along with a reference table identifying each data file and plot in Appendix C.

43. As shown in Figure 14, each lift of cold-cap grout was instrumented with five thermocouples at the block centerline to record continuous

temperature data during the filling operation. Lift 2 also was instrumented with six additional thermocouples to record temperature variations within the lift from the cube centerline to the outside wall. Figures 19 through 21 show temperature profile versus time recorded at the block centerline in each lift. Figures 22 and 23 show the temperature variation in lift 2 at positions 48 cm and 15 cm from the model face. As each new lift was added to the model, the lowest thermocouple in the new lift, which was also the thermocouple nearest the grout surface, experienced the widest range of temperature variation. These lift additions are represented by temperature spikes in Figures 20 through 23. The widest variation within a lift occurred in the third lift and measured 39 °C.

44. The Carlson strain meters placed throughout the model also measured temperature on a continuous basis, and this also provided information on the temperature gradient from the model centerline to the outside edges. Elevated temperature does not cause cracking in grout and concrete but temperature gradients do. For this reason the model dimensions were specifically chosen so that the block represented a corner of the vault which is the worst-case scenario in terms of temperature gradients to the outside walls and the top of the vault. Figures 24 through 53 illustrate the changes in grout temperature and thermal strain with time and space as the model was filled.

45. When adjacent Carlson meters in the same lift were compared, there was very little difference in temperature, with the centermost meter being only slightly hotter. However, there is a large difference in the measured strains among meters within a lift, with the innermost meter always recording substantially higher strains. This trend was true when measuring from the centerline out to the cube face and also when measuring along the cube face from the center of the face to a corner. This result is attributed to the restraint imposed upon the grout layer by the increased proximity of the side wall of the model. The meters nearest the cube faces and top also showed a measure of strain relief after the last lift had been placed as evidenced by the positive (compressive) strains noted with increasing time in Figures 29, 31, and 35. These strains continued to rise for approximately 20 days before leveling off despite a relatively flat temperature profile during this period. The temperatures recorded at the edges and top of the cube were in most cases only a few degrees lower than those measured at the cube centerline.

Volume Stability Measurements

46. After the final lift was placed the top of the cube, six dial gages were attached to a fixed support simulating the vault cover blocks above the grout surface. The locations of these gages are shown in Figure 54. The actual volume stability of the grout surface was measured to validate the data obtained from the laboratory prism specimens. Figure 55 shows the deflection of the surface with respect to the cover blocks as measured by five of the gages through 90 days age. The sixth gage malfunctioned soon after installation. The average deflection is 0.021 in (0.52 mm). When divided by the 54-in. (137 cm) depth of the cold-cap grout, the shrinkage of the cold cap is calculated to be 0.039 percent. This value meets the shrinkage requirement of 0.1 percent for the lower lifts but misses the 0.01 percent limit for the top lift.

Analyses of the Interface in the Physical Model

47. The interface between the layer of simulated wasteform grout and the first lift of cold-cap grout in the physical model was sampled by horizontal coring after these layers had been in contact for 4 months at the vault temperature. This interface was studied by the same techniques as were the smaller samples. Again, there was minimal bonding between these layers, which is desirable for materials with different moduli and coefficients of thermal expansion. The froth was absent. However, where the two grouts had separated, the lower surface of the cold cap showed what appeared to be small channels, <1 mm in diameter and several millimetres long, suggesting fluid movement. The chemical composition of grouts and interfacial region were similar to those of the smaller samples, although the phase assemblage differed in that three forms of calcium carbonate were identified on the wasteform surface, and no ettringite was detected at the interface.

Implications for Chemical Interaction

48. The presence of froth at the interface of samples from small plastic molds suggests that it was preserved where fluid movement was

restricted. Microchannels on the interface from the larger physical model are consistent with this interpretation. We did not isolate or verify the cause of these interfacial features. However, the formation of ettringite at the interface of the small samples may indicate increased availability of sulfate from PSW. Extensive carbonation of the surface of the wasteform grout in the Hanford demonstration vault is likely because of the probable use of forced-flow air filtration system during and soon after placement of wasteform grout.

PART V: SUMMARY

49. A nonradioactive sanded cold-cap grout was developed to serve as a void filler between the waste grout and the underside of the cover blocks in the first Hanford Grout Vault. Using a small amount of Class H oil-well cement, a large amount of ASTM Class F fly ash, a natural sand, and bentonite clay, a grout was developed which met a demanding set of physical and geochemical properties.

50. Based upon this study, the following observations and conclusions are offered:

a. The required fresh-concrete properties of 2-hr workability with 15-sec flow time combined with no bleeding and no segregation can be met with the right combination of materials.

b. Adiabatic temperature-rise tests indicated that the mixture may be too hot; however, the full-depth model test placed under vault-like conditions showed a peak temperature rise of only 41 °C and a maximum temperature of 61 °C, which is well within the project requirements.

c. Although the vault is basically a closed system following placement of the cold-cap grout, the physical model experienced drying of the surface of the grout layers. This induced drying shrinkage cracking especially at penetration points where the grout was restrained by gage supports or other hardware. Strain measurements exceeded the nominal strain capacity expected for conventional cement-based grouts. However, the second layer did not crack when wet cured by ponding.

Recommendations

51. We recommend research to establish the early-age modulus of the grout material. Minimizing time between successive lifts and ponding water on the surface of the grout between lifts may alleviate the potential for cracking, but the demonstration vault may be sealed well enough during and following closure that it does not experience this apparent water loss by evaporation. If lower thermal strain and closer volume tolerance are required, we recommend additional work to develop grout with a lower cement content.

REFERENCES

American Society for Testing and Materials. 1991. 1991 Annual Book of ASTM Standards, Philadelphia, PA.

a. Designation C 39-86. "Standard Test Method for Compressive Strength of Cylindrical Concrete Specimens."

b. Designation C 109-90. "Standard Test Method for Compressive Strength of Hydraulic Cement Mortars (Using 2-in. or 50-mm Cube Specimens)."

c. Designation C 127-88. "Standard Test Method for Specific Gravity and Absorption of Coarse Aggregate."

d. Designation C 128-88. "Standard Test Method for Specific Gravity and Absorption of Fine Aggregate."

e. Designation C 136-84a. "Standard Method for Sieve Analysis in Fine and Coarse Aggregates."

f. Designation C 150-89. "Standard Specification for Portland Cement."

g. Designation C 157-89. "Standard Test Method for Length Change of Hardened Hydraulic-Cement Mortar and Concrete."

h. Designation C 191-82. "Standard Test Method for Time of Setting of Hydraulic Cement by Vicat Needle."

i. Designation C 305-82. "Standard Practice for Mechanical Mixing of Hydraulic Cement Pastes and Mortars of Plastic Consistency."

j. Designation C 618-91. "Standard Specification for Fly Ash and Raw or Calcined Natural Pozzolan for Use as a Mineral Admixture in Portland Cement Concrete."

k. Designation C 939-87. "Standard Test Method for Flow of Grout for Preplaced-Aggregate Concrete (Flow Cone Method)."

l. Designation C 940-89. "Standard Test Method for Expansion and Bleeding of Freshly Mixed Grouts for Preplaced-Aggregate Concrete in Laboratory."

m. Designation C 953-87. "Standard Test Method for Time of Setting of Grouts for Preplaced-Aggregate Concrete in the Laboratory."

Barrow, S., and R. L. Carrasquillo. 1988. "The Effect of Fly Ash on the Temperature Rise in Concrete," Research Report 481-2, Center for Transportation Research, University of Texas at Austin.

Barrow, R. S., P. M. Hadchiti, and R. L. Carrasquillo. 1989. "Temperature Rise and Durability of Concrete Containing Fly Ash," Proceedings of the Third International Conference on the Use of Fly Ash, Silica Fume, Slag, and Natural Pozzolans in Concrete, American Concrete Institute, SP 114, pp 331-338.

Cline, M. W., A. R. Tedeschi, and A. K. Yoakum. 1990. "Phosphate/Sulfate Waste Grout Campaign Report," WHC-SA-0829-FP, prepared for the U.S. Department of Energy Assistant Secretary for Defense Programs by Westinghouse Hanford Company, P.O. Box 1970, Richland, WA.

Hanford Support Team. 1990. "Hanford Site Environmental Restoration Cost And Review," prepared for U.S. Department of Energy Office of Environmental Restoration and Waste Management by U.S. Army Corps of Engineers Division, North Pacific (CENPD), P.O. Box 2870, Portland, OR.

Lokken, R. O., Reimus, M. A., Martin, P. F. C., and Geldart, S. E. 1988. "Characterization of Simulated Low-Level Waste Grout Produced in a Pilot-Scale Test," PNL-6396, Pacific Northwest Laboratory.

Mindess, S. and J. F. Young. 1981. Concrete, 671 pp, Prentice-Hall, Englewood Cliffs, NJ.

Tikalsky, P. J., and R. L. Carrasquillo. 1988. "Effect of Fly Ash on the Sulfate Resistance of Concrete Containing Fly Ash," Research Report 481-1, Center for Transportation Research, University of Texas at Austin.

U.S. Army Corps of Engineers. 1949. Handbook for Concrete and Cement, U.S. Army Engineer Waterways Experiment Station, Vicksburg, MS (with quarterly supplements).

Table 1

Chemical and Physical Properties of Portland Cement

(API Type H) Used in Cold-Cap Grout

Chemical Analysis	Result	Spec Limits Type II	
SiO_2, %	23.6	20.0	min
Al_2O_3, %	2.7	6.0	max
Fe_2O_3, %	3.5	6.0	max
CaO, %	61.8	*	
MgO, %	3.4	6.0	max
SO_3, %	2.5	3.0	max
Loss on ignition, %	0.9	3.0	max
Insoluble residue, %	0.24	0.75	max
Na_2O, %	0.07	*	
K_2O, %	0.52	*	
Alkalies-total as Na_2O, %	0.41	0.60	max
TiO_2, %	0.19	*	
P_2O_5, %	0.07	*	
C_3A, %	2	8	max
C_3S, %	40	*	
C_2S, %	42	*	
C_4AF, %	11	*	
Physical Tests			
Heat of hydration, 7-day, cal/g	59	70	max
Surface area, m^2/kg (air permeability)	304	280	min
Autoclave expansion, %	0.06	0.80	max
Initial set, min. (Gillmore)	170	60	min
Final set, min. (Gillmore)	285	600	max
Air content, %	10	12	max
Compressive strength, 3-day, psi	1,700	1,000	min
Compressive strength, 7-day, psi	2,205	1,700	min
False set (final penetration), %	94	50	min

* ASTM C 150 contains no specification requirements for these chemical analysis results.

Table 2

Chemical and Physical Properties of Fly Ash

Chemical Analysis	Result	Spec Limits Class F	
SiO_2, %	48.5	*	
Al_2O_3, %	19.8	*	
Fe_2O_3, %	17.6	*	
Sum, %	85.9	70.0	min
MgO, %	0.8	*	
SO_3, %	1.1	5.0	max
Moisture content, %	0.2	3.0	max
Loss on ignition, %	3.2	6.0	max
Available alkalies (28-day), %	1.1	1.5	max
Physical Tests			
Fineness (45-μm (No. 375) sieve), % retained	24	34	max
Water requirement, %	103	105	max
Density, Mg/m^3	2.38	*	
Autoclave expansion, %	0.02	0.80	max
Pozzolanic activity w/lime, psi	1,020	900	min
Pozzolanic activity w/cement (28-day), %	119	75	min

Laboratory cement used: Lone Star Industries, Cape Girardeau, MO
Laboratory lime used: Chemstone

* ASTM C 618 contains no specification requirements for results of these determinations.

Table 3

Fine Aggregate Data

Material: Hanford natural basaltic sand, HAN-1 S-2

Bulk Specific Gravity = 2.695

Source: Acme Concrete Co.
Richland, WA

Absorption = 1.6%

Sieve Size	Cumulative Percent Ret.	Pass.
4.75-mm (No. 4)	0.8	99.2
2.36-mm (No. 8)	18.4	81.6
1.18-mm (No. 16)	27.9	72.1
600-μm (No. 30)	46.4	53.6
300-μm (No. 50)	73.0	27.0
150-μm (No. 100)	90.1	9.9
Finer than 150-μm (No. 100)	(100.0)	0

Fineness Modulus = 2.57
(No. 4 - No. 100)

Material: Laboratory stock crushed limestone sand, WESSC-9

Bulk Specific Gravity = 2.69

Source: Vulcan Materials Co.
Calera, AL

Absorption = 0.9%

Sieve Size	Cumulative Percent Ret.	Pass.
4.75-mm (No. 4)	1	99
2.36-mm (No. 8)	5	85
1.18-mm (No. 16)	50	50
600-μm (No. 30)	71	29
300-μm (No. 50)	85	15
150-μm (No. 100)	94	6
Finer than 150-μm (No. 100)	100.0)	0

Fineness Modulus = 3.06
(No. 4 - No. 100)

Table 4

Chemical Analysis of Bentonite

Material: Big Horn Gel
HAN-1 SM1

Density (Mg/m^3) = 2.32

Source: Wyo-Gen Inc.
Billings, MT

Pozzolanic Activity
w/Cement (psi) = 150

X-ray Fluorescence Chemical Analysis

Component	Result (Mass %)
SiO_2	77.64
Al_2O_3	16.40
Fe_2O_3	4.34
MgO	1.60
Na_2O	1.17
CaO	1.13
K_2O	0.37
P_2O_5	0.19
TiO_2	0.12
SO_3	0.08
Mn_2O_3	0.06
Total	103.10

Table 5

Mixture Proportion for Grouts selected for Testing in Phase II

Mixture Designation	Class H Cement (lb/cy)	Fly Ash (lb/cy)	Aggregate Type (sand:cement + fly ash)	Aggregate Weight (lb/cy)	Clay (lb/cy)	Water (lb/cy)	High-Range Water Reducer (lb/cy)	Set Retarder (oz/cy)	W/C Ratio*
CC 9/10	481	1182	Hanford (1/2:1)	800	38	670	2.9	5	0.40
CC 11/12	481	1182	Limestone (1/2:1)	844	38	670	2.9	5	0.40
CC 13/14	481	988	Limestone (1:1)	1340	38	580	4.72	8.2	0.40
CC 15/16	481	983	Hanford (1:1)	1260	38	572	4.72	8.2	0.39
CC 20	300	1112	Hanford (1:1)	1314	38	564	4.16	4.5	0.40

* Ratio of water (w) to cement + fly ash (c).

Table 6

Compressive Strength Data for

Five Phase II Mixtures

Mixture Designation	Compressive Strength @ 23 °C (psi)			Compressive Strength @ 38 °C (psi)		
	7 days	14 days	28 days	7 days	14 days	28 days
CC 9/10 Hanford 1/2:1	1060	1440	1780	2610	3400	3800
CC 11/12 Limestone 1/2:1	1240	1900	2400	3000	3560	4160
CC 13/14 Limestone 1:1	1520	1440	2600	3500	3400	4300
C 15/16 Hanford 1:1	1160	1920	1920	2980	3560	3730
CC 20 Hanford 1:1	610	1040	1330	*	*	*

* No specimens were tested at elevated temperature because all measured values for strength exceeded the performance requirement.

Table 7

Overview of Expansion Bar Data

Fine Aggregate:Cement Ratio and Curing Condition	Length Change (%)	
	Hanford	Limestone
@1/2:1 & 45 °C/100% RH*	+0.007	-0.002
@1/2:1 & 38 °C/40% RH*	-0.08	-0.082
@1:1 & 45 °C/100% RH*	+0.002	-0.004
@1:1 & 38 °C/40% RH*	-0.10	-0.078
@1:1 & 45 °C/100% RH**	-0.03	
@1:1 & 38 °C/40% RH**	-0.23	

* Mixtures containing 481 lb/cy of cement @ 150 days.
** Mixtures containing 300 lb/cy of cement @ 90 days.

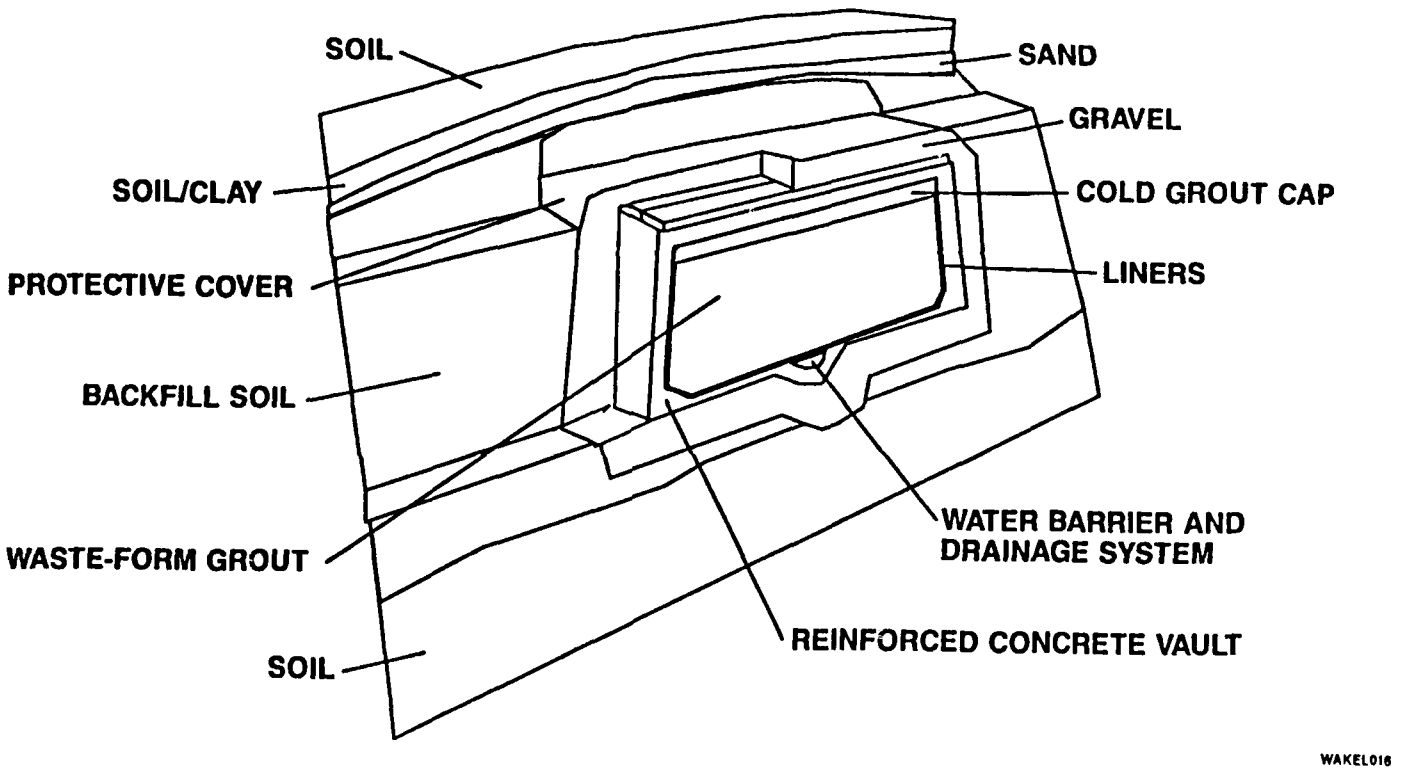

Figure 1. Grouted waste-disposal vault

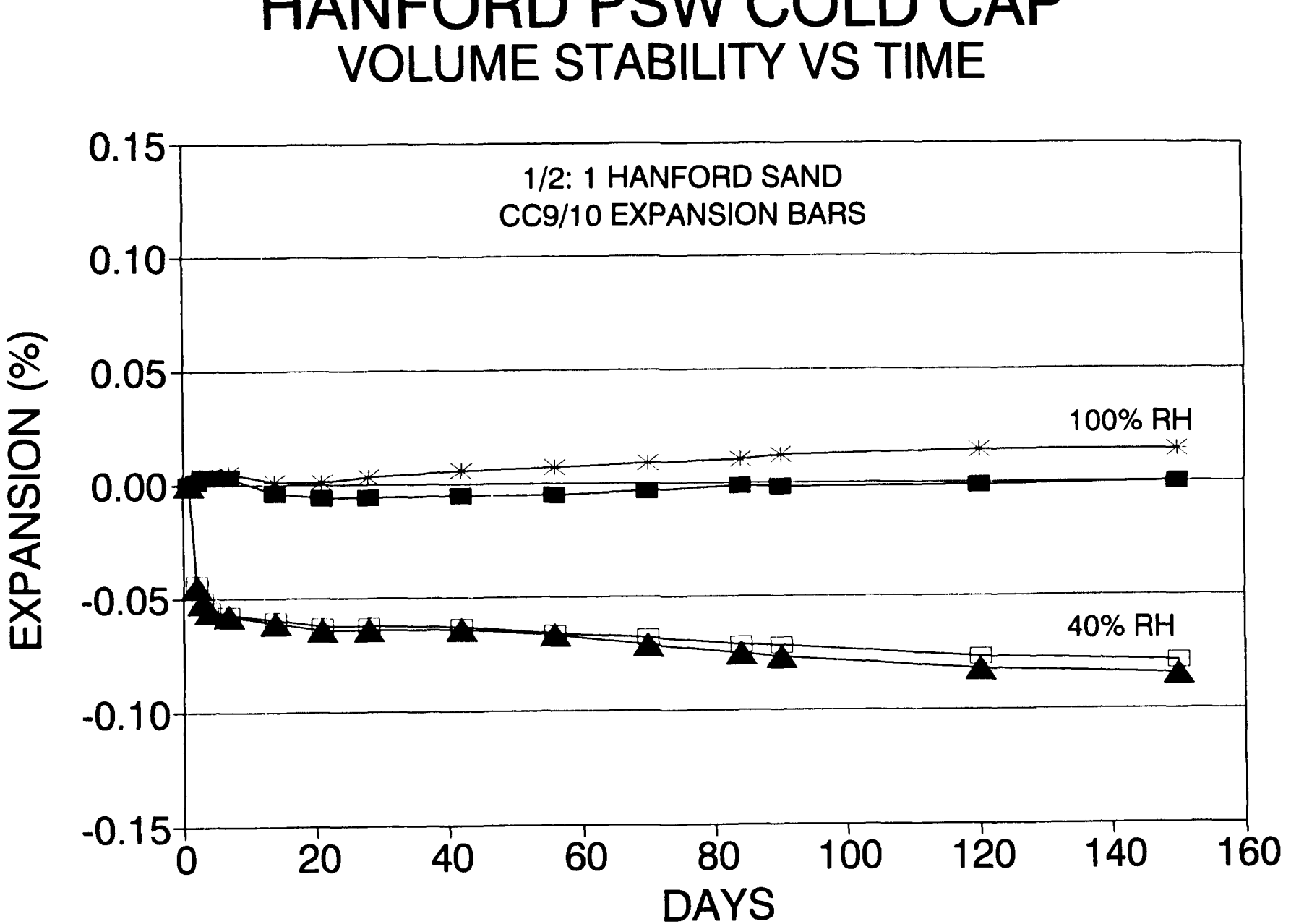

Figure 2. Plot of volume stability vs time for phase II expansion bars

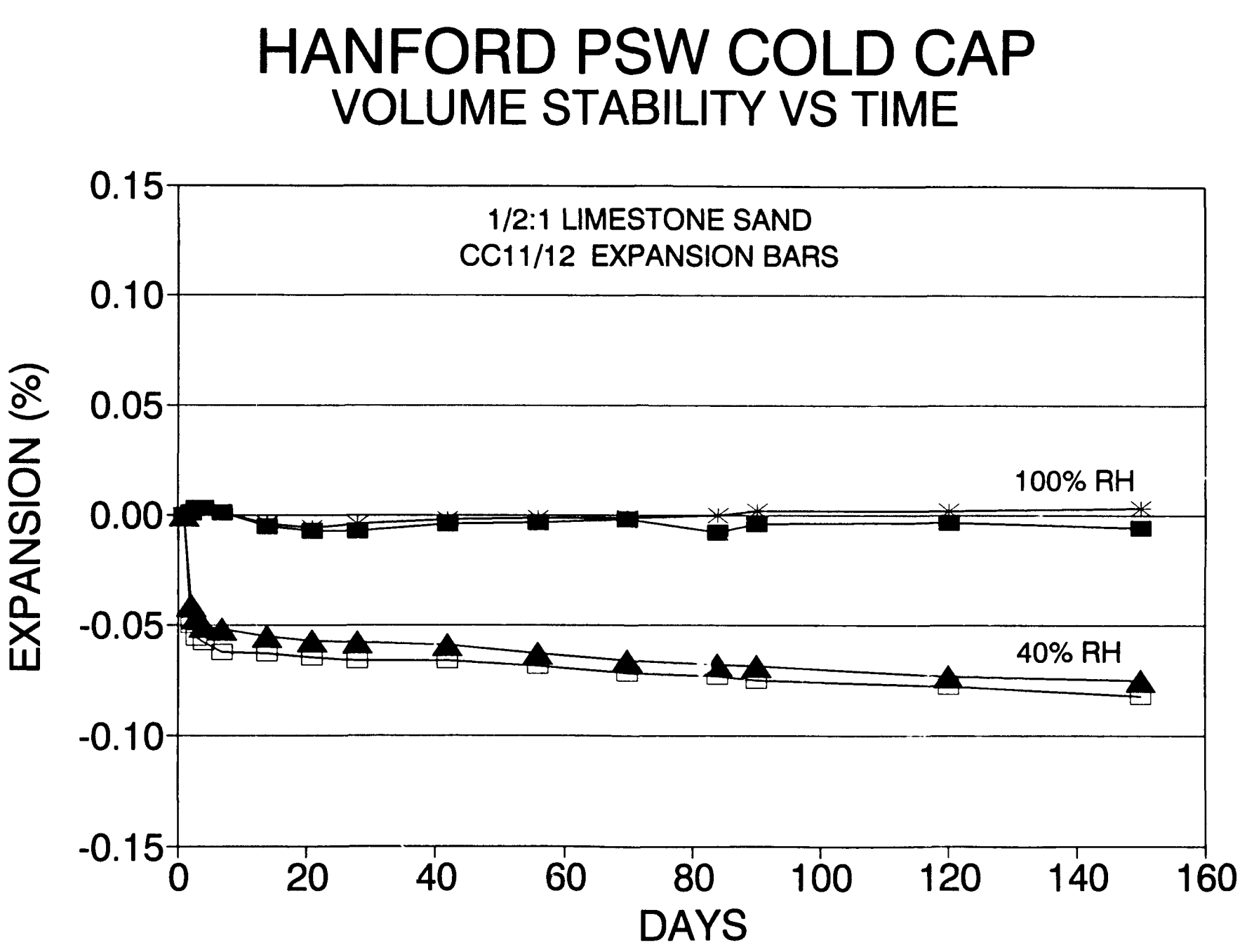

Figure 3. Plot of volume stability vs time for phase II expansion bars

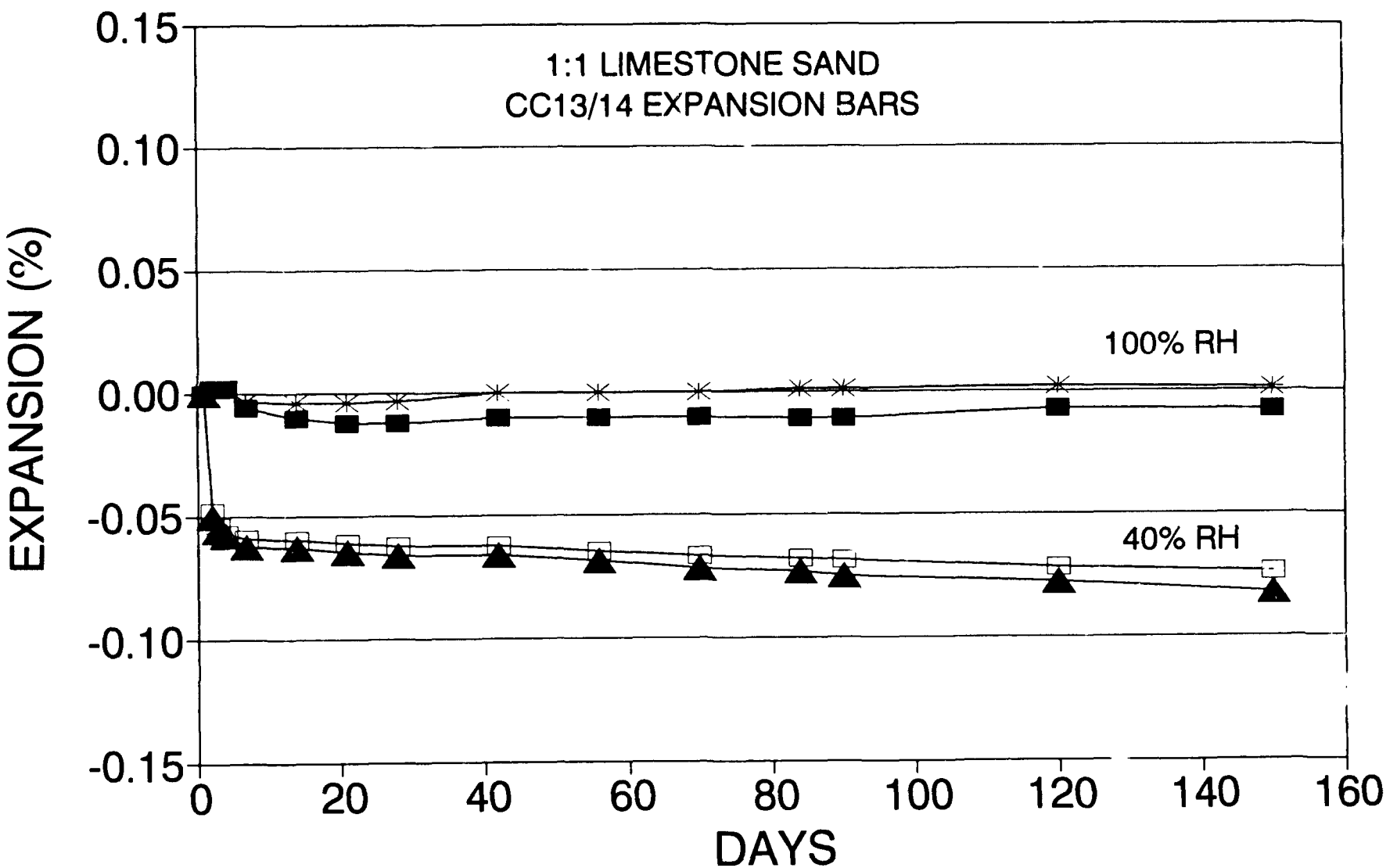

Figure 4. Plot of volume stability vs time for phase II expansion bars

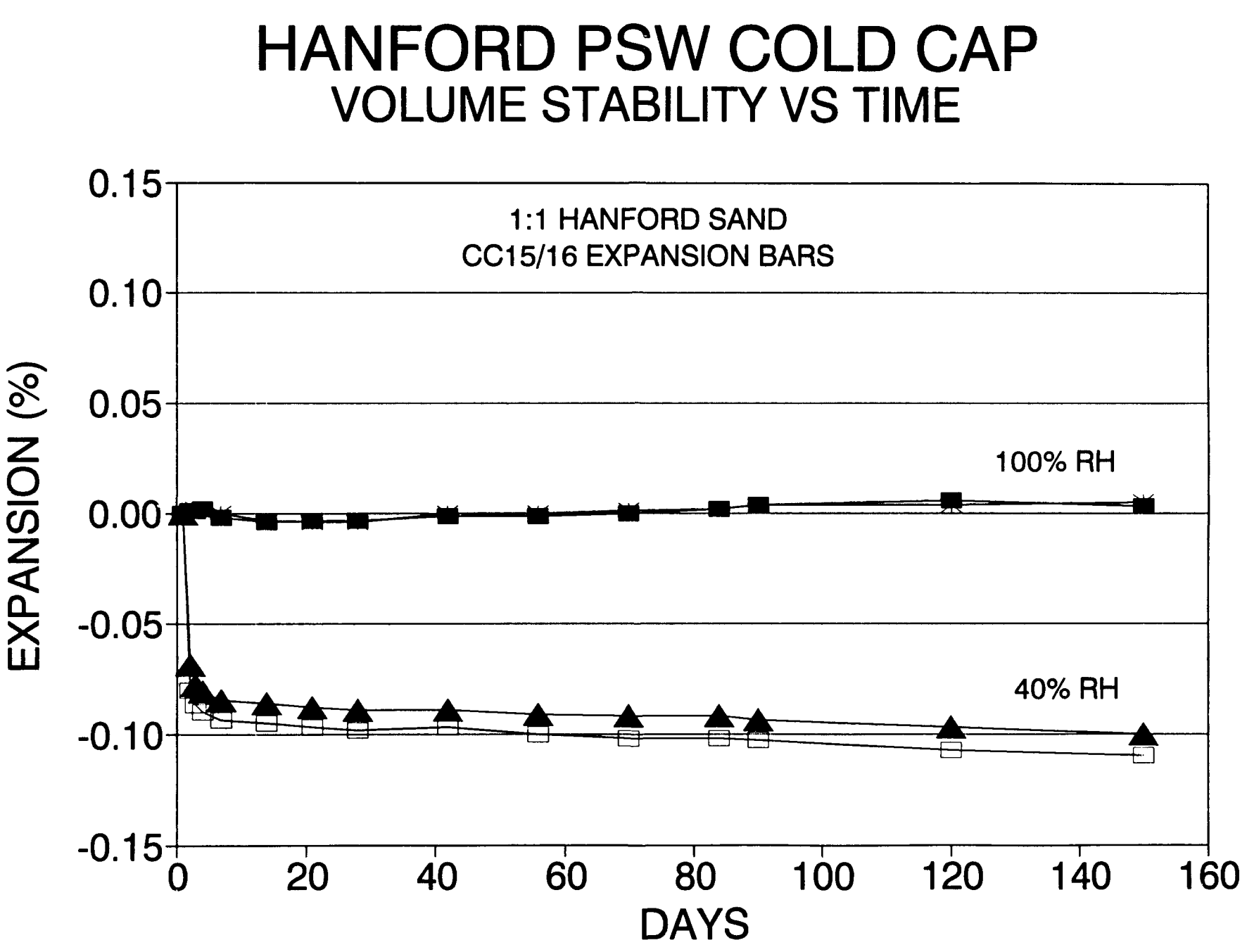

Figure 5. Plot of volume stability vs time for phase II expansion bars

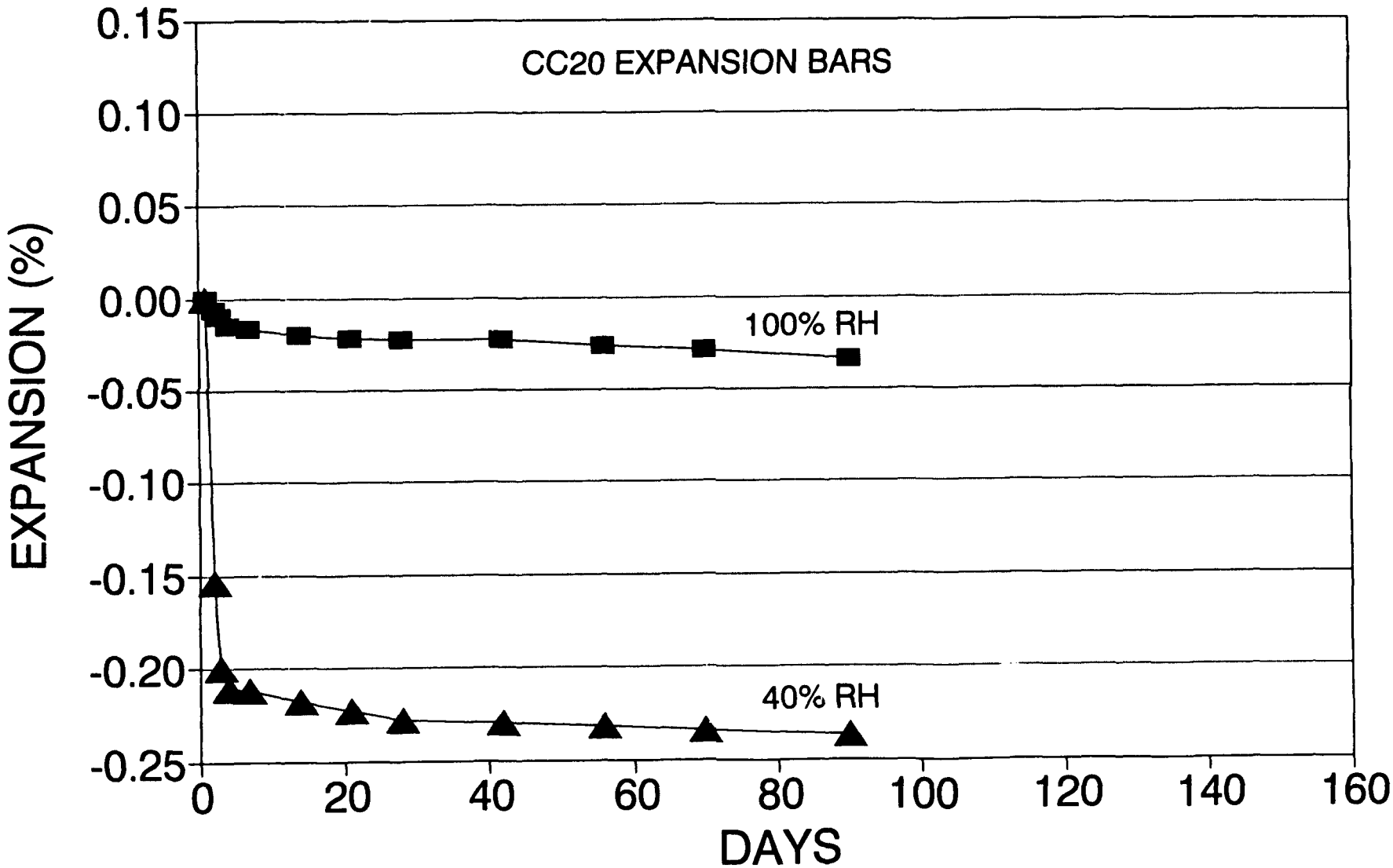

Figure 6. Plot of volume stability vs time for phase II expansion bars

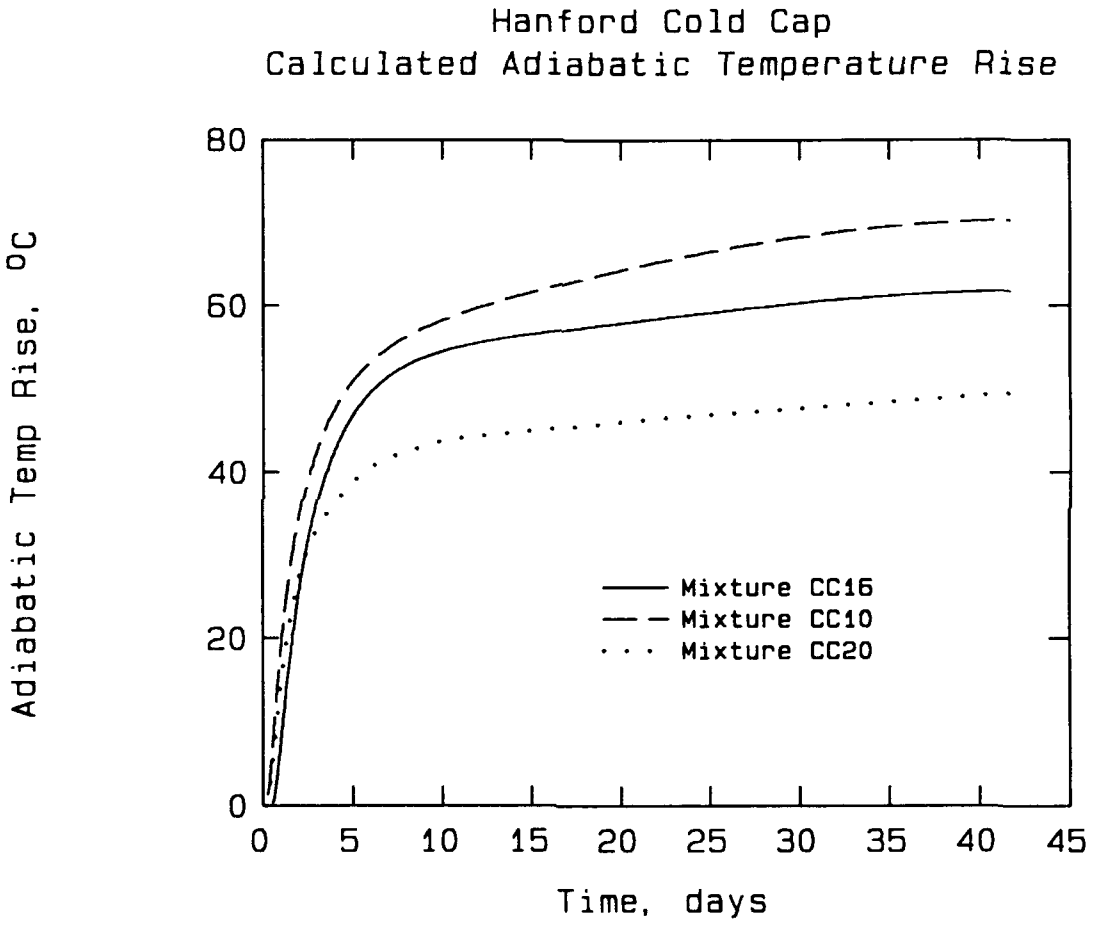

Figure 7. Calculated adiabatic temperature rise for mixtures CC10, CC16, and CC20 as predicted by the semiadiabatic test

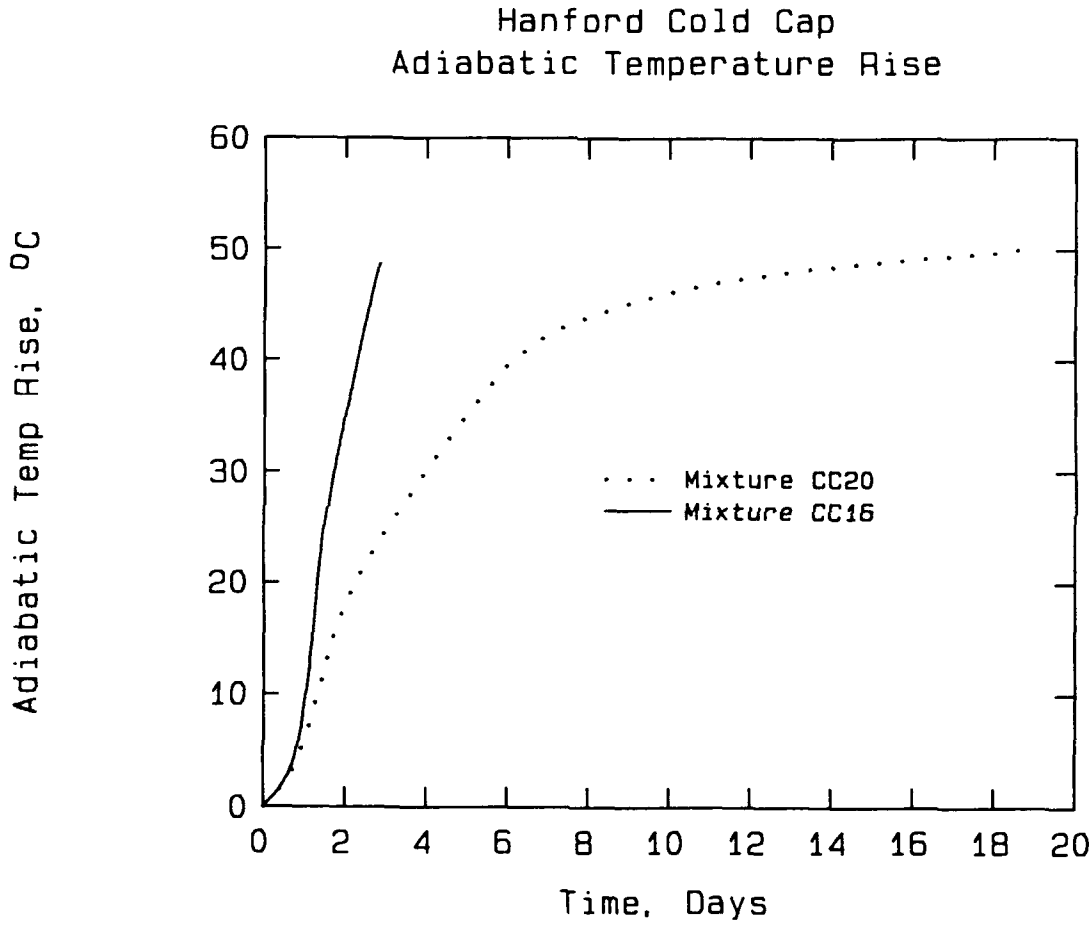

Figure 8. Adiabatic temperature rise for mixtures CC16 and CC20

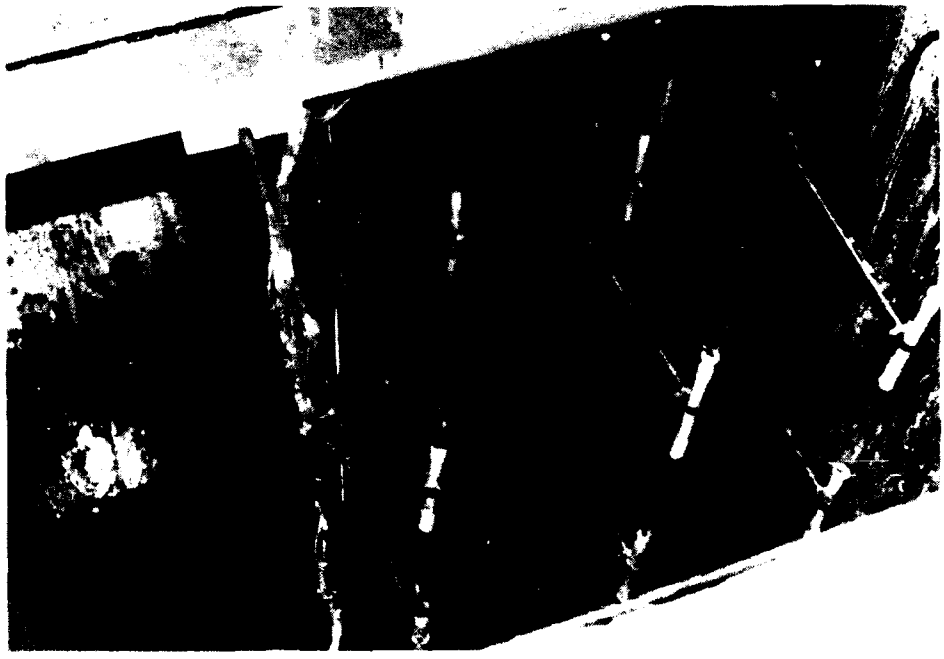

Figure 9. Photograph of inside of physical model immediately after placement of the first grout lift

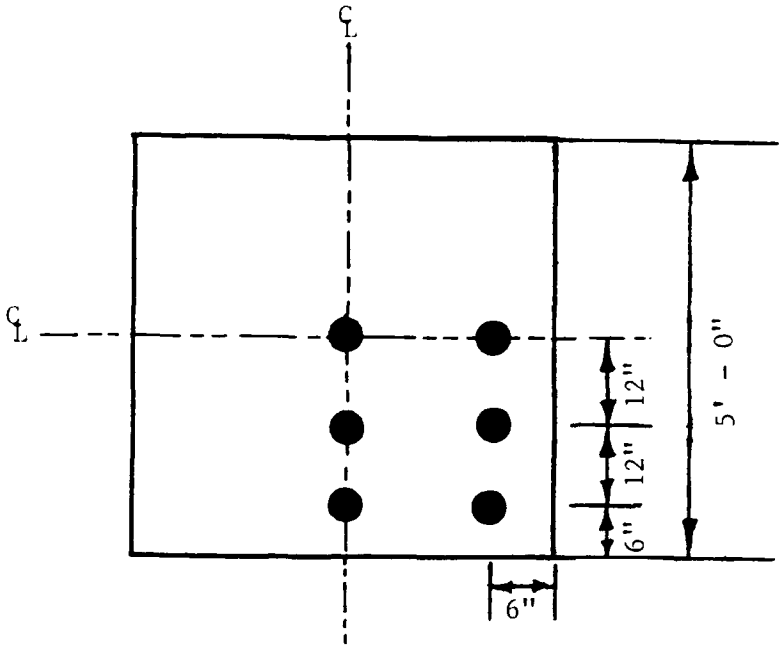

(a) Plan view

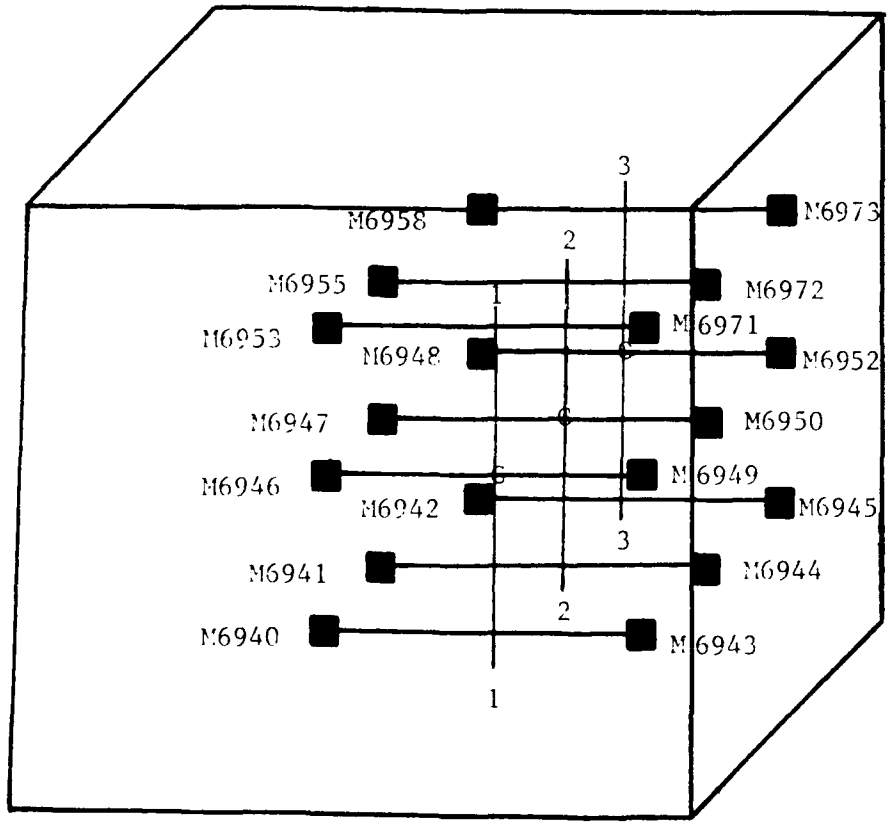

(b) Three dimensional

Figure 10. Drawing of physical model showing location of strain meters

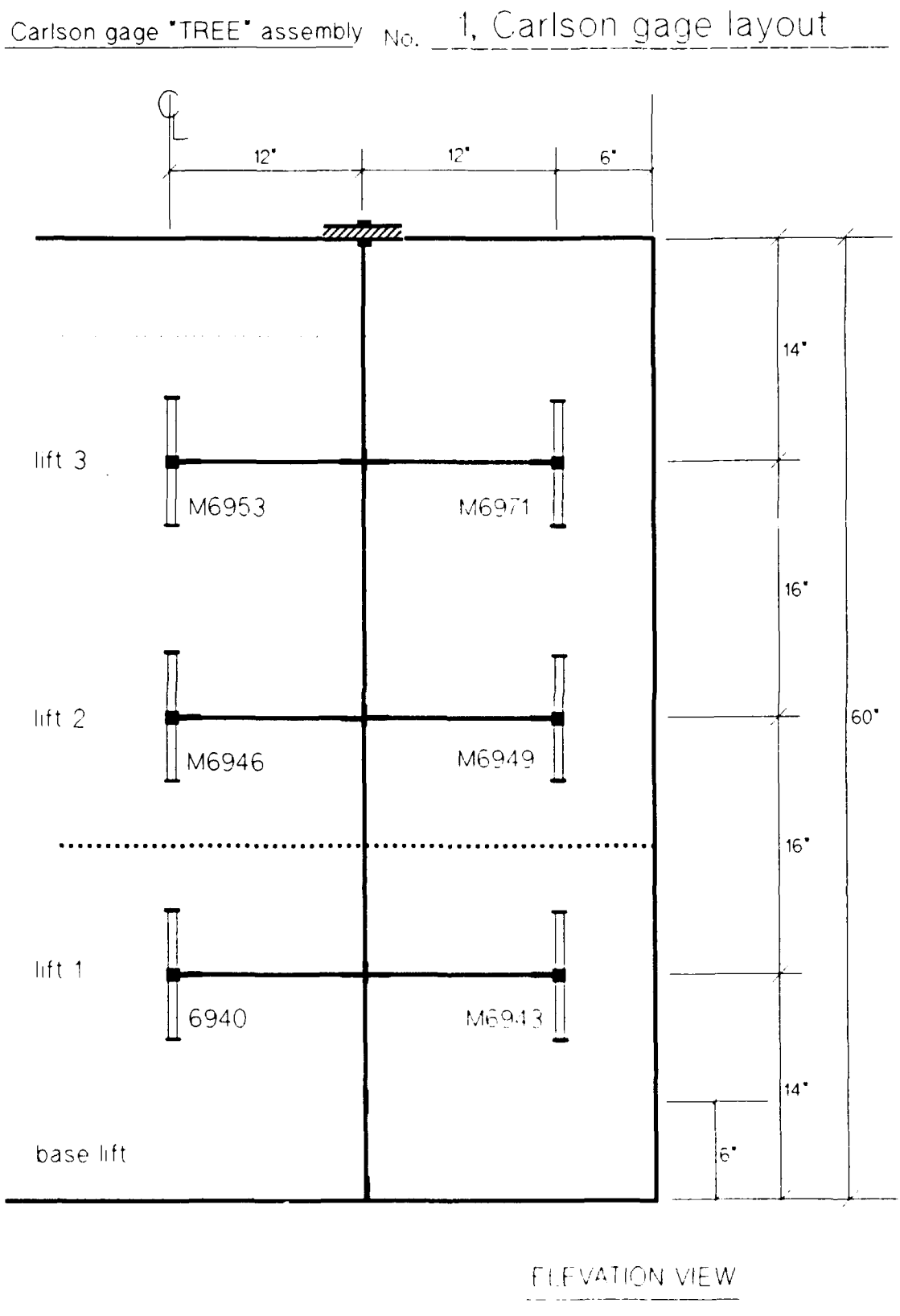

Figure 11. Layout drawing showing location of strain meters

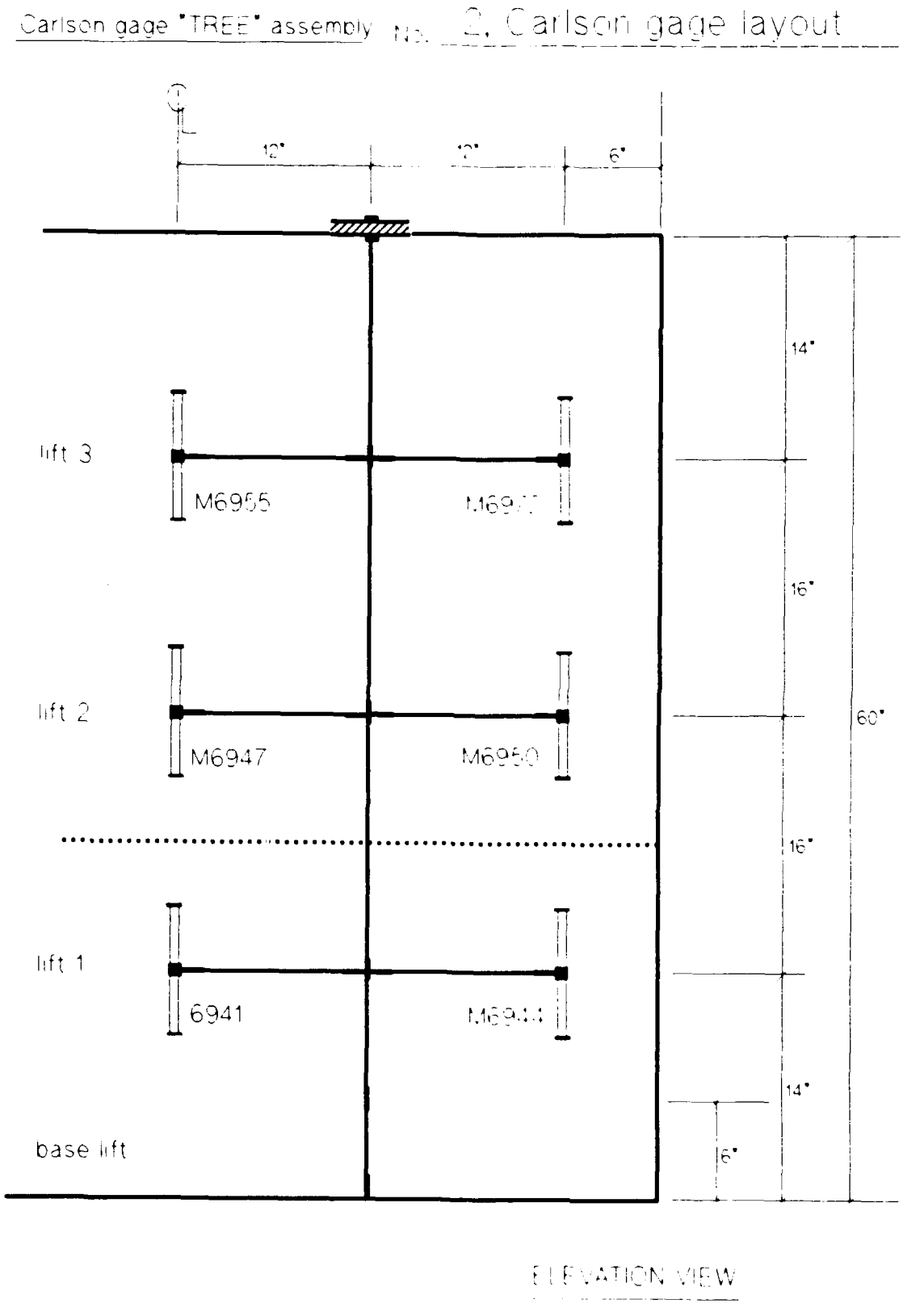

Figure 12. Layout drawing showing location of strain meters

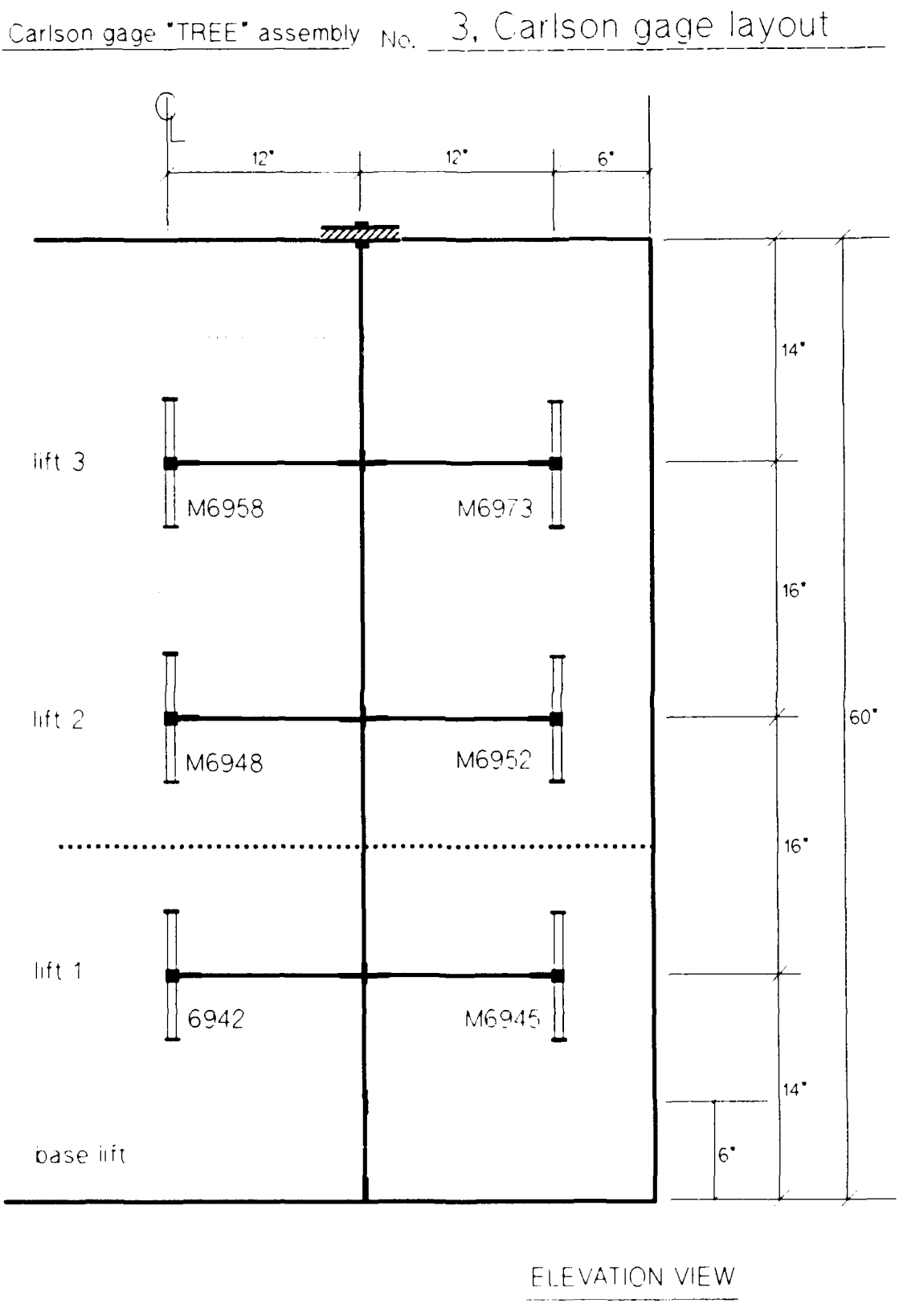

Figure 13. Layout drawing showing location of strain meters

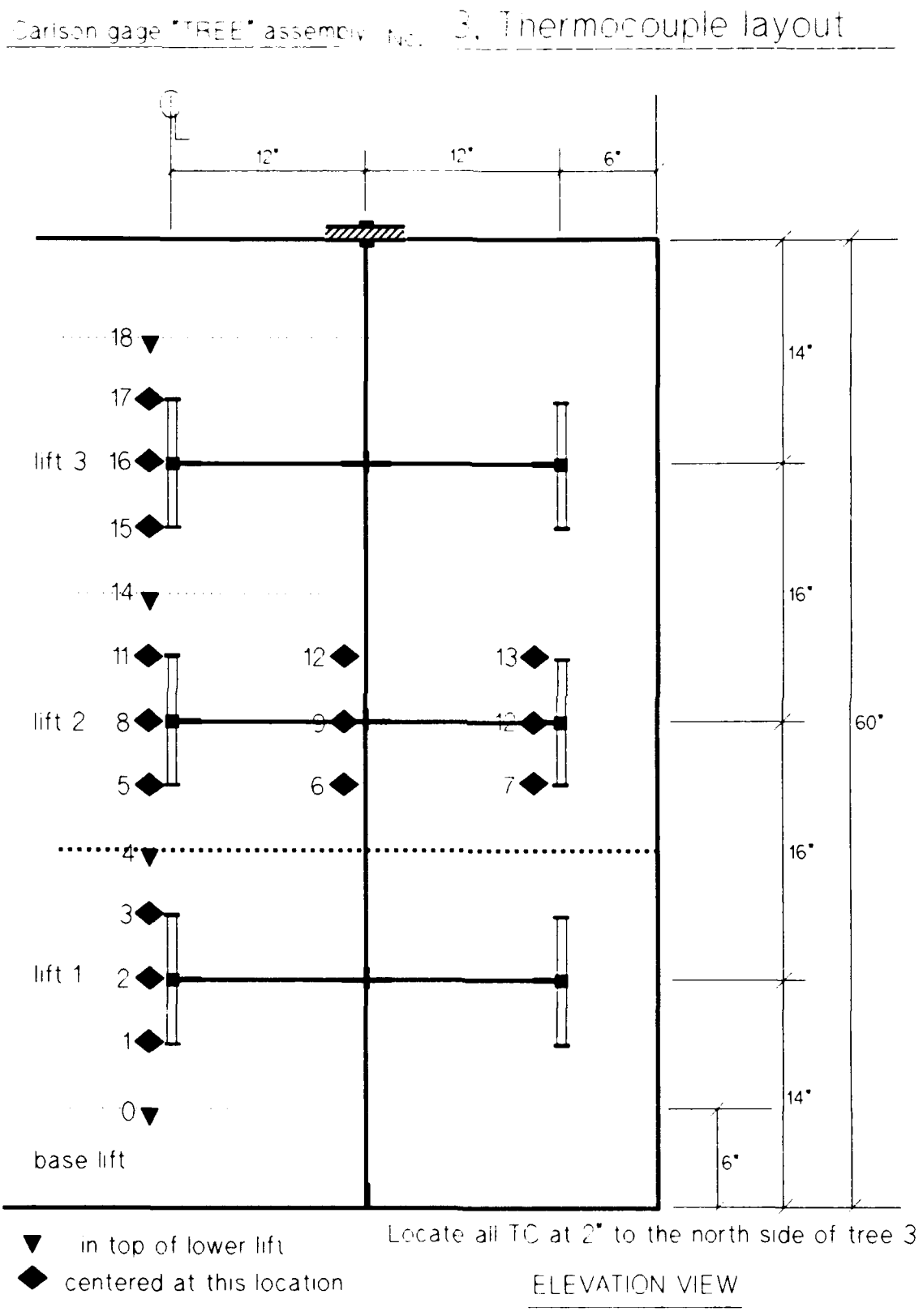

Figure 14. Layout drawing showing location of thermocouples

Figure 15. Photograph of discharging grout from the batch plant and pug mill

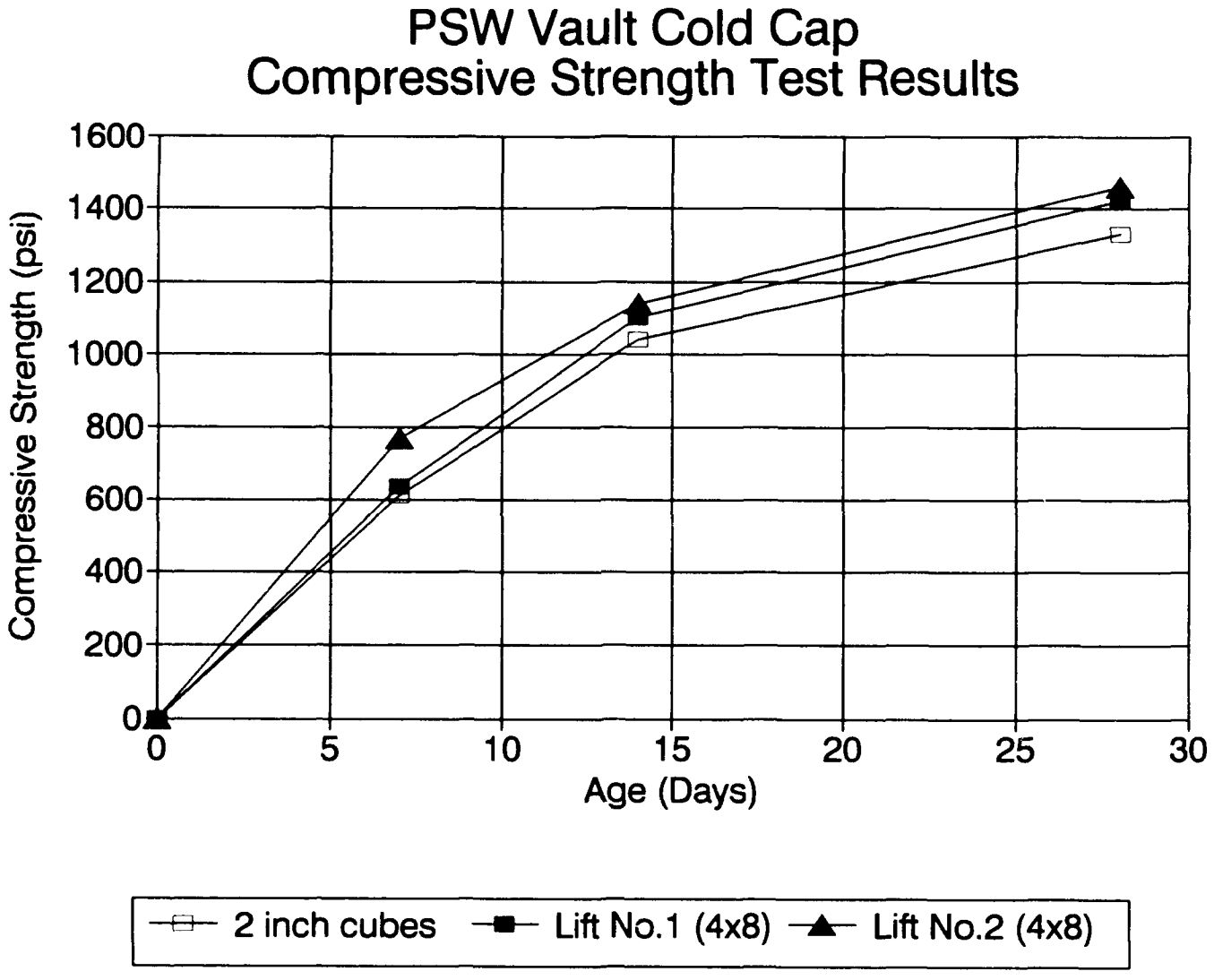

Figure 16. Compressive strength from lifts in physical model

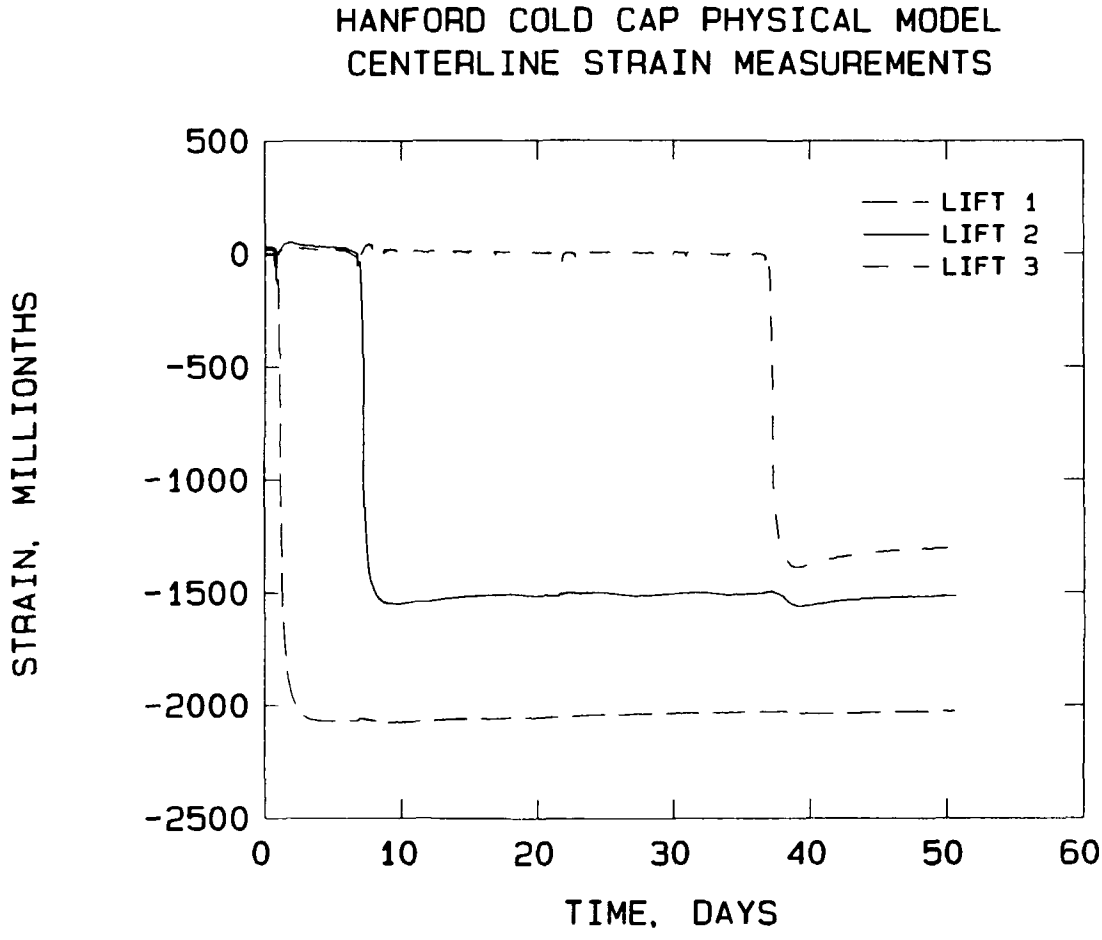

Figure 17. Centerline strain measurements plotted vs time

Figure 18. Photograph of the surface of lift 1 at 6 days of age, showing cracks

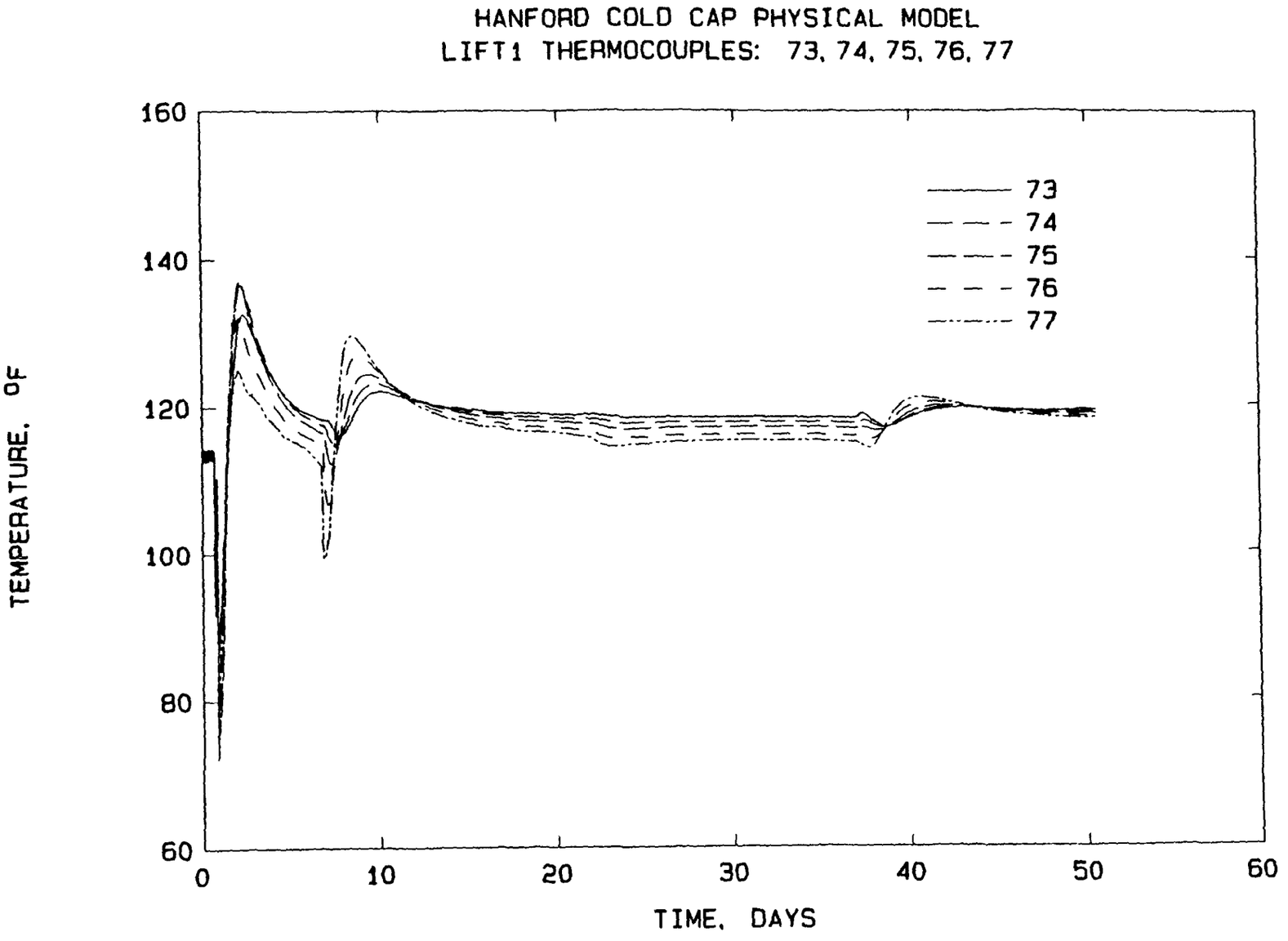

Figure 19. Temperature vs time measured in lift 1 at the centerline

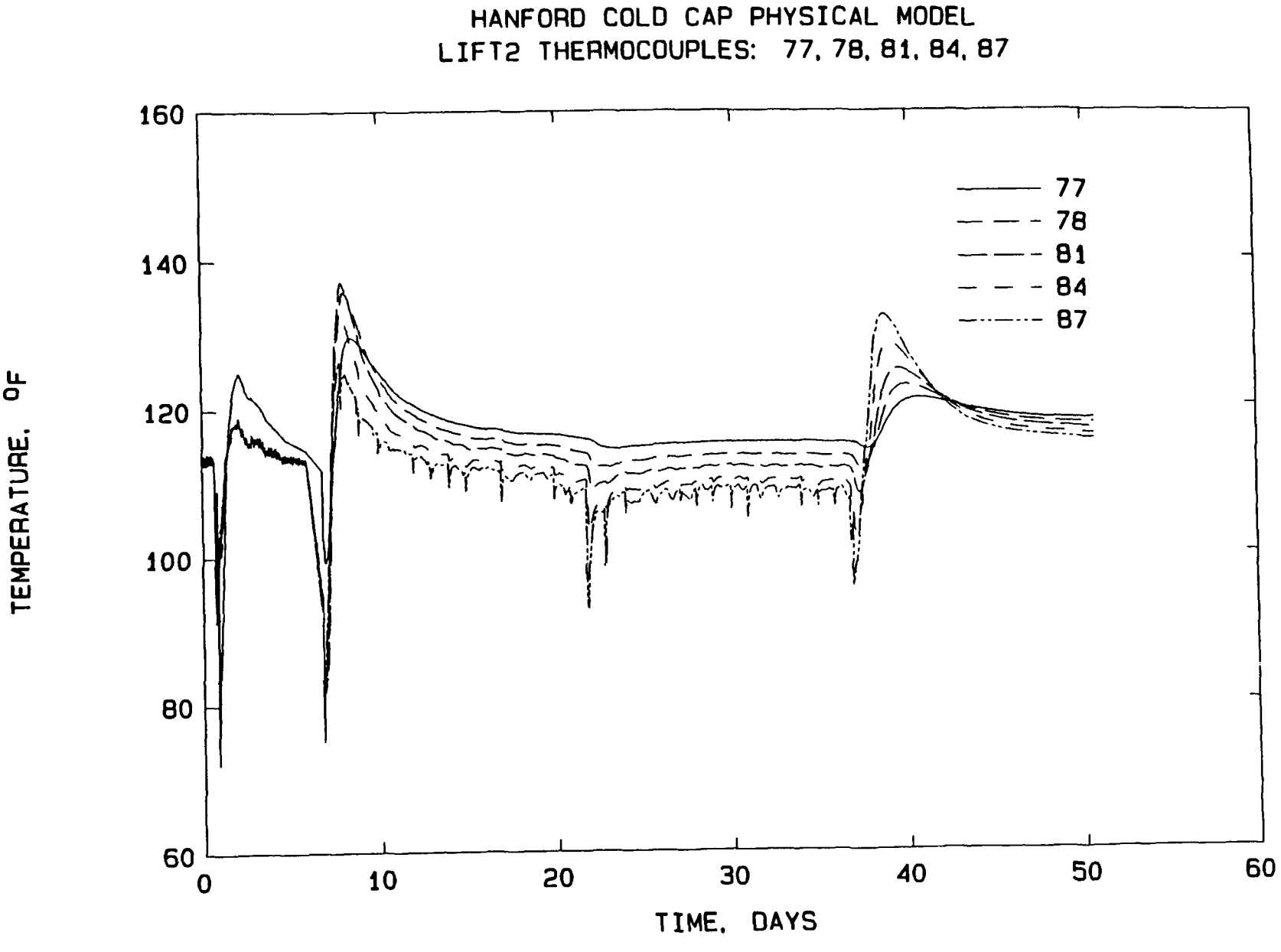

Figure 20. Temperature vs time measured in lift 2 at the centerline

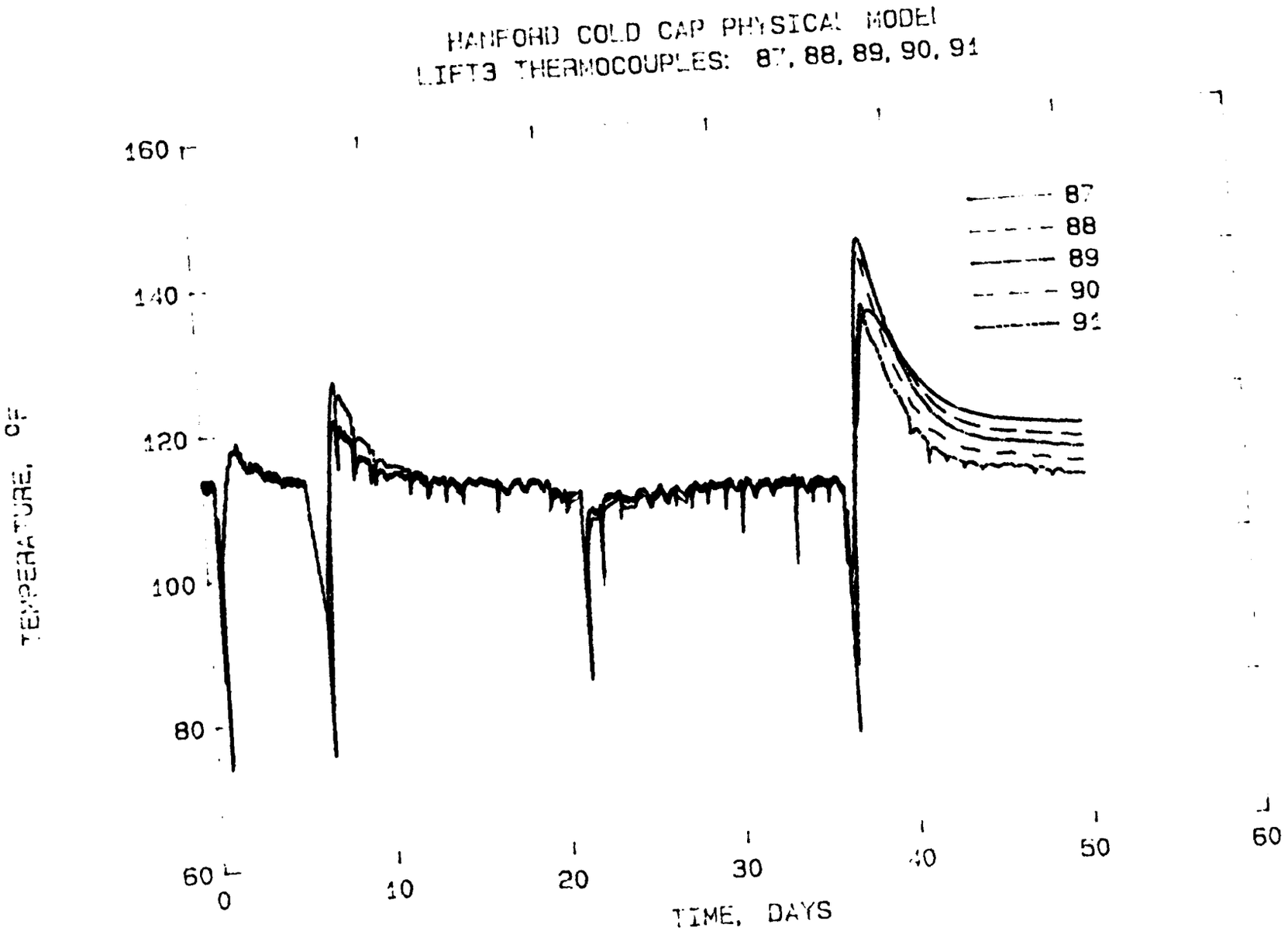

Figure 21. Temperature vs time measured in lift 3 at the centerline

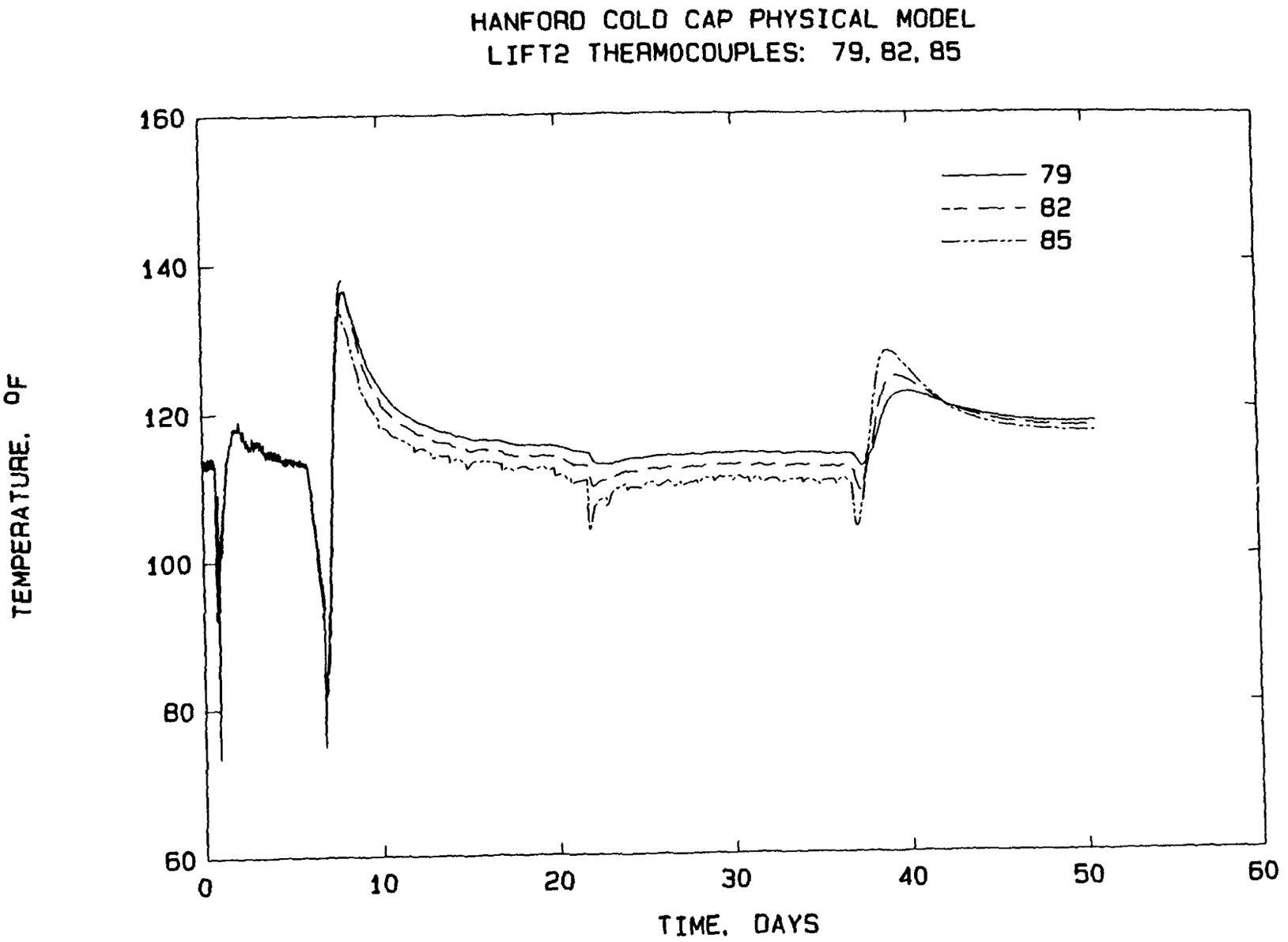

Figure 22. Temperature vs time measured in lift 2 at the 18 inches from outside wall

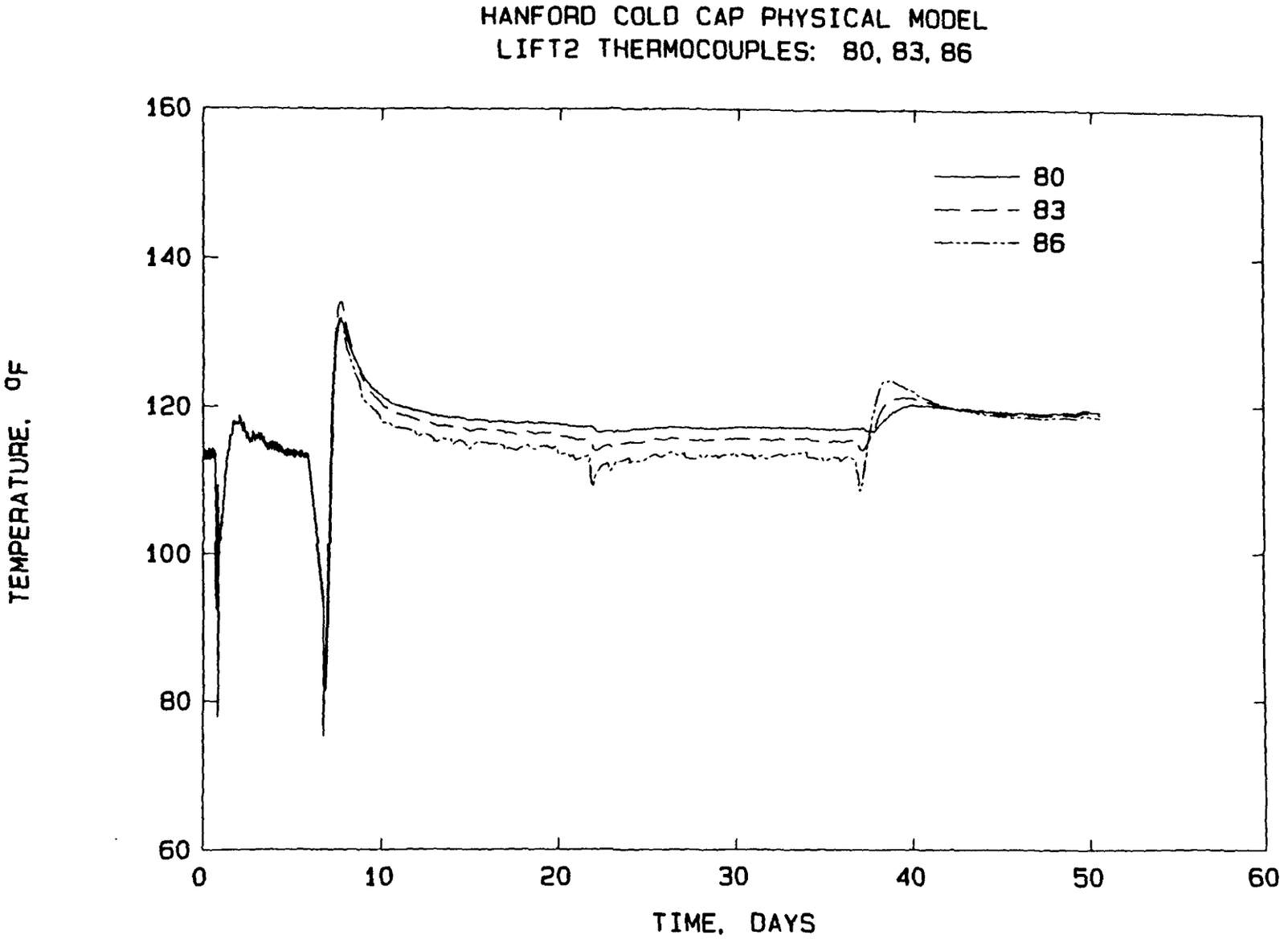

Figure 23. Temperature vs time measured in lift 2 at the 6 inches from outside wall

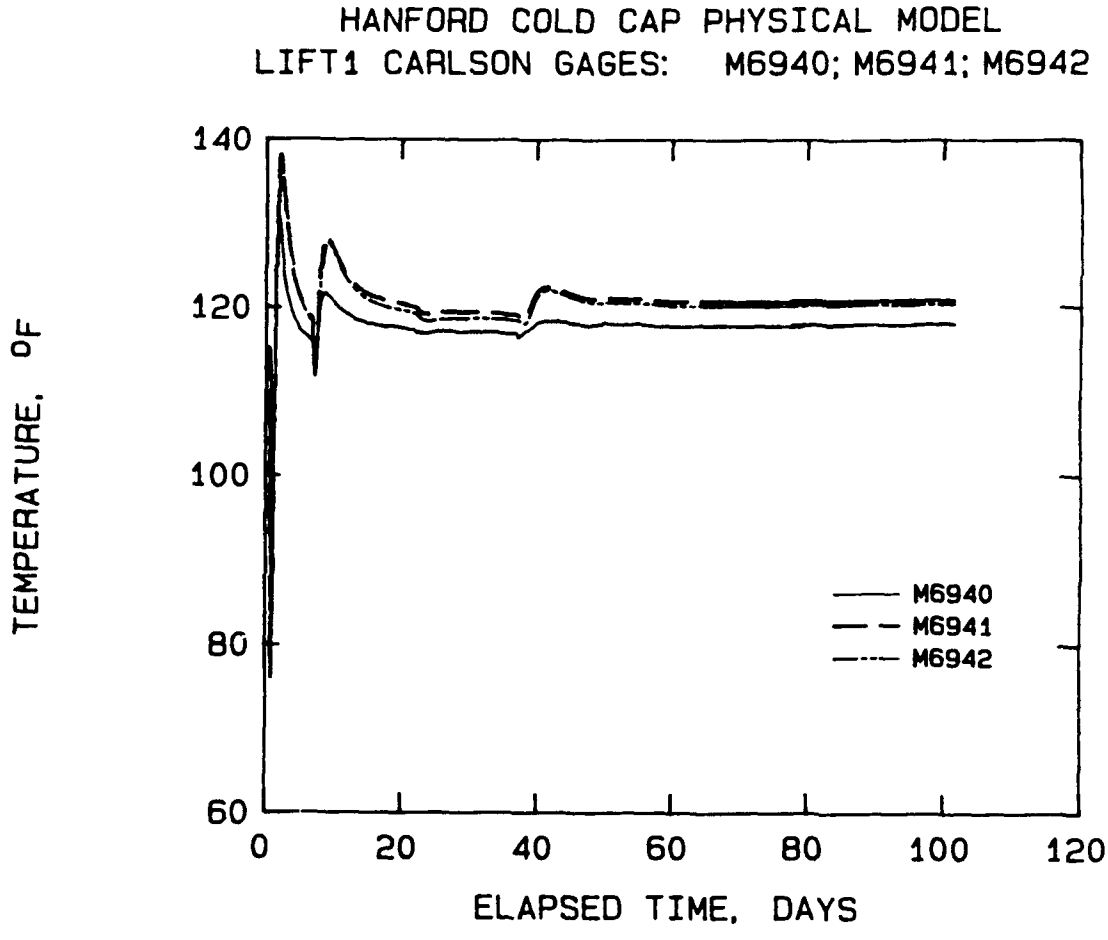

Figure 24. Plot of temperature vs time recorded by strain meters during grouting of lifts in the physical model

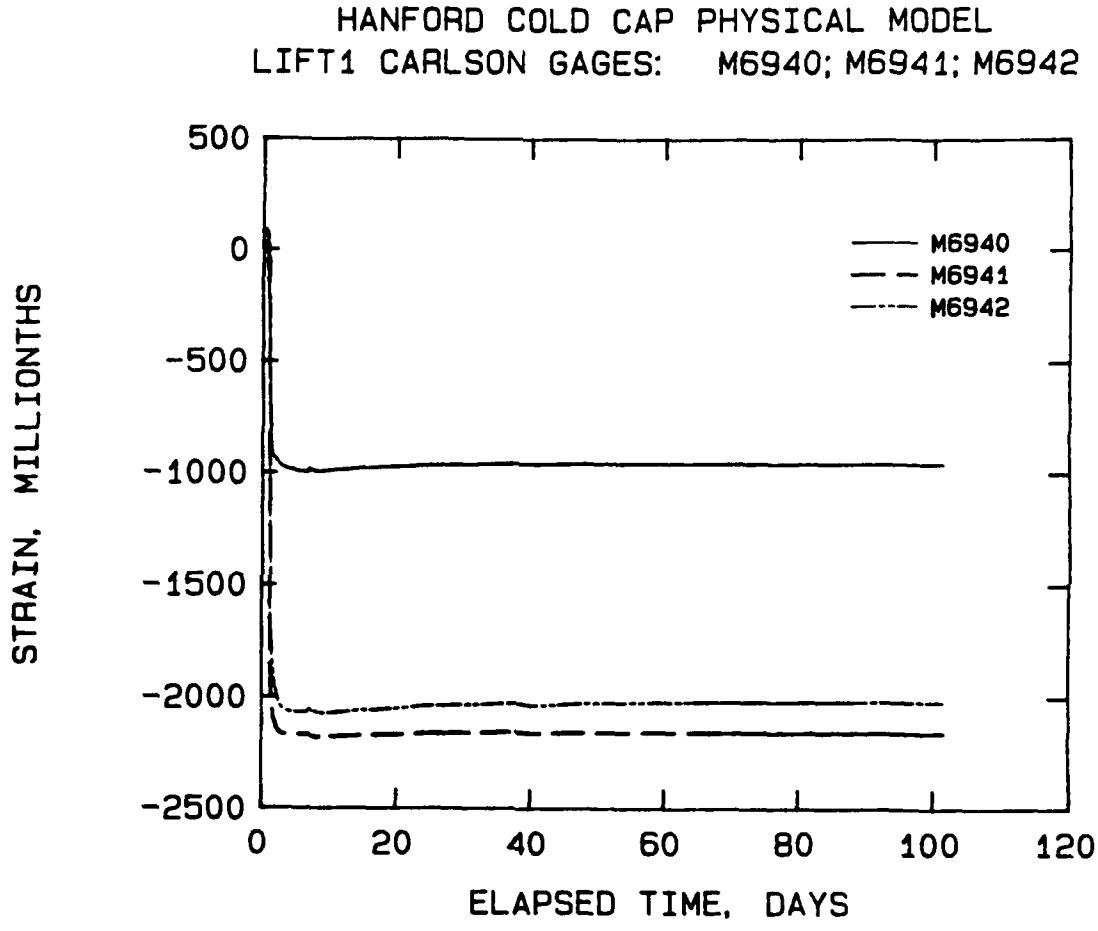

Figure 25. Plot of strain vs time recorded by strain meters during grouting of lifts in the physical model

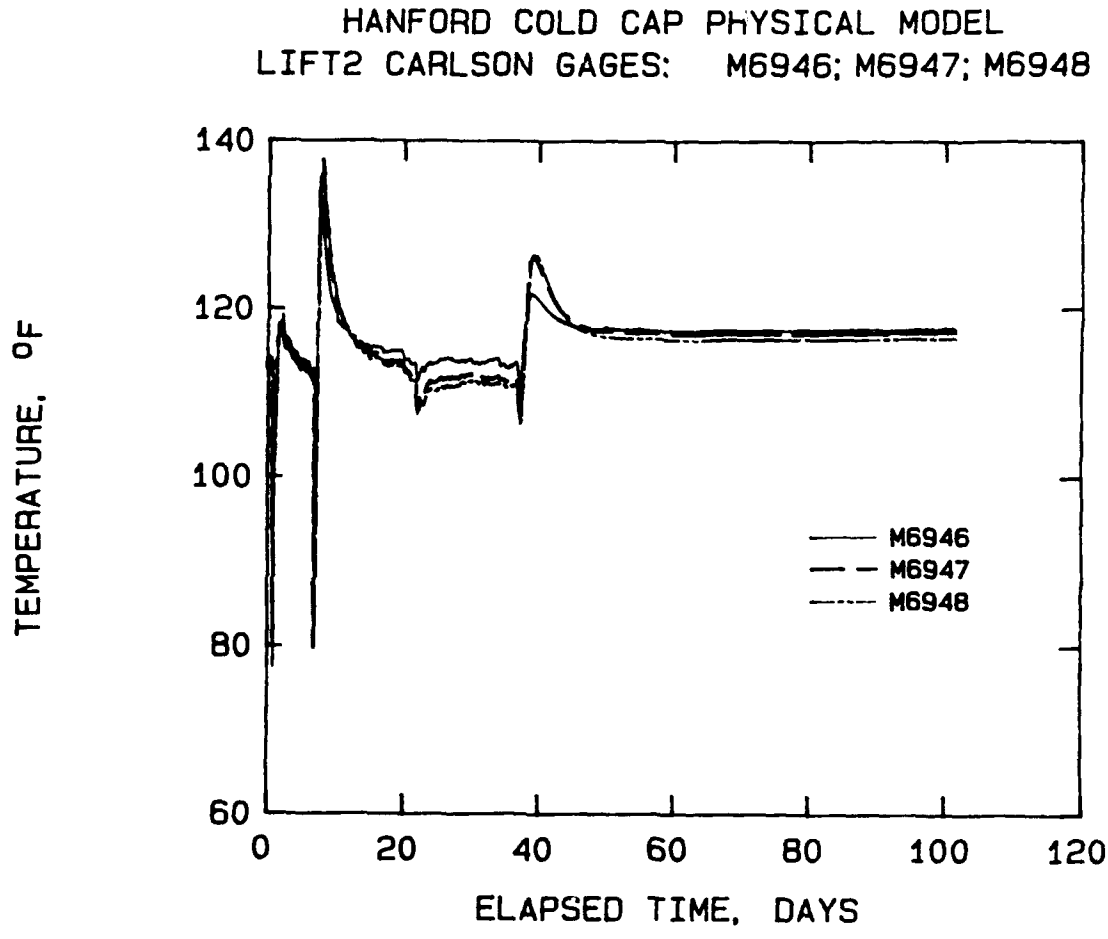

Figure 26. Plot of temperature vs time recorded by strain meters during grouting of lifts in the physical model

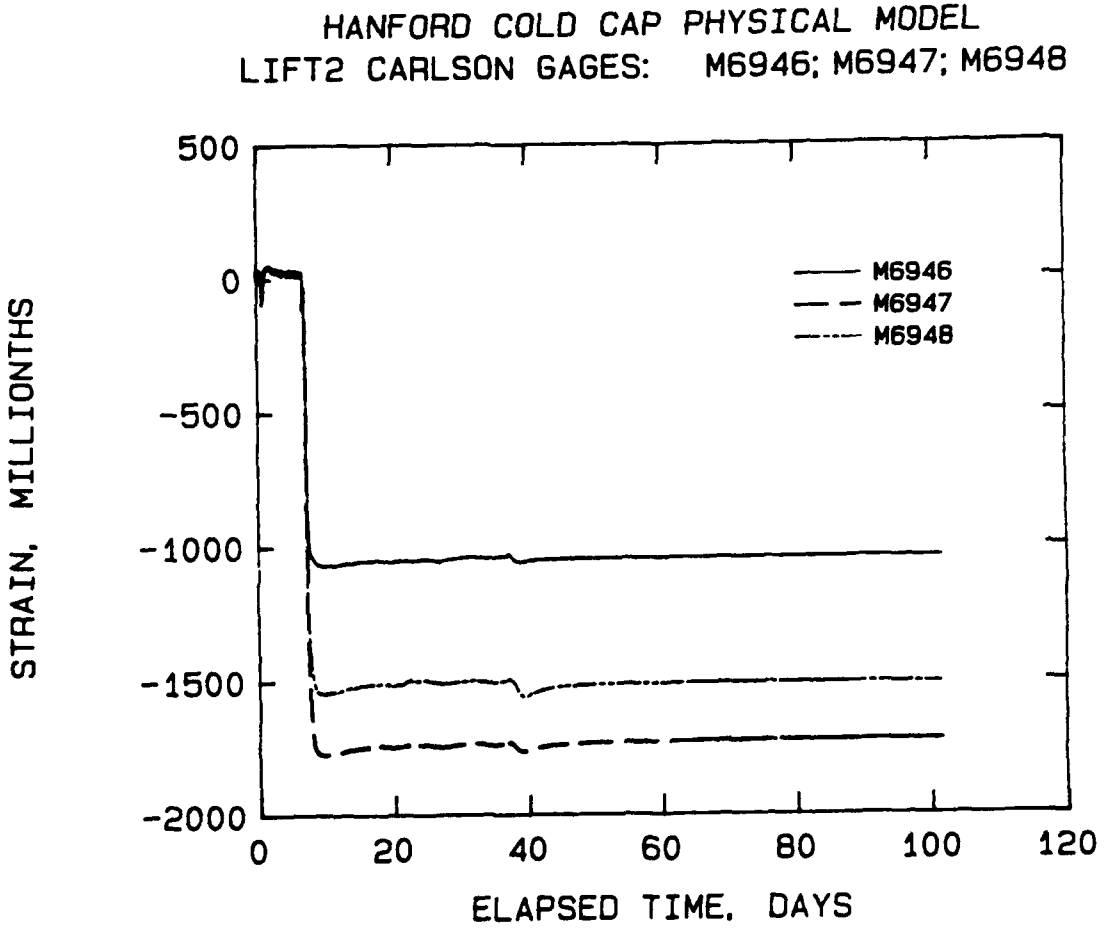

Figure 27. Plot of strain vs time recorded by strain meters during grouting of lifts in the physical model

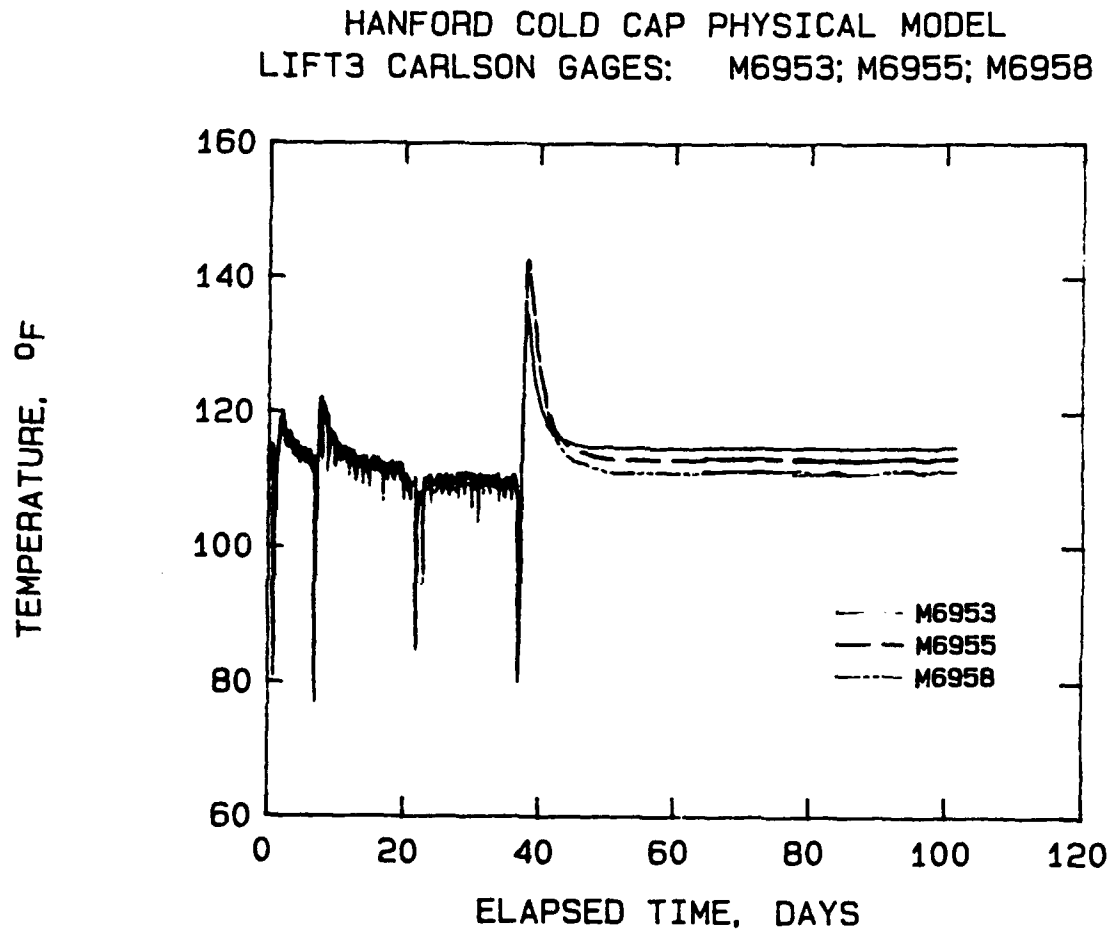

Figure 28. Plot of temperature vs time recorded by strain meters during grouting of lifts in the physical model

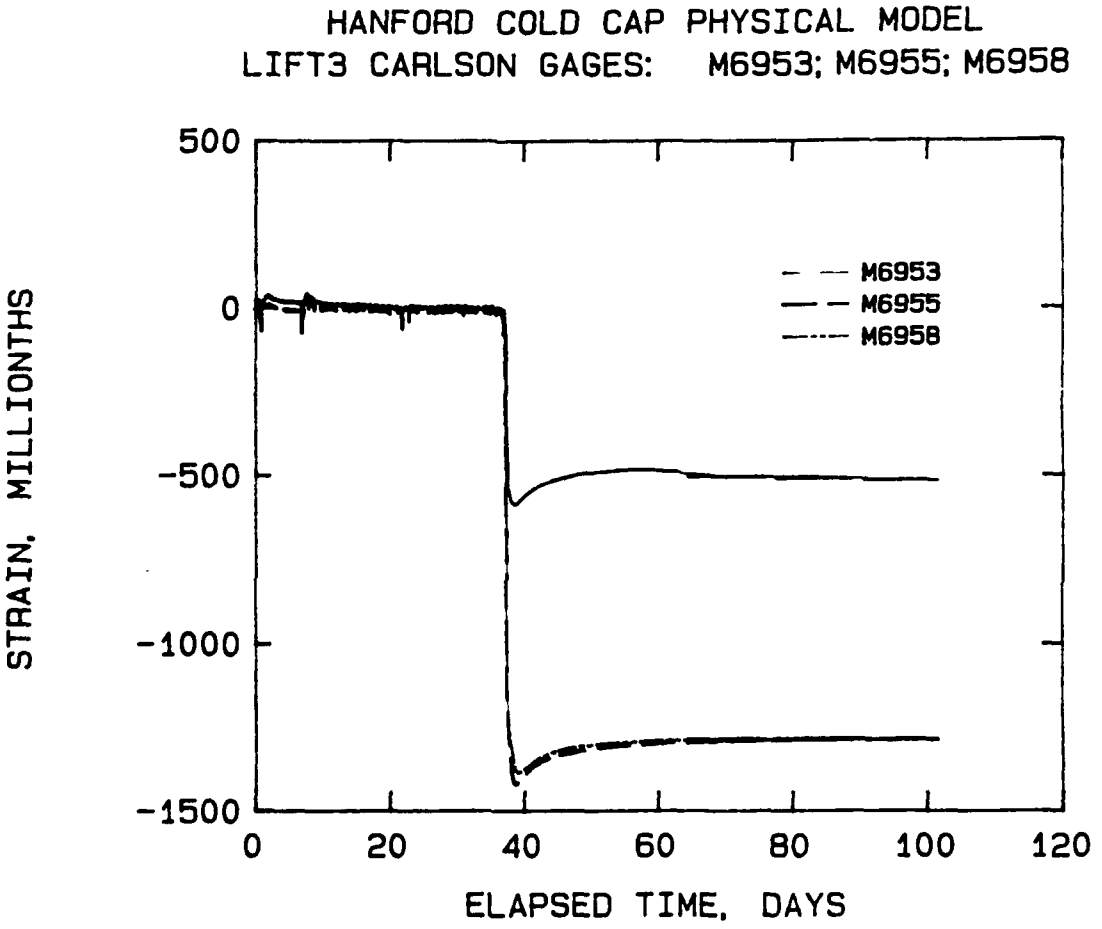

Figure 29. Plot of strain vs time recorded by strain meters during grouting of lifts in the physical model

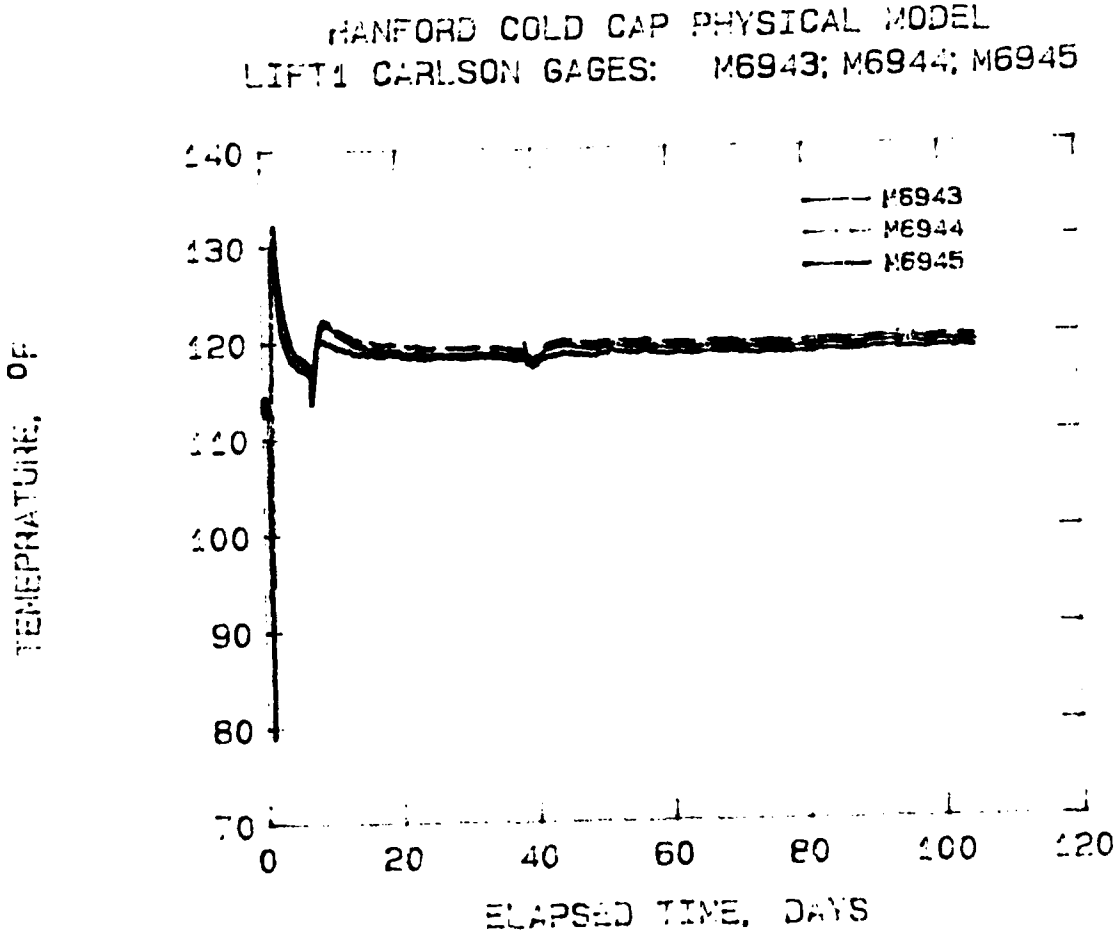

Figure 30. Plot of temperature vs time recorded by strain meters during grouting of lifts in the physical model

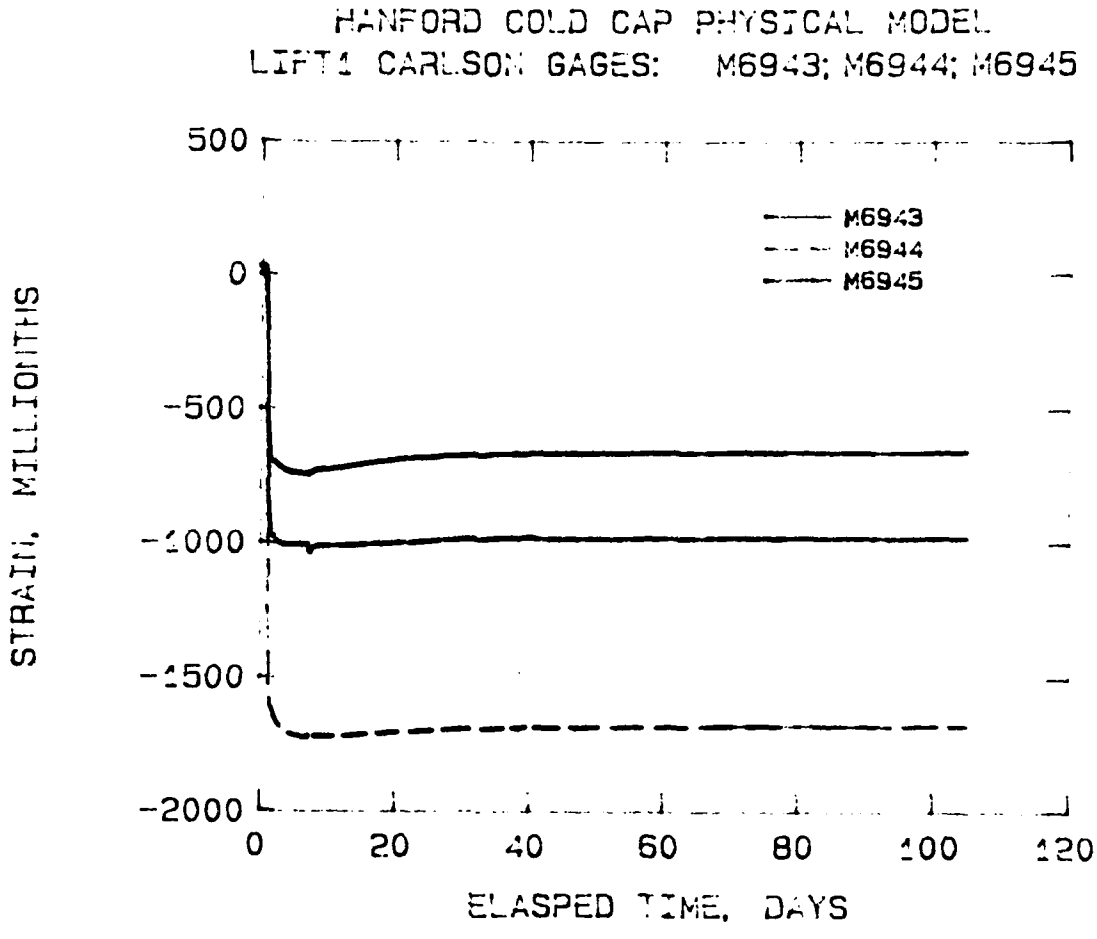

Figure 31. Plot of strain vs time recorded by strain meters during grouting of lifts in the physical model

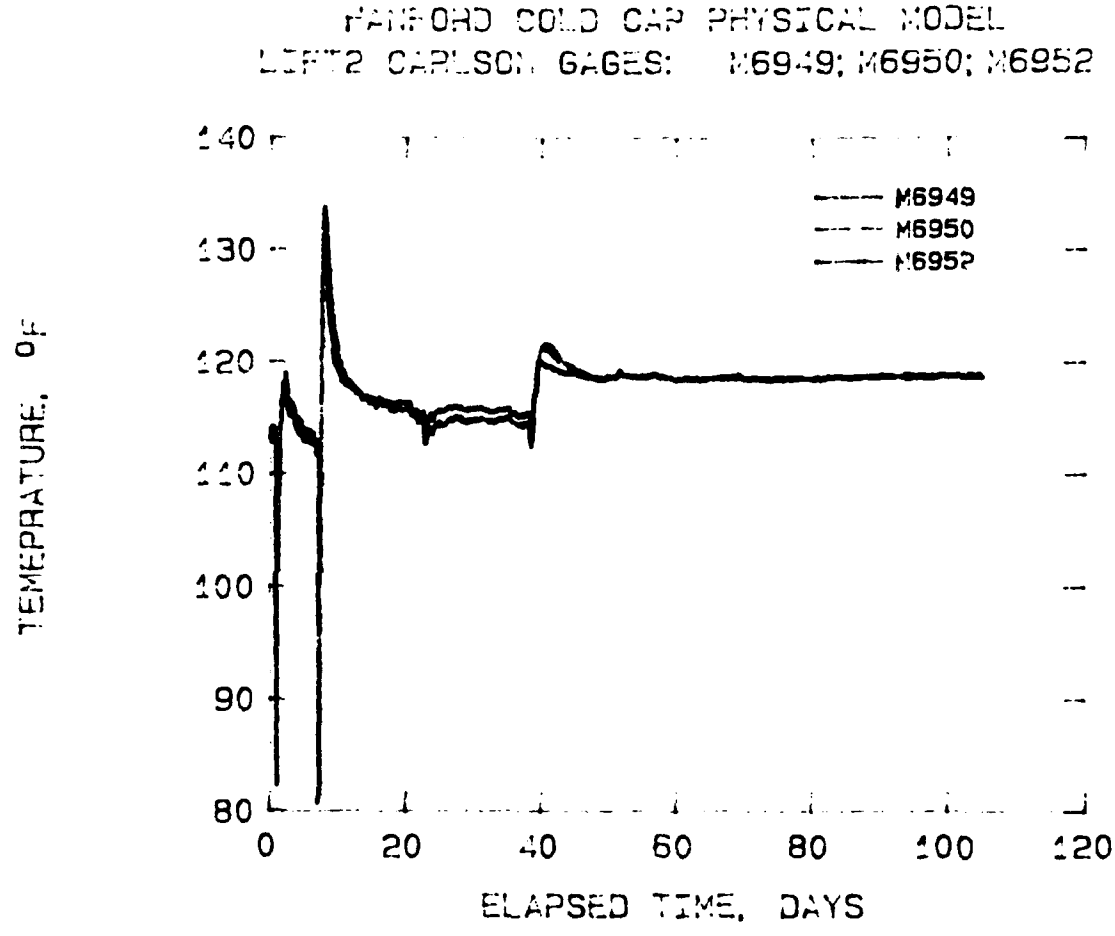

Figure 32. Plot of temperature vs time recorded by strain meters during grouting of lifts in the physical model

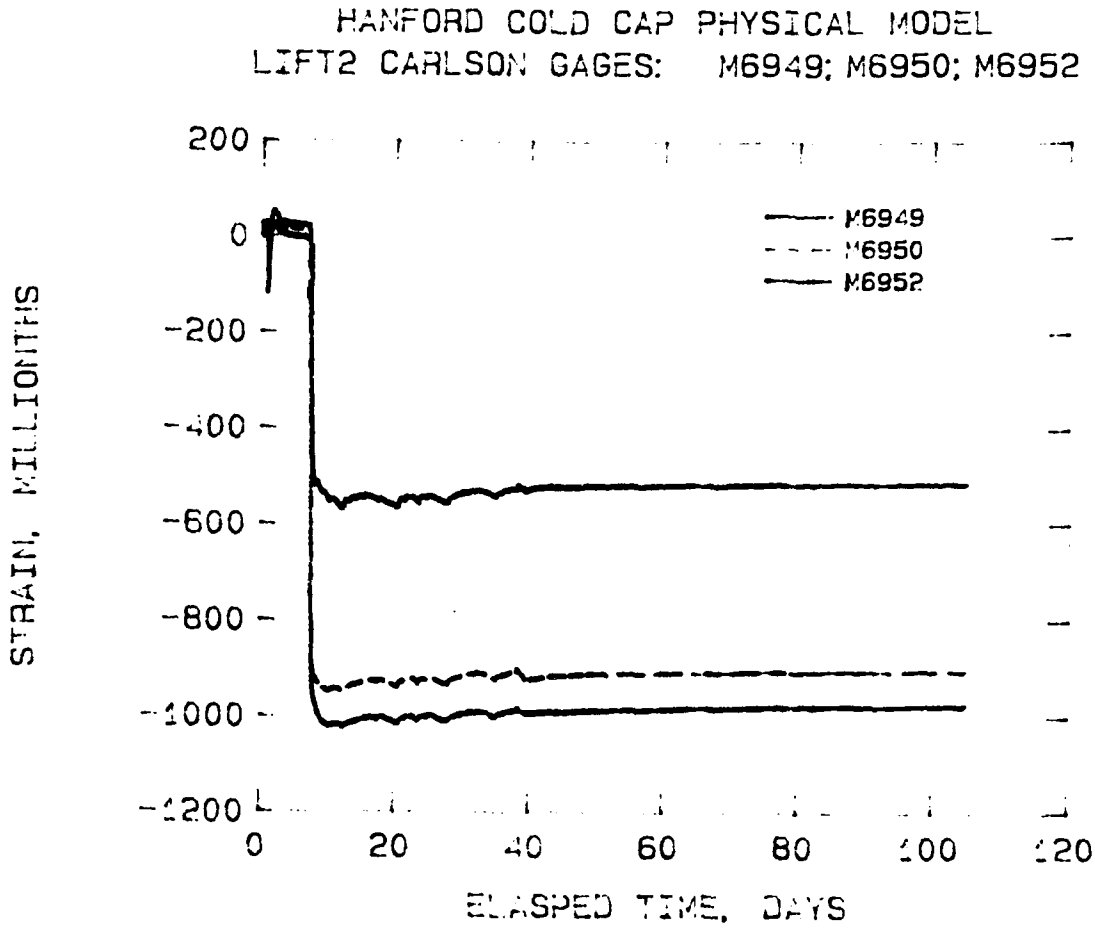

Figure 33. Plot of strain vs time recorded by strain meters during grouting of lifts in the physical model

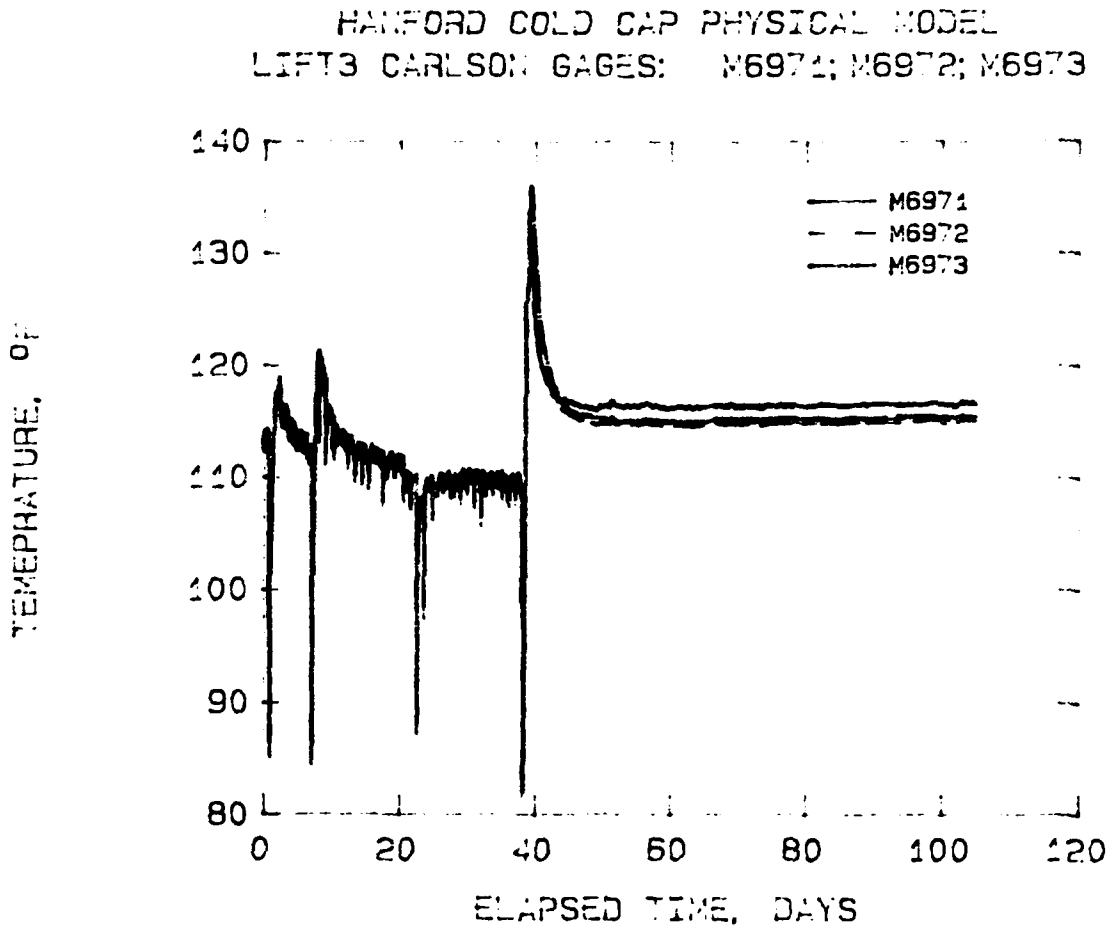

Figure 34. Plot of temperature vs time recorded by strain meters during grouting of lifts in the physical model

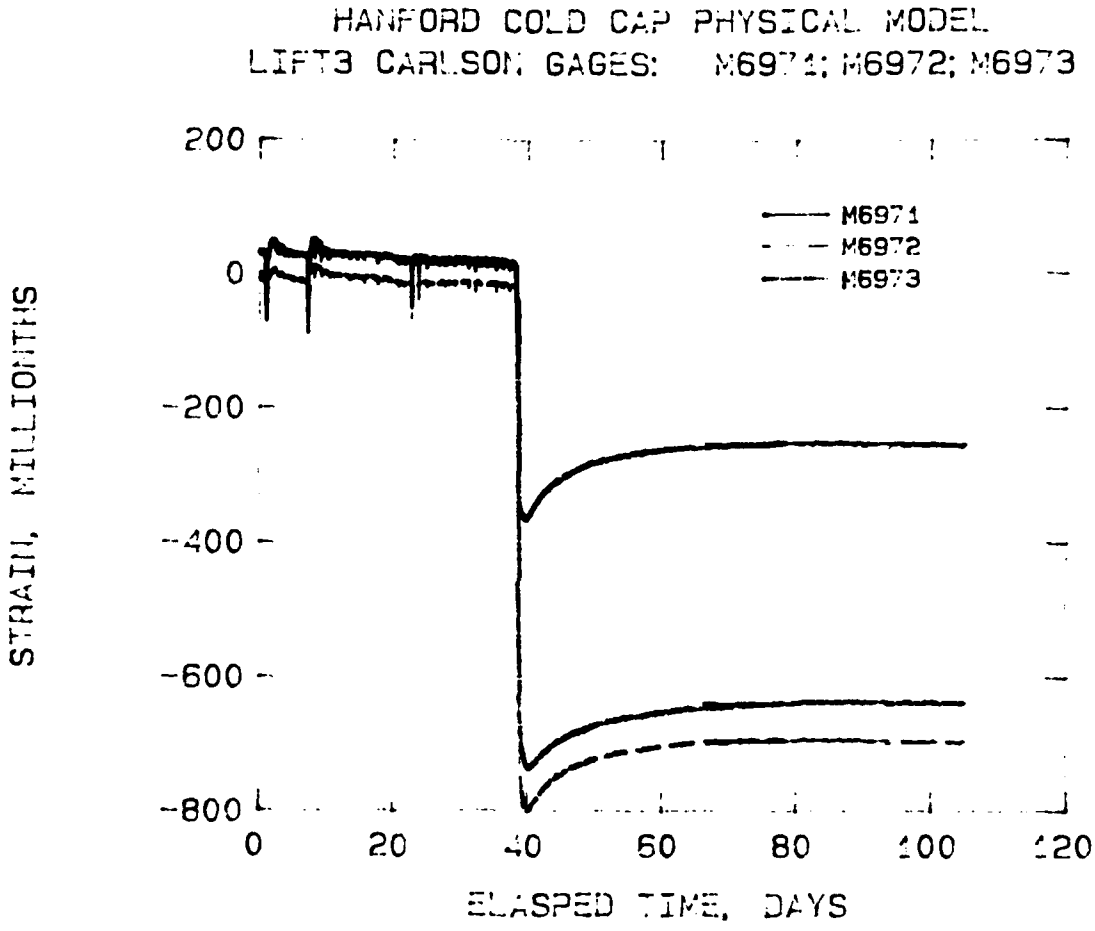

Figure 35. Plot of strain vs time recorded by strain meters during grouting of lifts in the physical model

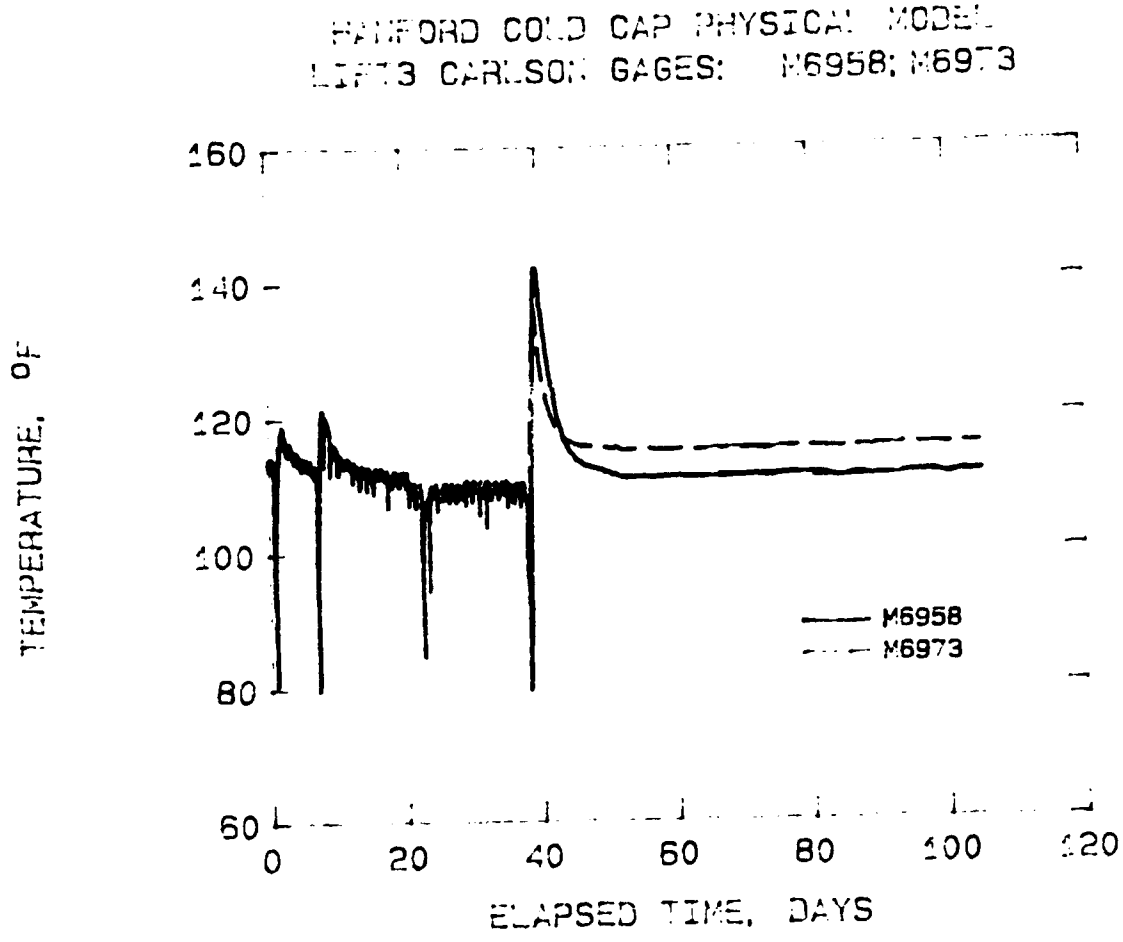

Figure 36. Plot of temperature vs time recorded by strain meters during grouting of lifts in the physical model

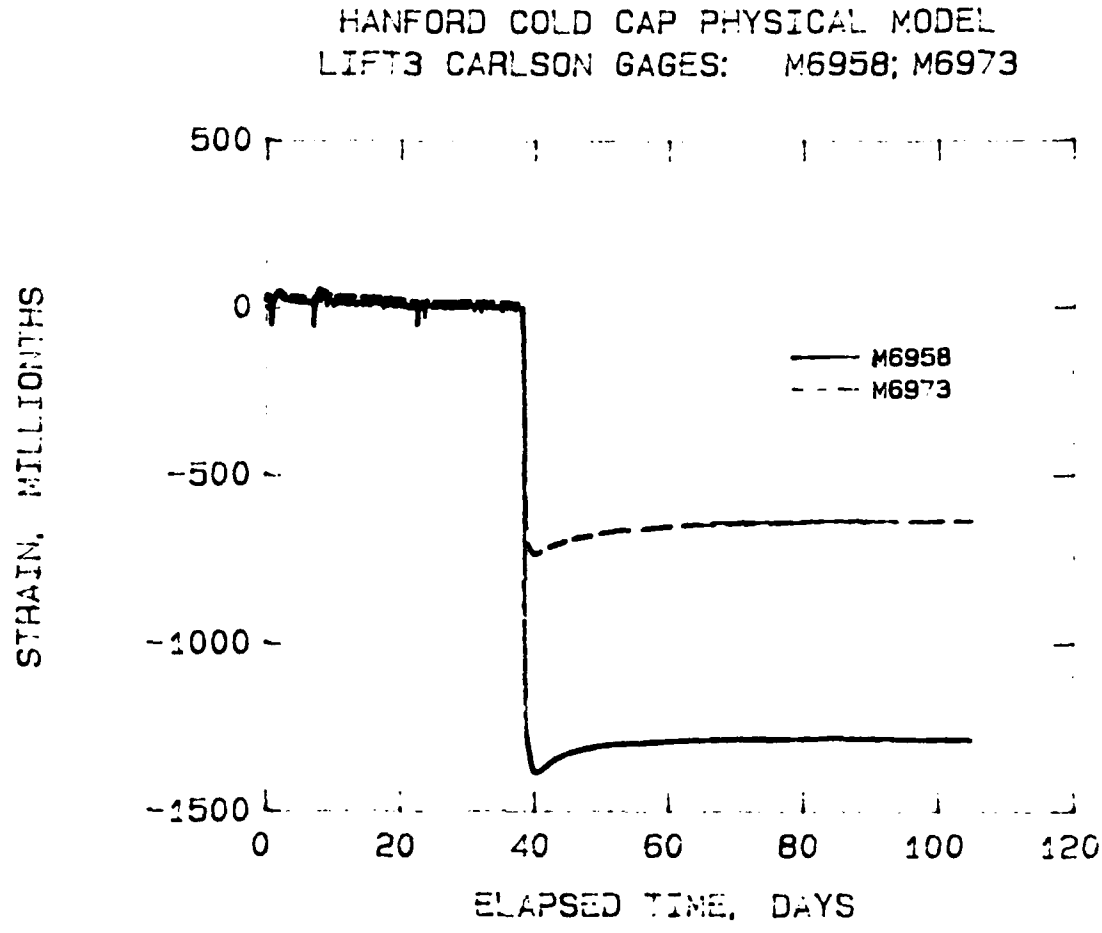

Figure 37. Plot of strain vs time recorded by strain meters during grouting of lifts in the physical model

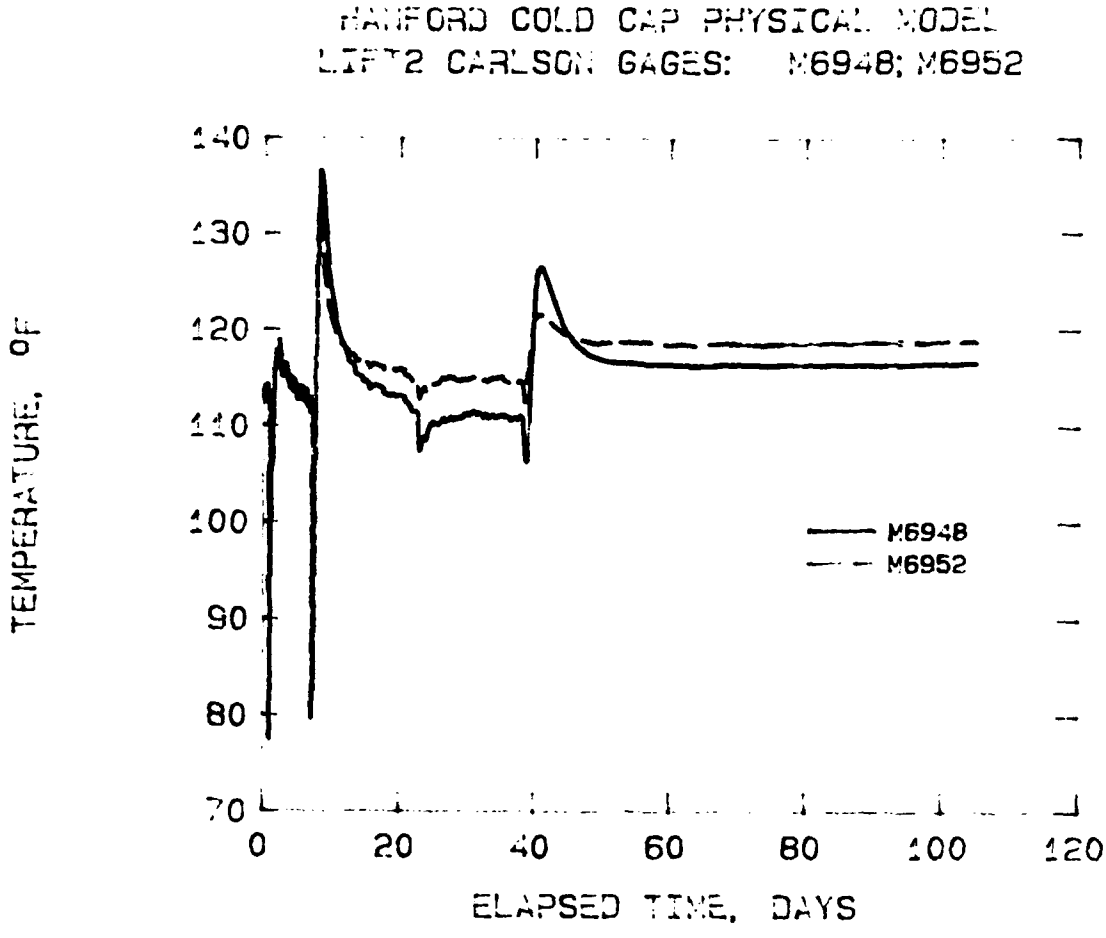

Figure 38. Plot of temperature vs time recorded by strain meters during grouting of lifts in the physical model

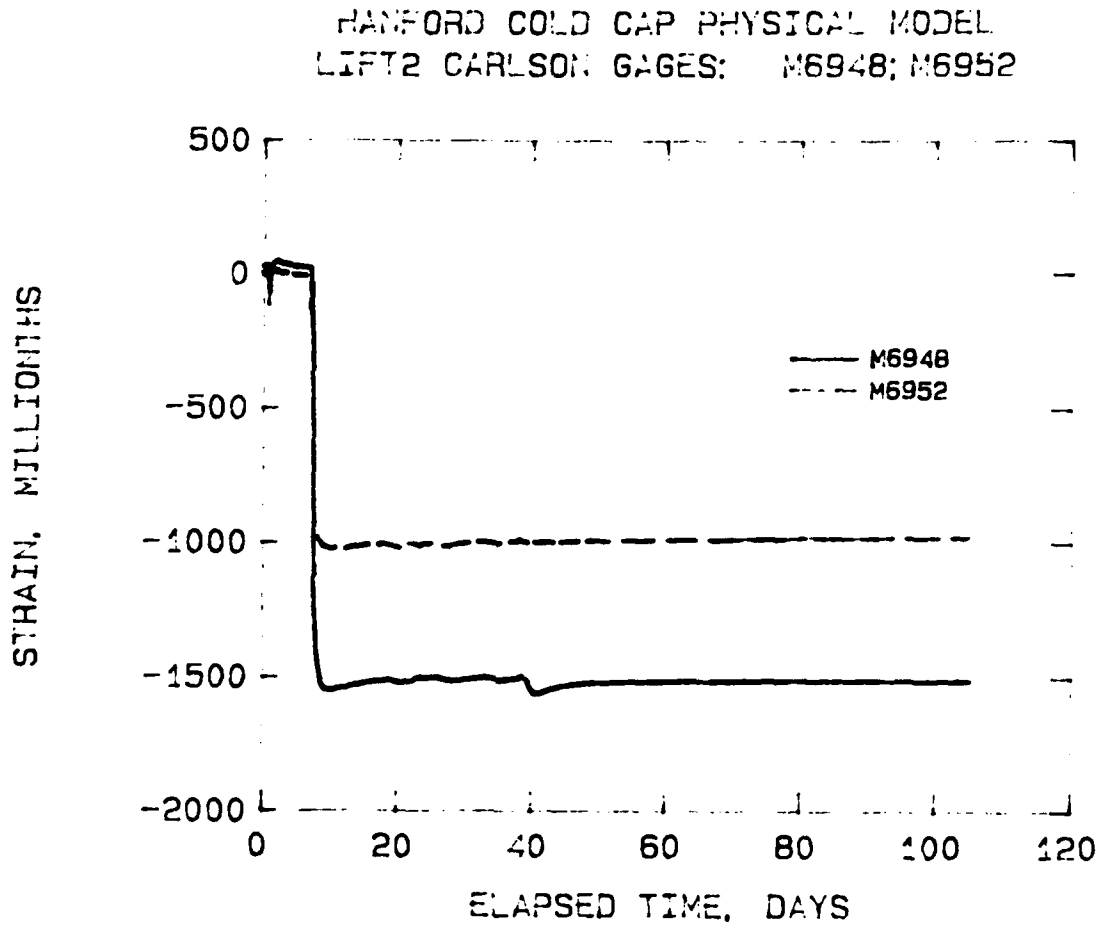

Figure 39. Plot of strain vs time recorded by strain meters during grouting of lifts in the physical model

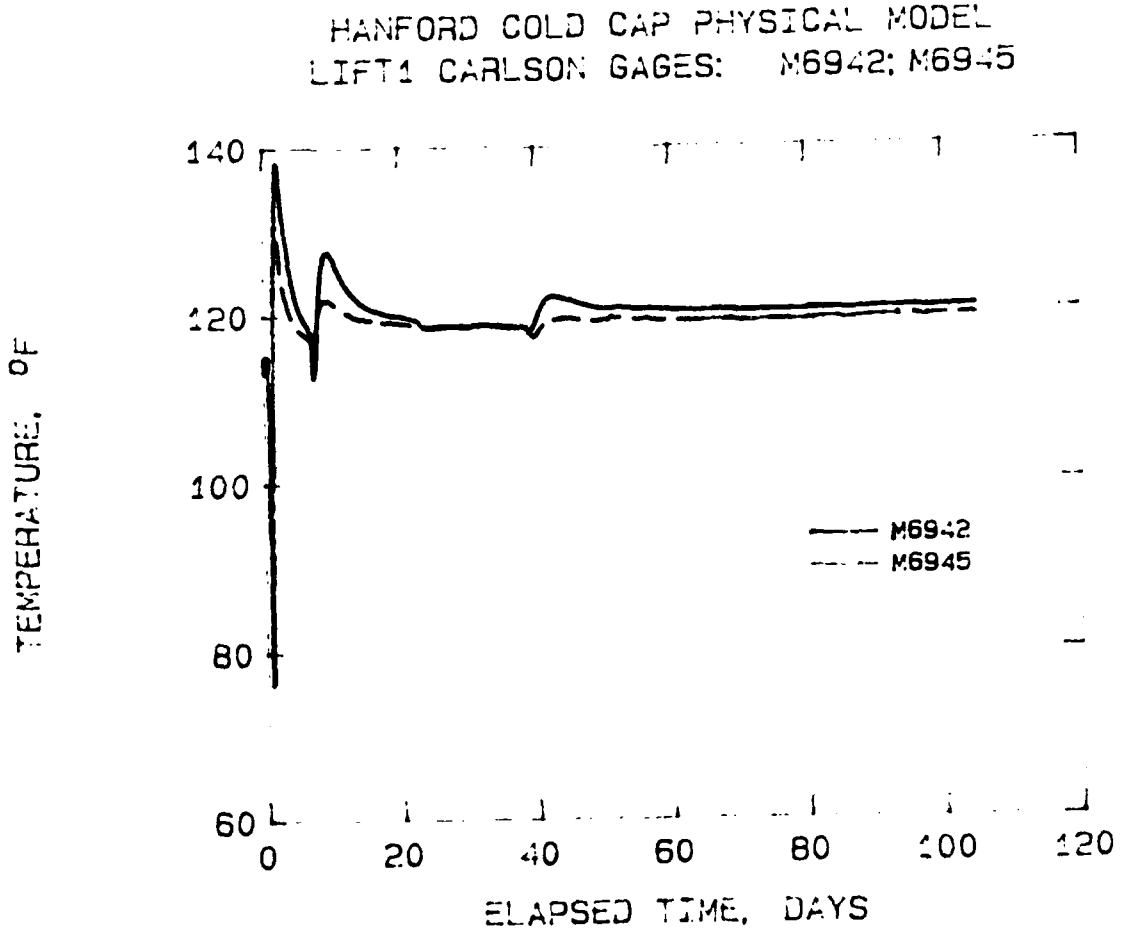

Figure 40. Plot of temperature vs time recorded by strain meters during grouting of lifts in the physical model

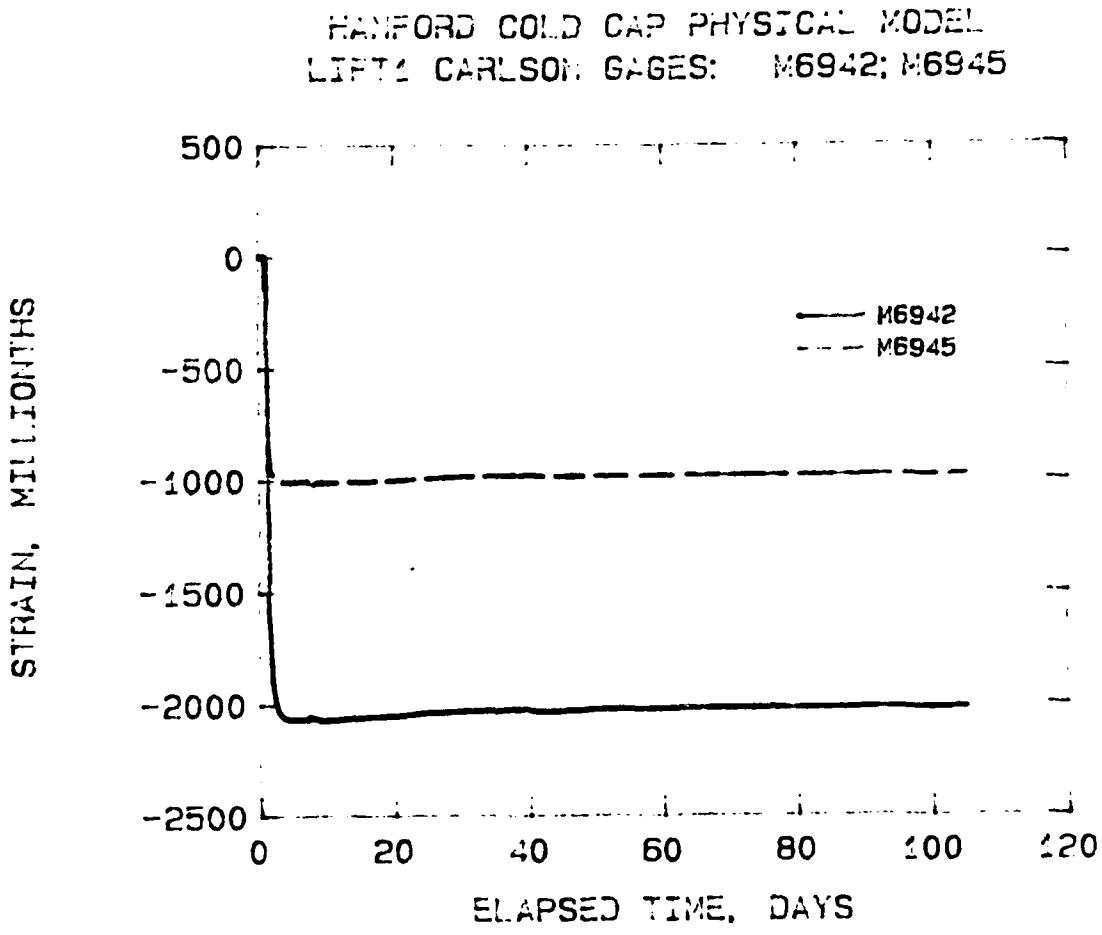

Figure 41. Plot of strain vs time recorded by strain meters during grouting of lifts in the physical model

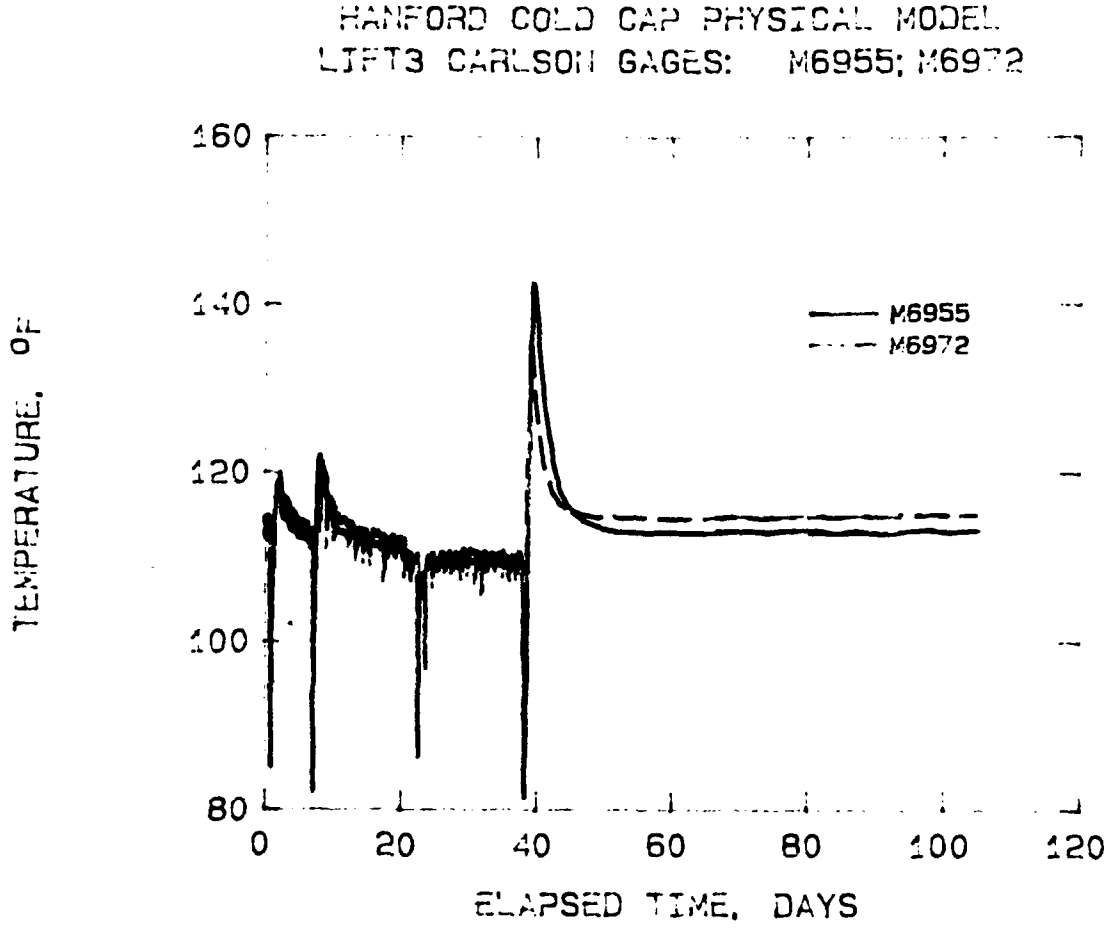

Figure 42. Plot of temperature vs time recorded by strain meters during grouting of lifts in the physical model

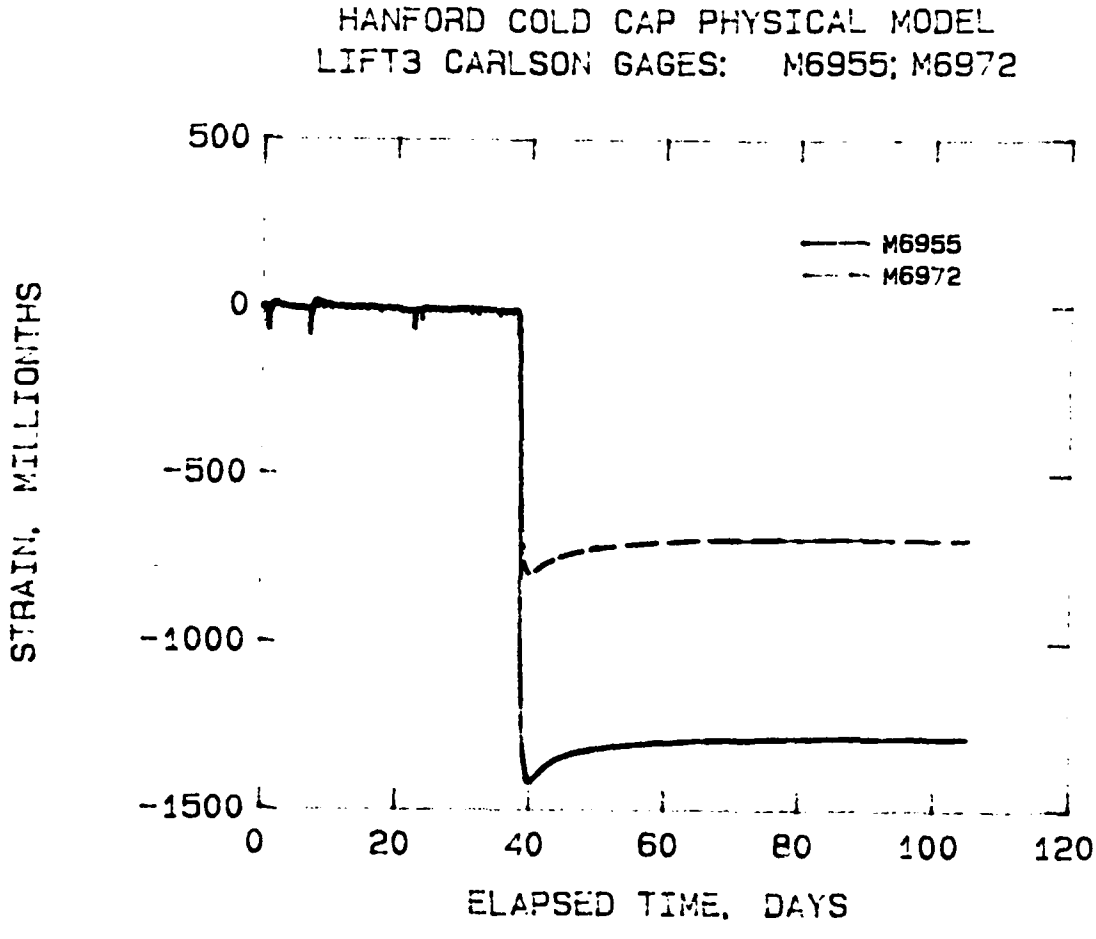

Figure 43. Plot of strain vs time recorded by strain meters during grouting of lifts in the physical model

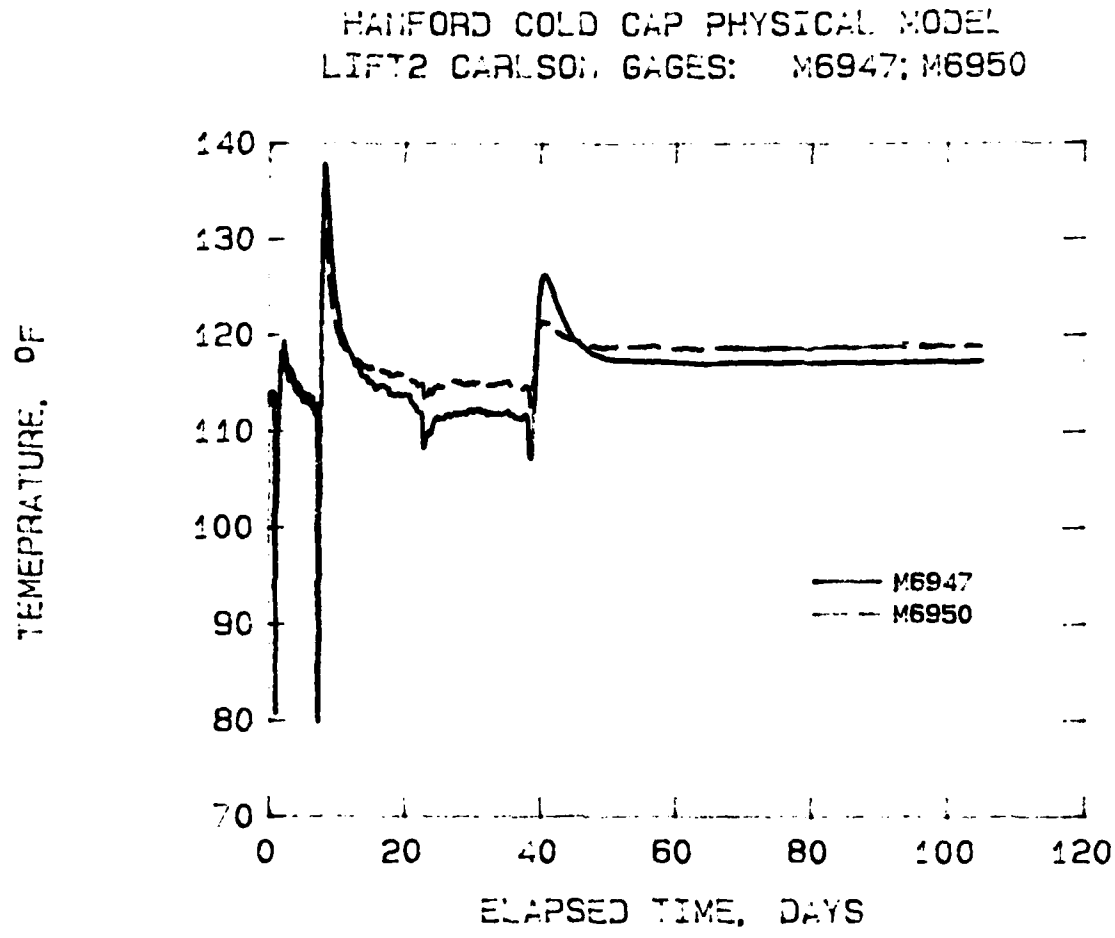

Figure 44. Plot of temperature vs time recorded by strain meters during grouting of lifts in the physical model

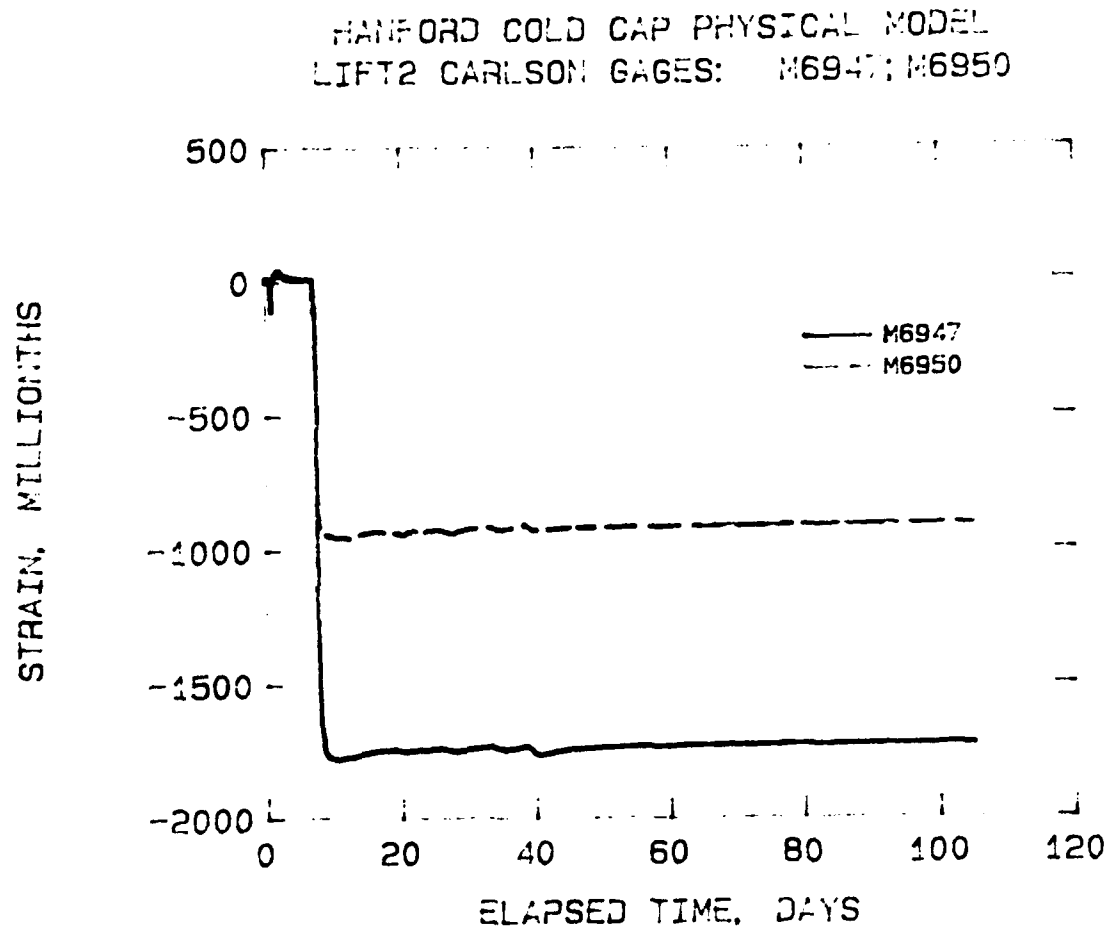

Figure 45. Plot of strain vs time recorded by strain meters during grouting of lifts in the physical model

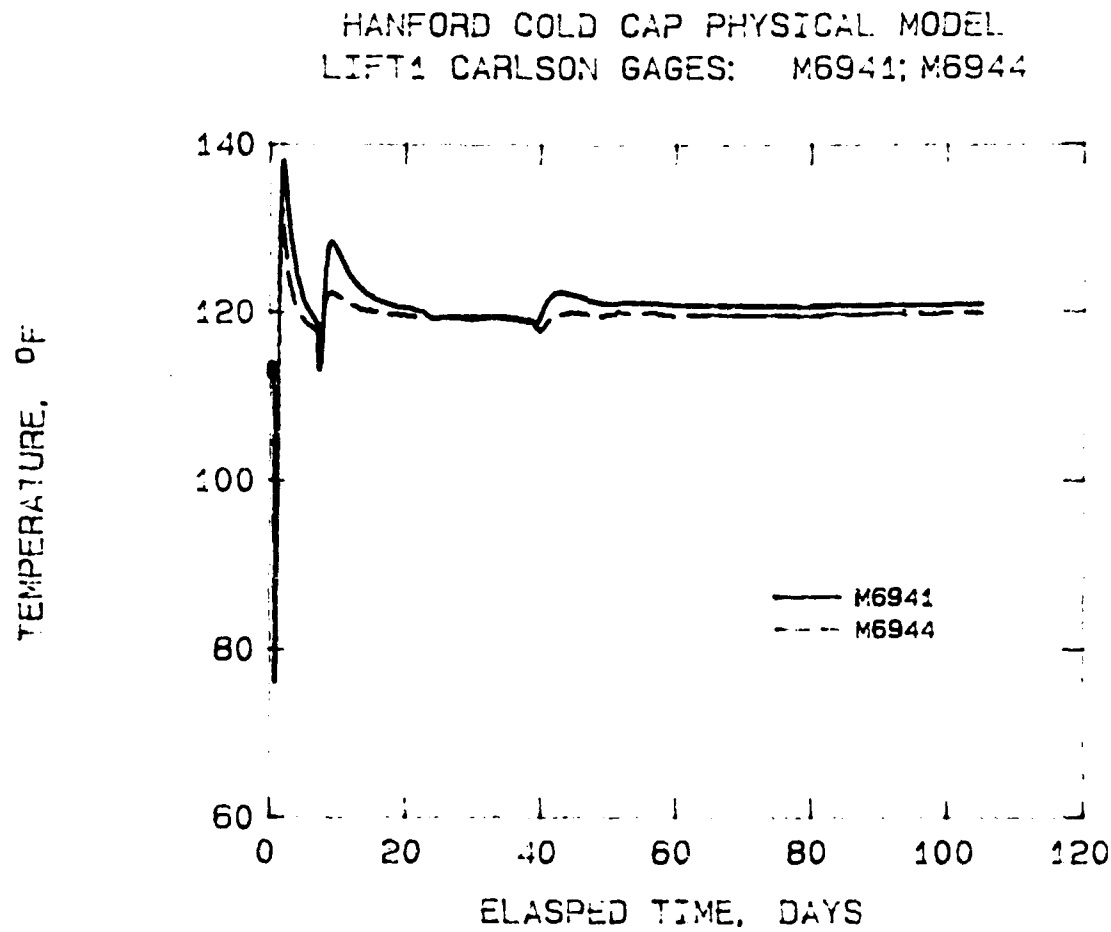

Figure 46. Plot of temperature vs time recorded by strain meters during grouting of lifts in the physical model

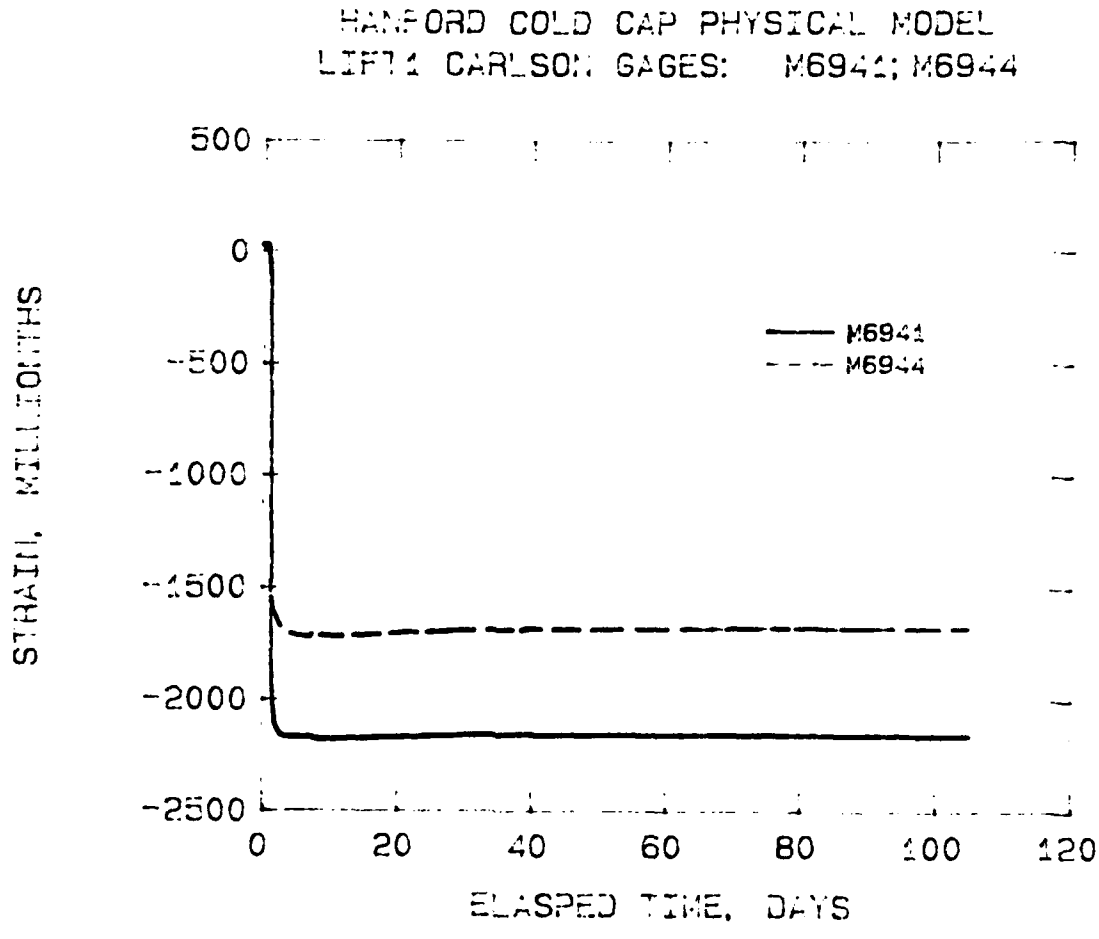

Figure 47. Plot of strain vs time recorded by strain meters during grouting of lifts in the physical model

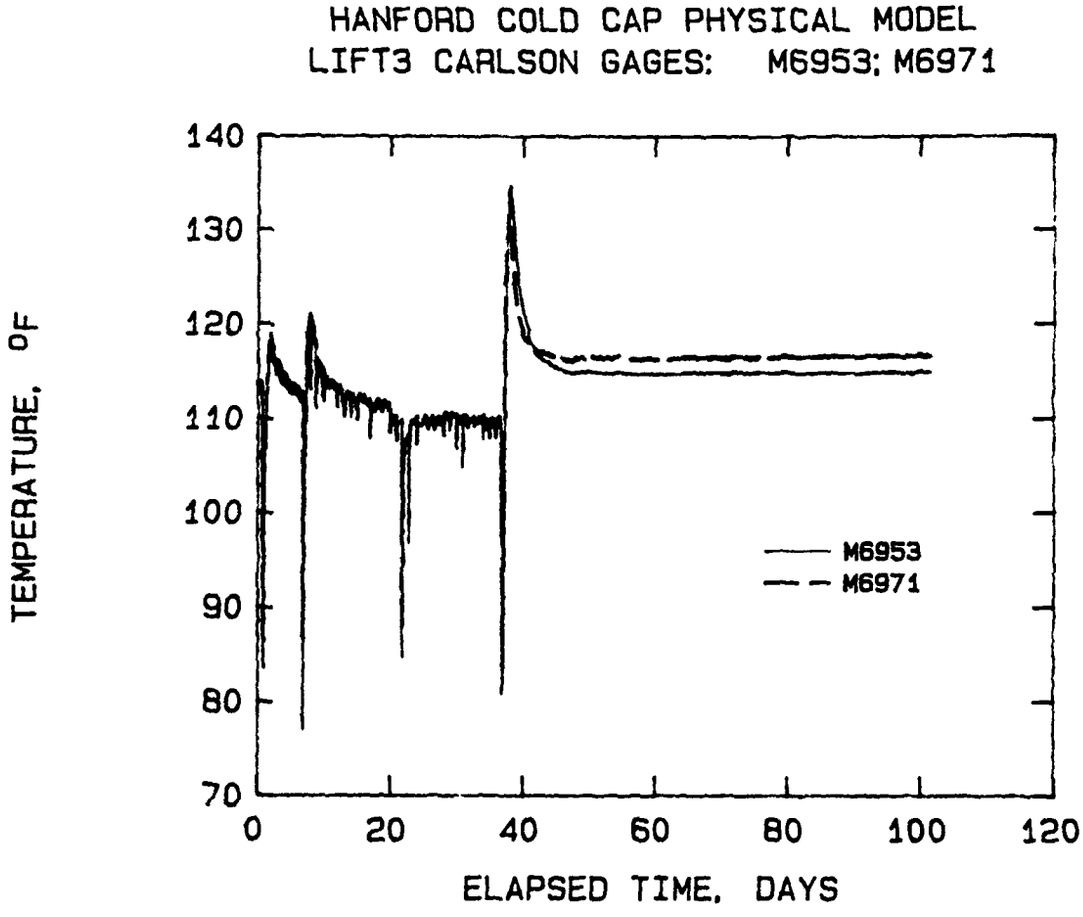

Figure 48. Plot of temperature vs time recorded by strain meters during grouting of lifts in the physical model

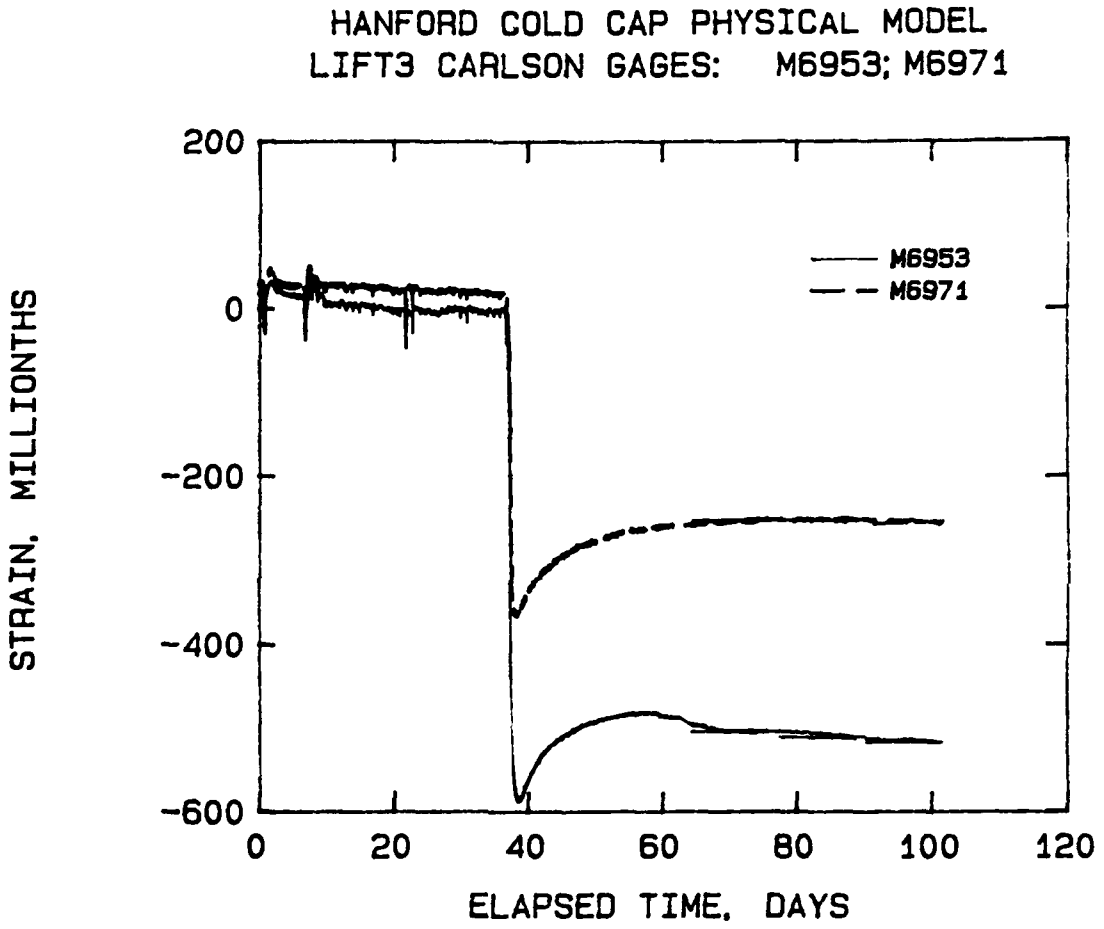

Figure 49. Plot of strain vs time recorded by strain meters during grouting of lifts in the physical model

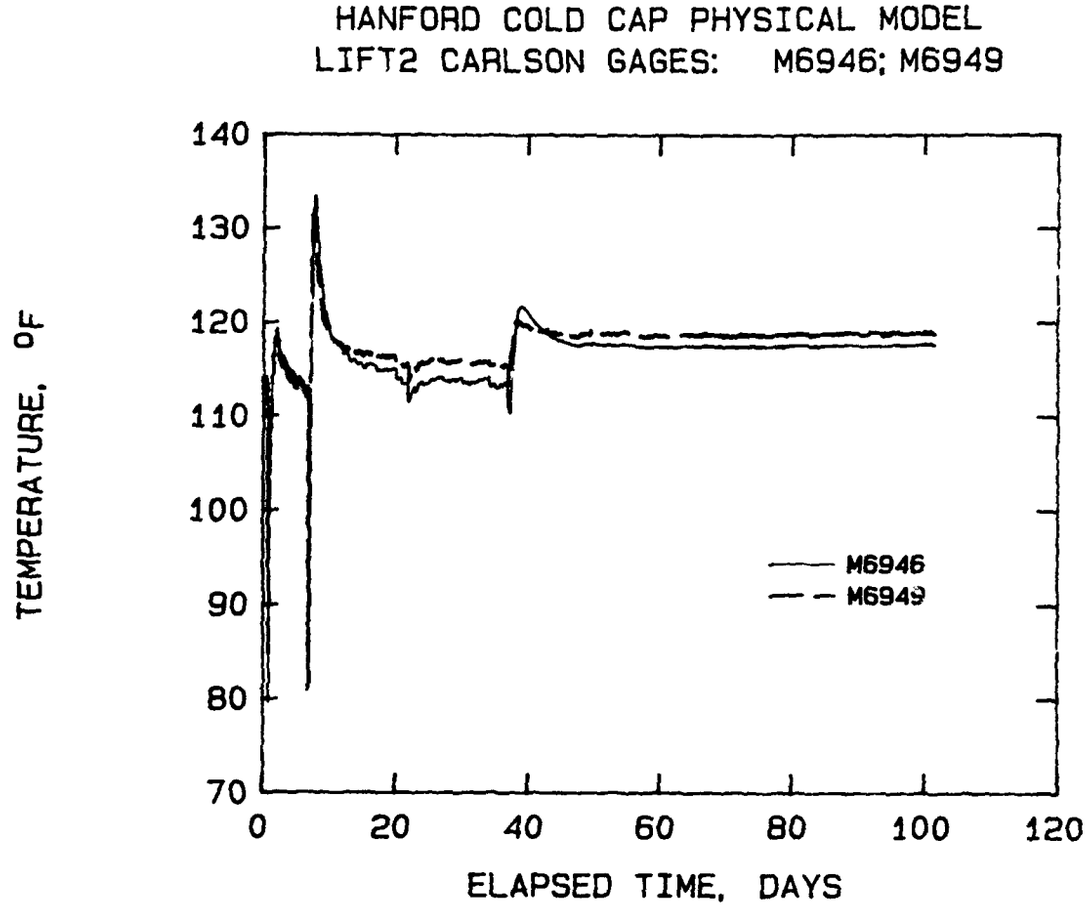

Figure 50. Plot of temperature vs time recorded by strain meters during grouting of lifts in the physical model

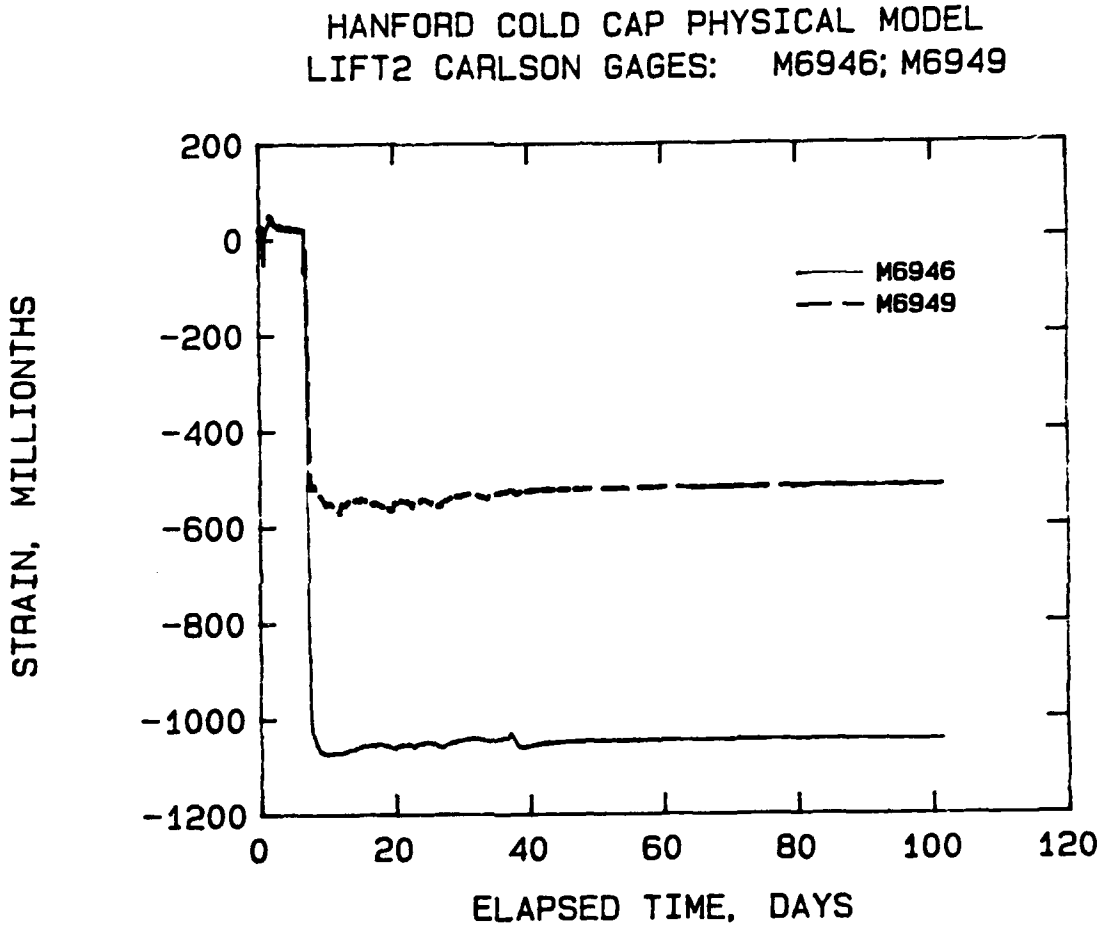

Figure 51. Plot of strain vs time recorded by strain meters during grouting of lifts in the physical model

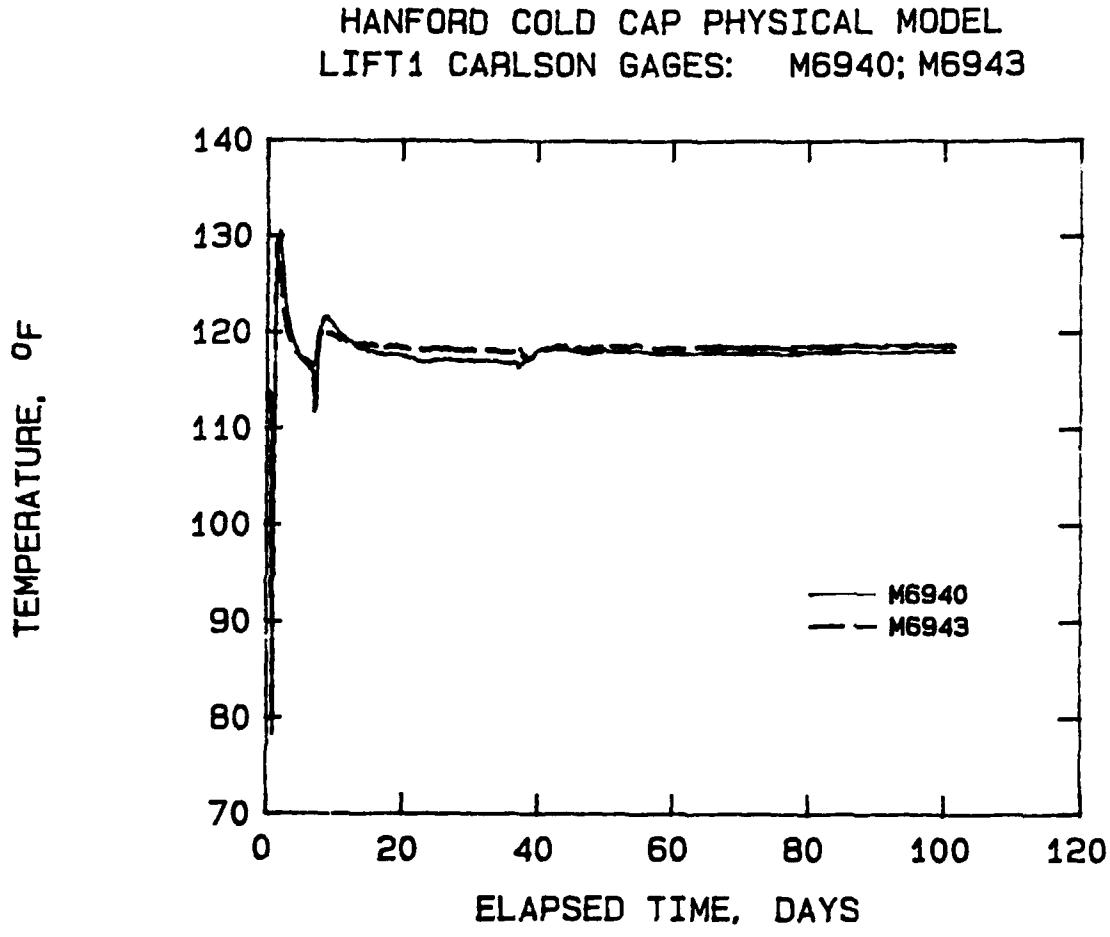

Figure 52. Plot of temperature vs time recorded by strain meters during grouting of lifts in the physical model

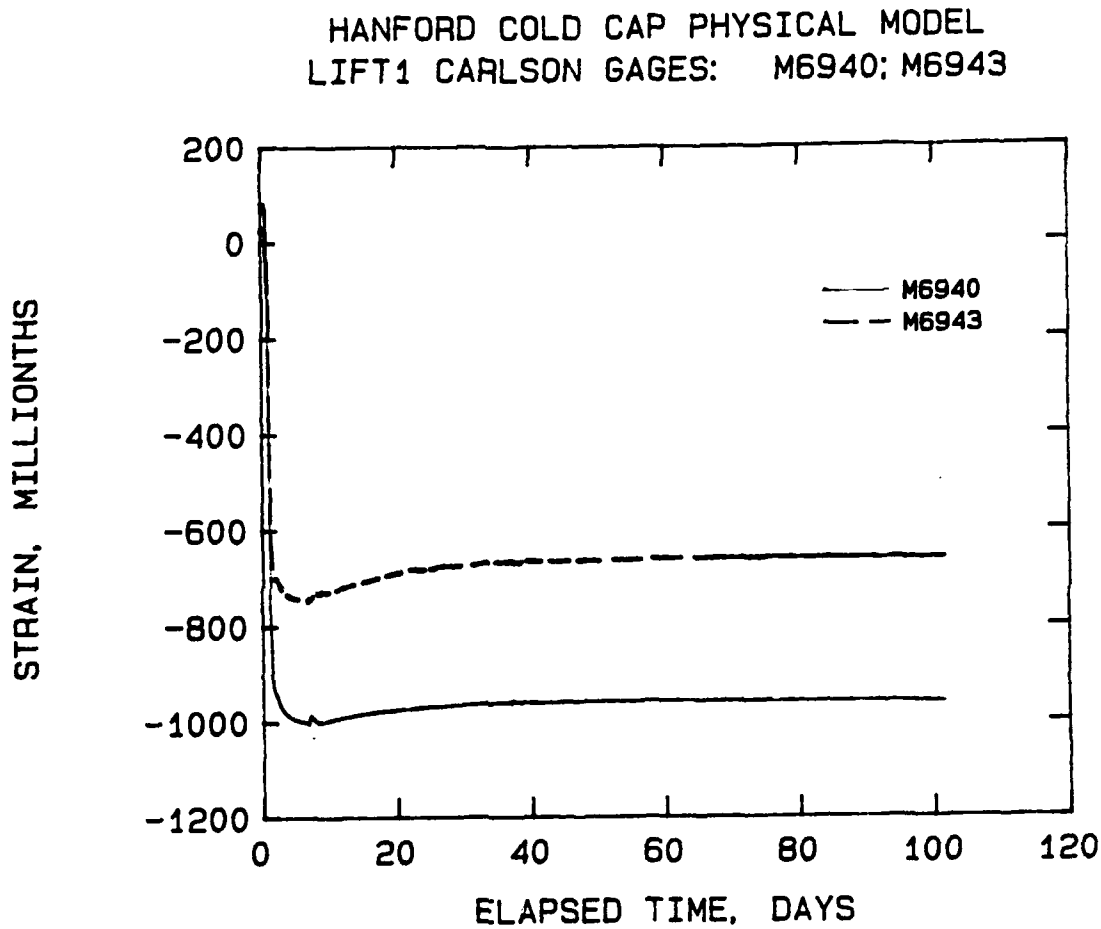

Figure 53. Plot of strain vs time recorded by strain meters during grouting of lifts in the physical model

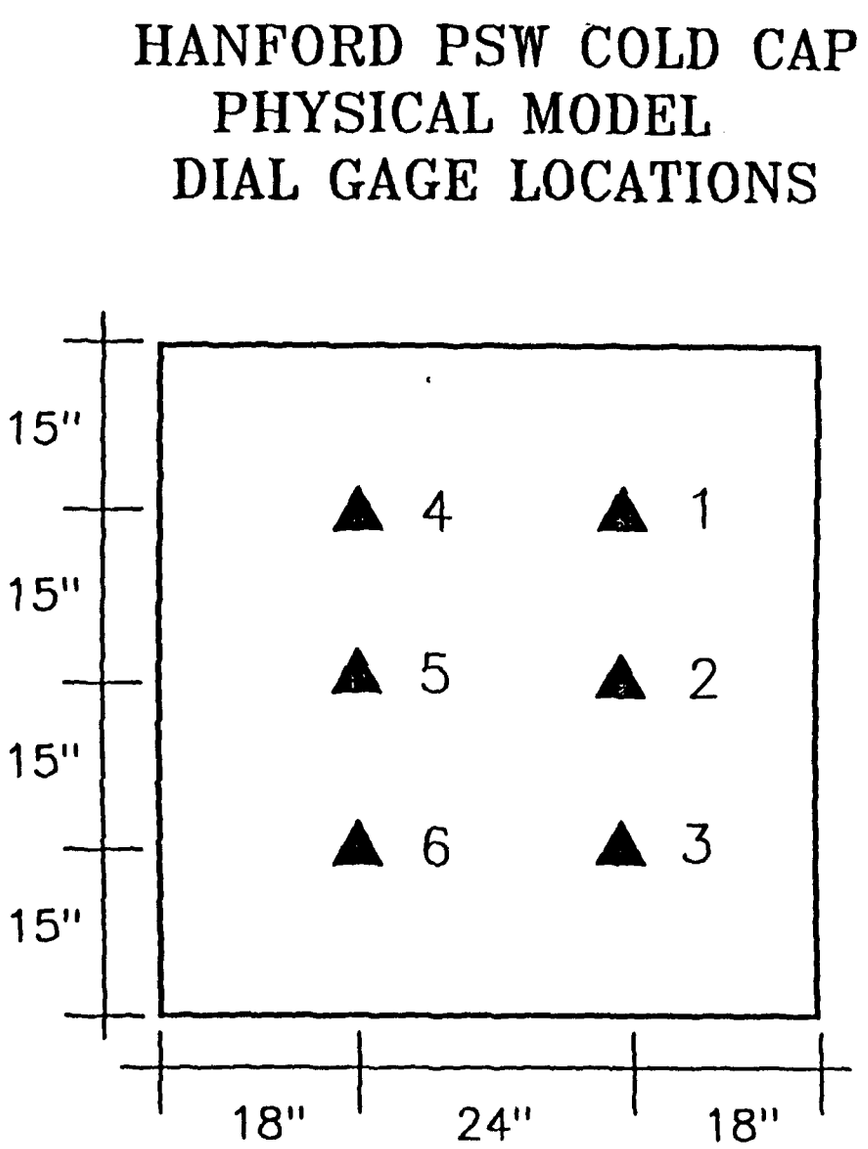

Figure 54. Plan view of physical model showing location of dial gages

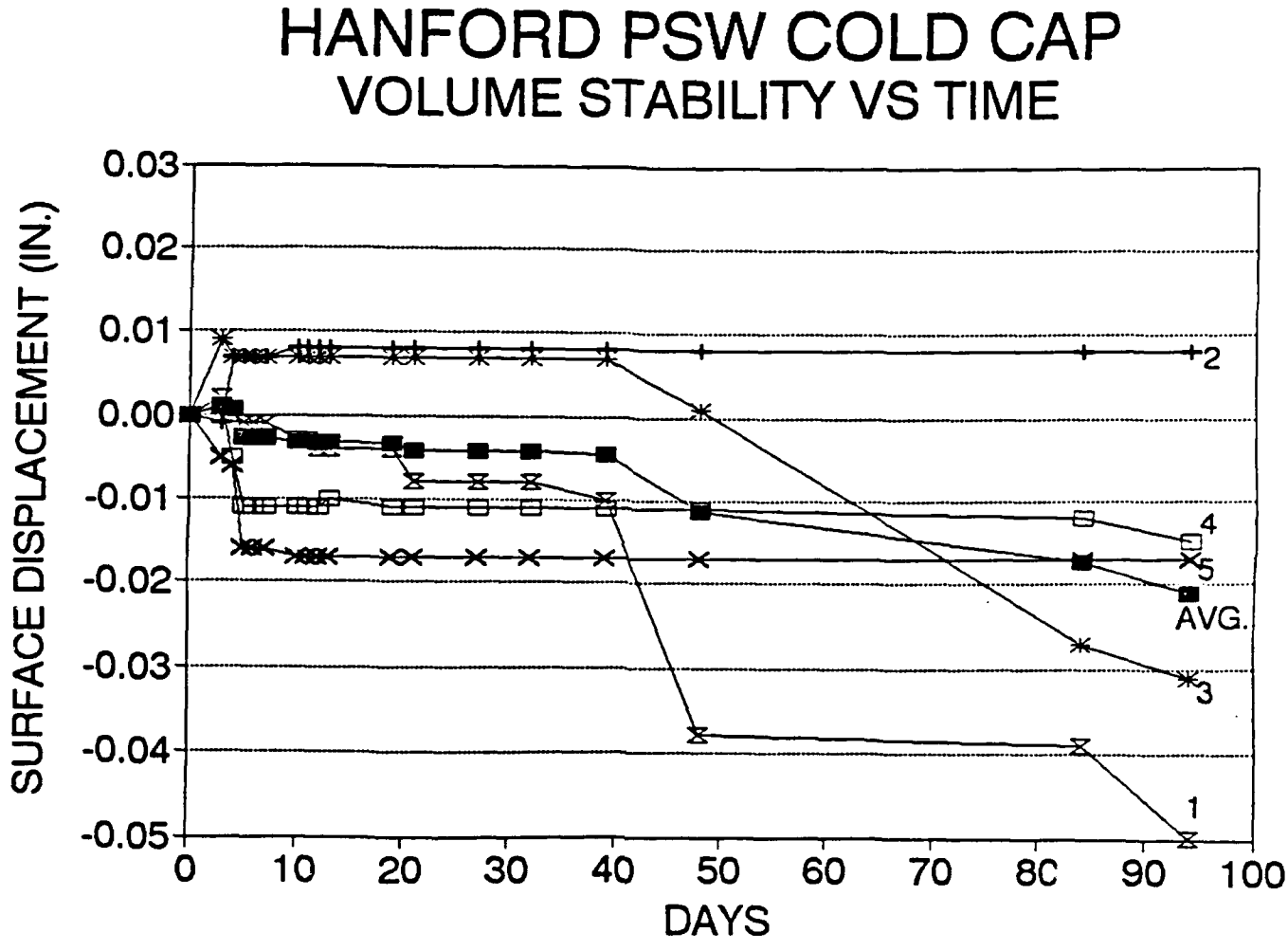

Figure 55. Deflection of the vault surface vs time

APPENDIX A:

PROPORTIONS OF EXPERIMENTAL GROUT MIXTURES TESTED DURING GROUT DEVELOPMENT

MIXTURE 2B

Mixture Proportions		Flow Properties		
Material	Lb/Cy	Time (min)	Flow (sec)	Comments
Class H Cement	432	5	13.1	Compressive strength at 7 days (140 °F) = 1,900 psi
Class F Fly Ash	980	15	11.5	
Masonry Sand	1,113	45	12.8	
Bentonite	27	75	15.0	Estimated volume loss to bleed = 1 percent
Water	664	105	17.6	
HRWRA	0.78			
Retarder	0 oz			

MIXTURE 3B

Mixture Proportions		Flow Properties		
Material	Lb/Cy	Time (min)	Flow (sec)	Comments
Class H Cement	486	5	11.0	Compressive strength at 7 days (140 °F) = 3,920 psi
Class F Fly Ash	851	30	11.0	
Basalt Sand	1,215	60	11.0	
Bentonite	27	90	11.2	Estimated volume loss to bleed = 8.7 percent
Water	664	120	11.3	
HRWRA	1.1			
Retarder	26 oz			

MIXTURE 3B-1

Mixture Proportions		Flow Properties		
Material	Lb/Cy	Time (min)	Flow (sec)	Comments
Class H Cement	468	5	14.0	Cast specimens after 1 hr. Mixture was too thick to use.
Class F Fly Ash	826	30	14.5	
Basalt Sand	1,215	60	16.3	Estimated volume loss to bleed = 1 percent
Bentonite	54	90		
Water	664	120		
HRWRA	1.1			
Retarder	26 oz			

MIXTURE 3B-2

Mixture Proportions		Flow Properties		
Material	Lb/Cy	Time (min)	Flow (sec)	Comments
Class H Cement	486	5	11.6	Estimated volume loss to bleed = 4 percent
Class F Fly Ash	845	30	11.6	
Basalt Sand	1,215	60	11.7	
Bentonite	34	90	11.9	
Water	664	120	12.0	
HRWRA	1.1			
Retarder	26 oz			

MIXTURE 5B

Mixture Proportions		Flow Properties		
Material	Lb/Cy	Time (min)	Flow (sec)	Comments
Class H Cement	486	5	15.0	Slight fallout of aggregate until 30 minutes.
Class F Fly Ash	851	30	15.0	
Basalt Sand	1,350	60	15.6	Compressive strength at 7 days (140 °F) = 4,055 psi
Bentonite	54	90	16.0	
Water	599	120	17.0	
HRWRA	2.43			
Retarder	26 oz			

MIXTURE 7B

Mixture Proportions		Flow Properties		
Material	Lb/Cy	Time (min)	Flow (sec)	Comments
Class H Cement	486	5	≈ 30 sec	Aggregate fellout excessively.
Class F Fly Ash	1,586	30		
Basalt Sand	540	60		Estimated volume loss to bleed = 3.5 percent
Bentonite	27	90		
Water	621	120		
HRWRA	1.1			
Retarder	26 oz			

MIXTURE 8B

Mixture Proportions		Flow Properties		
Material	Lb/Cy	Time (min)	Flow (sec)	Comments
Class H Cement	486	5		Did not test flow - mixtures experienced excessive fallout and bleed.
Class F Fly Ash	1,207	30		
Basalt Sand	810	60		
Bentonite	0	90		
Water	675	120		
HRWRA	1.35			
Retarder	16 oz			

MIXTURE 9B

Mixture Proportions		Flow Properties		
Material	Lb/Cy	Time (min)	Flow (sec)	Comments
Class H Cement	486	5	13.0	Cast specimens after 30 minutes.
Class F Fly Ash	1,156	30	14.7	
Basalt Sand	810	60		
Bentonite	54	90		
Water	675	120		
HRWRA	3.0			
Retarder	0 oz			

MIXTURE 10B

Mixture Proportions		Flow Properties		
Material	Lb/Cy	Time (min)	Flow (sec)	Comments
Class H Cement	486	5	13.8	Slight fallout of aggregate at 30 minutes.
Class F Fly Ash	1,182	30	11.8	
Basalt Sand	810	60	11.9	No fallout after 60 minutes of mixing.
Bentonite	27	90	11.9	
Water	675	120	12.0	
HRWRA	2.67			
Retarder	15.4 oz			

MIXTURE 12B

Mixture Proportions		Flow Properties		
Material	Lb/Cy	Time (min)	Flow (sec)	Comments
Class H Cement	486	5	12.5	Slight fallout of aggregate at 60 minutes.
Class F Fly Ash	1,000	30	13.2	
Basalt Sand	1,280	60	14.0	
Bentonite	13			
Water	594			
HRWRA	2.43			
Retarder	13.5 oz			

MIXTURE 1L

Mixture Proportions		Flow Properties		
Material	Lb/Cy	Time (min)	Flow (sec)	Comments
Class H Cement	432	5	12.0	Slight fallout of aggregate at 30 minutes.
Class F Fly Ash	967	30	12.0	
Limestone Sand	1,160	60	12.5	Compressive strength at 7 days (140 °F) = 2,330 psi
Bentonite	54	90	13	
Water	664	120	13.6	Estimated volume loss to bleed = 2 percent
HRWRA	1.1			
Retarder	23 oz			

MIXTURE 4L

Mixture Proportions		Flow Properties		
Material	Lb/Cy	Time (min)	Flow (sec)	Comments
Class H Cement	468	5	13.0	Compressive strength at 7 days (140 °F) = 3,180 psi
Class F Fly Ash	869	30	12.7	
Limestone Sand	1,215	60	13.0	Estimated volume loss to bleed = 3 percent
Bentonite	67.5	90	13.0	
Water	664	120	13.8	
HRWRA	2.43			
Retarder	31 oz			

MIXTURE 6L

Mixture Proportions		Flow Properties		
Material	Lb/Cy	Time (min)	Flow (sec)	Comments
Class H Cement	468	5	13.8	Compressive strength at 7 days (140 °F) = 3,480 psi
Class F Fly Ash	869	30	13.8	
Limestone Sand	1,350	60	14.5	
Bentonite	54	90	15.5	
Water	619	120	17.3	
HRWRA	2.43			
Retarder	26 oz			

MIXTURE 10L

Mixture Proportions		Flow Properties		
Material	Lb/Cy	Time (min)	Flow (sec)	Comments
Class H Cement	468	5	13.2	
Class F Fly Ash	1,182	30	13.0	
Limestone Sand	854	60	13.0	
Bentonite	27	90	13.2	
Water	675	120	13.4	
HRWRA	0.9			
Retarder	15 oz			

MIXTURE 11L

Mixture Proportions		Flow Properties		
Material	Lb/Cy	Time (min)	Flow (sec)	Comments
Class H Cement	468	5	14.5	Specimens cast after 60 minutes of mixing.
Class F Fly Ash	999	30	13.4	
Limestone Sand	1,350	60	13.0	
Bentonite	13	90		
Water	594	120		
HRWRA	2.43			
Retarder	13.5 oz			

MIXTURE 17

Mixture Proportions		Flow Properties		
Material	Lb/Cy	Time (min)	Flow (sec)	Comments
Class K Cement	500	5	11.2	Compressive strength at 7 days (73 °F) = 810 psi
Class F Fly Ash	1,000	30	13.0	
Basalt Sand	1,233	60	12.5	Specimens cast after 60 minutes of mixing.
Bentonite	0	90		
Water	600	120		
HRWRA	0			
Retarder	0			

MIXTURE 18

Mixture Proportions		Flow Properties		
Material	Lb/Cy	Time (min)	Flow (sec)	Comments
Class K Cement	500	5	13.6	Compressive strength at 7 days (73 °F) = 880 psi
Class F Fly Ash	1,000	30	13.8	
Basalt Sand	850	60	14.0	
Bentonite	0	90		
Water	750	120		
HRWRA	2.6			
Retarder	15 oz			

MIXTURE 19

Mixture Proportions		Flow Properties		
Material	Lb/Cy	Time (min)	Flow (sec)	Comments
Class K Cement	400	5	12.2	Slight aggregate fallout at 5 minutes.
Class F Fly Ash	1,072	30	13.0	
Basalt Sand	1,233	60	13.0	No fallout at 60 minutes.
Bentonite	0	90		Compressive strength at 7 days (73 °F) = 700 psi
Water	600	120		
HRWRA	0			
Retarder	12 oz			

MIXTURE 20

Mixture Proportions		Flow Properties		
Material	Lb/Cy	Time (min)	Flow (sec)	Comments
Class H Cement	300	5	19	
Class F Fly Ash	1,112	30	17.4	
Basalt Sand	1,314	60	17.9	
Bentonite	38	90	17.8	
Water	564	120	18.6	
HRWRA	4.86			
Retarder	4.6 oz			

MIXTURE 21

Mixture Proportions		Flow Properties		
Material	Lb/Cy	Time (min)	Flow (sec)	Comments
Class K Cement	607	5	27	Mixture not fluid enough.
Class F Fly Ash	1,087	30	22	
Basalt Sand	835	60	17.8	
Bentonite	48	90	20.0	
Water	677	120	16.8	
HRWRA	10.3			
Retarder	8.3 oz			

MIXTURE 22

Mixture Proportions		Flow Properties		
Material	Lb/Cy	Time (min)	Flow (sec)	Comments
Class H Cement	350	5	16.8	
Class F Fly Ash	1,077	30	17.1	
Basalt Sand	1,296	60	17.3	
Bentonite	42	90	17.9	
Water	571	120	19.3	
HRWRA	5.4			
Retarder	5.4 oz			

APPENDIX B:

REPORTS FROM EXAMINATION OF CEMENT, AGGREGATES, AND INTERFACE BETWEEN COLD-CAP GROUT AND SIMULATED WASTE

US Army Engineer Waterways Experiment Station 3909 Halls Ferry Road Vicksburg, Mississippi 39180-6199	SUBJECT: Petrographic Examination of a Class H Oil Well Cement (HAN-1 C-1) DATE: 22 March 1991

1. In March 1991, you requested a petrographic examination of a Class H Oil Well cement received from the Lone Star Industries, Inc., Mary Neal, Texas. The cement was assigned the Structures Laboratory serial No. HAN-1 C-1.

2. A composite of the as-received cement was examined by X-ray diffraction (XRD).

3. Approximately 5-g was treated for 30 min in a 20 percent solution of maleic acid in methanol. This test was done to remove the silicates, alite (C_3S) and belite (C_2S), from the sample. The insoluble material was collected on filter paper, dried and weighed. The percent of silicates in the sample were calculated. A composite of the residue was examined by XRD.

4. The residue left after the maleic acid treatment was next treated for one hour with a 10 percent solution of ammonium chloride (NH_4Cl) in deionized water. This test will remove sulfates. The insoluble material was collected on filter paper, dried and weighed. The percent of material lost was calculated. A composite of the residue was examined by XRD.

5. The tests by selective dissolution to determine the percent of silicates and sulfates in the sample showed that 81.7 percent were C_3S and C_2S. Of the 18.3 percent insoluble, 4.9 percent was lost during the NH_4Cl treatment. However, some MgO was lost during the NH_4Cl test, as evidenced by the loss in intensity of MgO XRD lines after treatment with NH_4Cl. A good estimate of total sulfates in the sample would be approximately three percent.

6. The crystalline phases present, as determined by XRD are:

Alite (C_3S)
Belite (C_2S)
Calcium aluminoferrite (C_4AF)
MgO
Gypsum ($C\bar{S}\cdot 2H$)
Anhydrite ($C\bar{S}$)
Calcium sulfate hemihydrate ($C\bar{S}\cdot 1/2H$)
Quartz (tr)

A trace of potassium sulfate, and a trace of the substituted (NC_8A_3) calcium aluminate was tentatively identified. Alite was the major phase.

WES FORM No. 1115-E
Rev May 1990

US Army Engineer Waterways Experiment Station 3909 Halls Ferry Road Vicksburg, Mississippi 39180-6199	SUBJECT: Examination of HAN-1 S-3 Sand DATE: 8 March 1991

1. A small plastic bag containing several pounds of basaltic sand from Acme Materials, Richland, WA, was received for tests. A composite of the sand was separated into six sieve sizes. The percent by weight of each size was determined (Table B1).

2. X-ray diffraction was used to determine the mineralogy of sand collected on sieve sizes No. 4 (4.75 mm), No. 100 (150 μm), and Pan (Table B2).

3. A stereomicroscope was used to examine the sand. Particle shapes were determined.

4. Selected particles from each sample were picked to be examined as immersion mounts prepared using an oil with a refractive index of n = 1.544. The mounts were examined with a polarizing microscope.

5. Chert was found. Some has an index of refraction lower than n = 1.544.

6. The examination showed that this sand, and sand HAN-1 S-2 which was a previous batch from Acme Materials, are similar. The color, mineralogical composition, and shapes of particles are alike. The finer sieve fractions of both HAN-1 S-2 and S-3 contain considerable quartz.

7. The characteristics of this natural sand make it suitable for use as a fine aggregate for grout or concrete.

Table B1

Size Fractions by Weight of HAN-1 S-3

Sieve Size	Percent Contained
No. 4 (4.75 mm)	2.7
No. 8 (2.36 mm)	19.3
No. 16 (1.18 mm)	13.0
No. 100 (150 μm)	59.0
No. 200 (75 μm)	4.4
Pan	1.1
Total	100

WES FORM No. 1115-E
Rev May 1990

Table B2

Mineralogical Composition by X-ray Diffraction of HAN-1 S-3

Constituents	HAN-1 S-3
Clay	
Smectite	Prob.
Clay mica	X
Chlorite	X
Kaolinite group	Poss.
Nonclays	
Quartz	X
Plagioclase Feldspar	X
Potassium Feldspar	X
Calcite	X
Pyroxene*	X
Amphibole*	X
Magnetite	X
Hematite	X
Glass	X

* Monoclinic crystal structure

US Army Engineer Waterways Experiment Station 3909 Halls Ferry Road Vicksburg, Mississippi 39180-6199	SUBJECT: Petrographic Examination of Specimen CC-9, Hanford Cold-Cap Grout DATE: 3 April 1991

1. Background. Samples of interfaces between candidate cold-cap grouts CC-9 through CC-16 and simulated wasteform grout were examinated to determine characteristics of the interface. Samples were laboratory-cast 2- by 4-in. cylinders, the lower half of each being simulated wasteform grout. Interfaces were studied for phase composition (X-ray diffraction (XRD)), chemical composition (energy-dispersive X-ray (EDX)), and physical appearance (microscopy and scanning electronic microscopy (SEM)). These studies revealed no notable differences among all candidate grouts. Results of the studies of CC-9 and CC-11 interfaces are reported here as examples.

2. The interface between cold-cap grout and wasteform had a thin layer of frothy material for both specimens. The frothy material was filled with air voids. No bond was formed. Grout and wasteform fell apart when the two specimens were demolded. No evidence of fluid movement was found by visual examination.

3. Examination of the froth by EDX showed sodium (Na) was a little high. Tables B3 and B4 gives a semiquantitative listing of chemical elements found in froth from the cold-cap and wasteform, respectively.

4. Eleven EDX spectrum were made from a specimen of the cold-cap grout. Ten of the spectrum were collected within 5-mm of the interface with wasteform. One spectrum was collected near the top of the cold-cap, on opposite end from the wasteform. Figure B1 shows the two spectrum that were collected at opposite ends, superimposed to show that a phosphorus (P) peak is probably present in the cold-cap grout at the interface, but not present at the other (top) end of the grout. Table B5 gives a semiquantitative listing of chemical elements in one of the spectrum collected near the interface.

5. SEM examination of pieces of cold-cap and wasteform material showed C-S-H gel was common to both materials. Small thin platelets of calcium hydroxide (CH) were also present in both materials. Figures B2 and B3 shows some C-S-H gel that was typical to both the cold-cap and wasteform, respectively. Figure B2 shows thin platelets of what is probably CH in the top portion of the photomicrograph. Figure B3 shows thin CH platelets in the lower right corner of the bottom portion of the photomicrograph. The C-S-H gel in both have the Type II reticular network morphology.

6. X-ray diffraction examination of the two froth samples examined showed several crystalline phases present. Ettringite, CH, and C-S-H gel were identified by XRD. Tetracalcium aluminate carbonate-11-hydrate ($C_4A\bar{C}H_{11}$) was present in the froth from the cold-cap, but not in froth from the wasteform. Unhydrated portland cement and fly ash were present in both froth samples; however, more was present in the cold-cap froth than the froth from wasteform.

7. Examination by XRD of a piece of wasteform, and a piece of the cold-cap both from near the contact zone, showed broad, but well defined peaks of C-S-H

gel. Calcium hydroxide was also identified in both samples. No ettringite or $C_4A\bar{C}H_{11}$ were identified. Calcite and dolomite probably from the palygorskite, were present in the wasteform material. The cold-cap material showed peaks of plagioclase feldspar from the basalt aggregate. No crystalline clay remains in the wasteform.

Table B3

FILE NAME: SPT DIG01B
LABEL: FROTH CC-9 COLD CAP GROUT
STORED ELEMENTS
CA NA MG AL SI P S K TI CR
MN FE
X-AXIS LABEL: ENERGY (KEV)
SPECTRUM STATUS:
LINEAR BACKGROUND SUBTRACTION
NOT FILTERED
SPECTRUM HAS BEEN PROCESSED BY QUANT
SPECTRUM HAS NOT BEEN SMOOTHED
LIVE TIME (SEC): 100.00
ACCELER. VOLT. (KEV): 21
COLLECTION DATE: 3/28/91
START OF SPECTRUM: 0.000
END OF SPECTRUM: 20000.00
NUMBER OF CHANNELS IN SPECTRUM: 2000
BEGINNING OF QUANT DATA
TAKE OFF ANGLE [DEG]: 35
TILT ANGLE [DEG]: 0
PROBE CURRENT [AMPS]: 0.54E-09

ELEMENT	METHOD	VALENCE	K-RATIO	WT %
CA	K	2.00	0.23717	27.0491
NA	K	1.00	0.02617	6.3045
MG	K	2.00	0.01577	2.9587
AL	K	3.00	0.11234	17.6140
SI	K	4.00	0.20761	34.9049
P	K	5.00	0.00181	0.3858
S	K	6.00	0.00911	1.5108
K	K	1.00	0.01075	1.2684
TI	K	4.00	0.02036	2.6176
CR	K	3.00	0.00199	0.2384
MN	K	2.00	0.00000	0.0005
FE	K	2.00	0.04447	5.1472

OF ELEMENTS ANALYZED BY QUANT: 12

Table B4

FILE NAME: SPT DIG02B
LABEL: FROTH CC-9 WASTE GROUT
STORED ELEMENTS
CA NA MG AL SI P S K TI CR
MN FE
X-AXIS LABEL: ENERGY (KEV)
SPECTRUM STATUS:
LINEAR BACKGROUND SUBTRACTION
NOT FILTERED
SPECTRUM HAS BEEN PROCESSED BY QUANT
SPECTRUM HAS NOT BEEN SMOOTHED
LIVE TIME (SEC): 100.00
ACCELER. VOLT. (KEV): 21
COLLECTION DATE: 3/28/91
START OF SPECTRUM: 0.000
END OF SPECTRUM: 20000.00
NUMBER OF CHANNELS IN SPECTRUM: 2000
BEGINNING OF QUANT DATA
TAKE OFF ANGLE [DEG]: 35
TILT ANGLE [DEG]: 0
PROBE CURRENT [AMPS]: 0.54E-09

ELEMENT	METHOD	VALENCE	K-RATIO	WT %
CA	K	2.00	0.25001	28.4356
NA	K	1.00	0.03047	7.3835
MG	K	2.00	0.01351	2.6007
AL	K	3.00	0.11262	17.8884
SI	K	4.00	0.18823	31.9687
P	K	5.00	0.00131	0.2720
S	K	6.00	0.01661	2.6992
K	K	1.00	0.00963	1.1313
TI	K	4.00	0.01936	2.4985
CR	K	3.00	0.00091	0.1091
MN	K	2.00	0.00000	0.0000
FE	K	2.00	0.04328	5.0130

OF ELEMENTS ANALYZED BY QUANT: 12

Table B5

FILE NAME: SPT DIG09B
LABEL: HANFORD CC-9 COLD CAP GROUT
STORED ELEMENTS
CA NA MG AL SI P S K TI CR
MN FE
X-AXIS LABEL: ENERGY (KEV)
SPECTRUM STATUS:
LINEAR BACKGROUND SUBTRACTION
NOT FILTERED
SPECTRUM HAS BEEN PROCESSED BY QUANT
SPECTRUM HAS NOT BEEN SMOOTHED
LIVE TIME (SEC): 88.84
ACCELER. VOLT. (KEV): 21
COLLECTION DATE: 3/29/91
START OF SPECTRUM: 0.000
END OF SPECTRUM: 20000.00
NUMBER OF CHANNELS IN SPECTRUM: 2000
BEGINNING OF QUANT DATA
TAKE OFF ANGLE [DEG]: 35
TILT ANGLE [DEG]: 0
PROBE CURRENT [AMPS]: 0.54E-09

ELEMENT	METHOD	VALENCE	K-RATIO	WT %
CA	K	2.00	0.30845	34.5640
NA	K	1.00	0.01341	3.6046
MG	K	2.00	0.01369	2.6290
AL	K	3.00	0.10644	16.8832
SI	K	4.00	0.18631	31.1610
P	K	5.00	0.00180	0.3663
S	K	6.00	0.00476	0.7607
K	K	1.00	0.00803	0.9168
TI	K	4.00	0.02097	2.7407
CR	K	3.00	0.00245	0.2959
MN	K	2.00	0.00031	0.0373
FE	K	2.00	0.05192	6.0406

OF ELEMENTS ANALYZED BY QUANT: 12

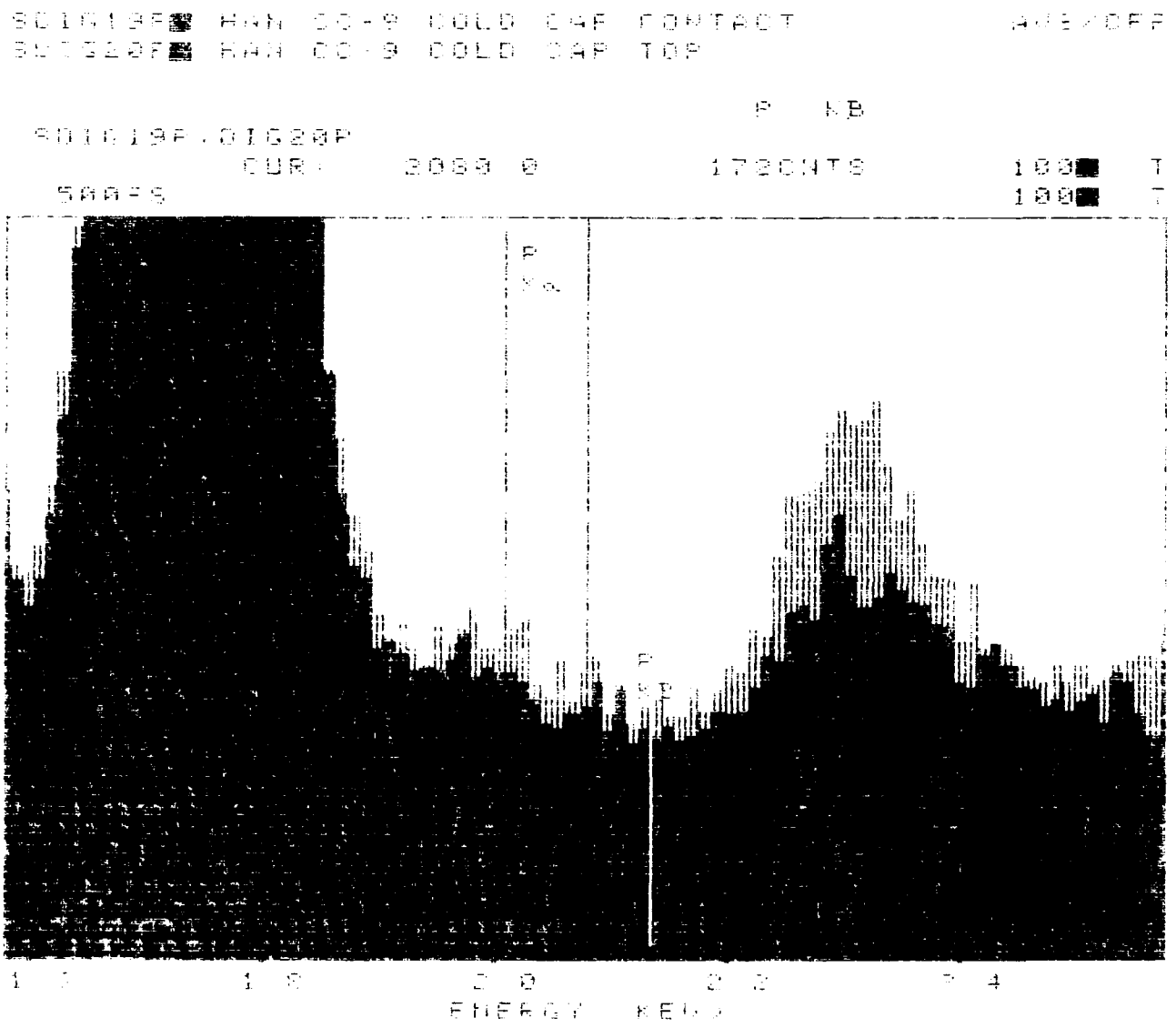

Figure 31. The dark portion is the spectrum collected at the top of cold-cap grout. The light portion is the spectrum collected near the interface of cold-cap and wasteform. A slight peak at 2.013 kev is probably P. Sulfur is probably higher near the interface, also.

Figure B2

Figure B2

Photomicrograph 1. Hanford CC-9 cold-cap. The lower half is magnified X 5,000. The upper half consists of the area in the rectangle magnified X 25,000. C-S-H gel with type II reticular network morphology is present. Thin platelets of CH appear to be present in the upper portion.

Figure B3

Figure B3

Photomicrograph 2. Hanford CC-9 wasteform. The lower half is magnified X 5,000. The upper half consists of the area in the rectangle magnified X 25,000. Type II reticular network morphology C-S-H gel is present. Thin platelets of CH are present in the lower right corner of the micrograph.

April 20, 1992

From: Dr. Charles A. Weiss, Jr./J. Pete Burkes

To: Dr. Lillian Wakeley

Subject: Mineralogy and Chemistry of Longitudinal Core Samples Taken from Interface between simulated Waste and Cold-Cap Grout in Physical Model

X-ray Analysis

X-ray diffraction analysis of bulk samples revealed the presence of the following minerals from most to least abundant.

(A) Cold Cap Distal from Interface
Quartz
Na, Ca-Feldspar
Diopside [$CaMg(SiO_3)_2$] - minor
Ca_2SiO_4 (C_2S) - minor

(B) Interface - Cold Cap Side
Quartz
Na, Ca-Feldspar
Diopside [$CaMg(SiO_3)_2$] - minor
Ca_2SiO_4 (C_2S) - minor
Dolomite - minor

(C) Material on Contact - Waste Side
Quartz
Albite
Calcite
Hematite
Iron

(D) Interface - Waste Side
Calcite
Quartz
Aragonite
Vaterite

(E) Waste Side Distal from Interface
Calcite
Quartz
Dolomite

In addition there is an amorphous component present in all the samples.

Elemental Analysis

(E) Waste vs. (A) Cold Cap
20% less SiO_2
4% less Al_2O_3
1% more P_2O_5
22% more CaO

(C) Material on Waste Side vs. (B) Cold Cap Interf.
6.5% less SiO_2
2% more Al_2O_3
1.5% more CaO
2.5% more Fe_2O_3

(C) Material on Waste Side vs. (A) Distal from Cold Cap
3% less SiO_2
2.5% more Al_2O_3
1% less CaO

(C) Material on Waste Side vs. (D) Waste Interf.
15.5% more SiO_2
6% more Al_2O_3
1% less P_2O_5
24% less CaO

On the waste side of the interface the 3 polymorphs of $CaCO_3$, Calcite, Aragonite, and Vaterite are observed. Since neither Vaterite, nor Aragonite are observed in any of the other samples, this indicates that they were formed in situ and not transported from either the waste or cold cap. As with the cold cap-9 samples, the carbonate minerals probably formed prior to the emplacement of the cold cap. The source for the Ca^{2+} is the waste grout which has 37% CaO far from the interface and 40% CaO at the interface. The source of CO_2 is most likely to be the air over the waste.

The other elements in the waste grout are minor compared to water Ca (37%), Al (13%), Si (35%), and Fe (4%) which are presumably derived from the solid components added to the waste, i.e., the Type I/II Portland Cement, the Class F Fly Ash, and the clays.

The material found adhered to the waste side of the interface was derived from the cold cap due to the presence of Na, Ca-Feldspar which is only found in the cold cap. The elemental analyses supports this hypothesis, because the chemistry more closely resembles that of the bulk chemistry for the cold cap.

Dr. Charles A. Weiss, Jr.
Geochemist

J. Pete Burkes
Geologist

APPENDIX C:

PLOTS OF THE DATA FROM INDIVIDUAL STRAIN METERS

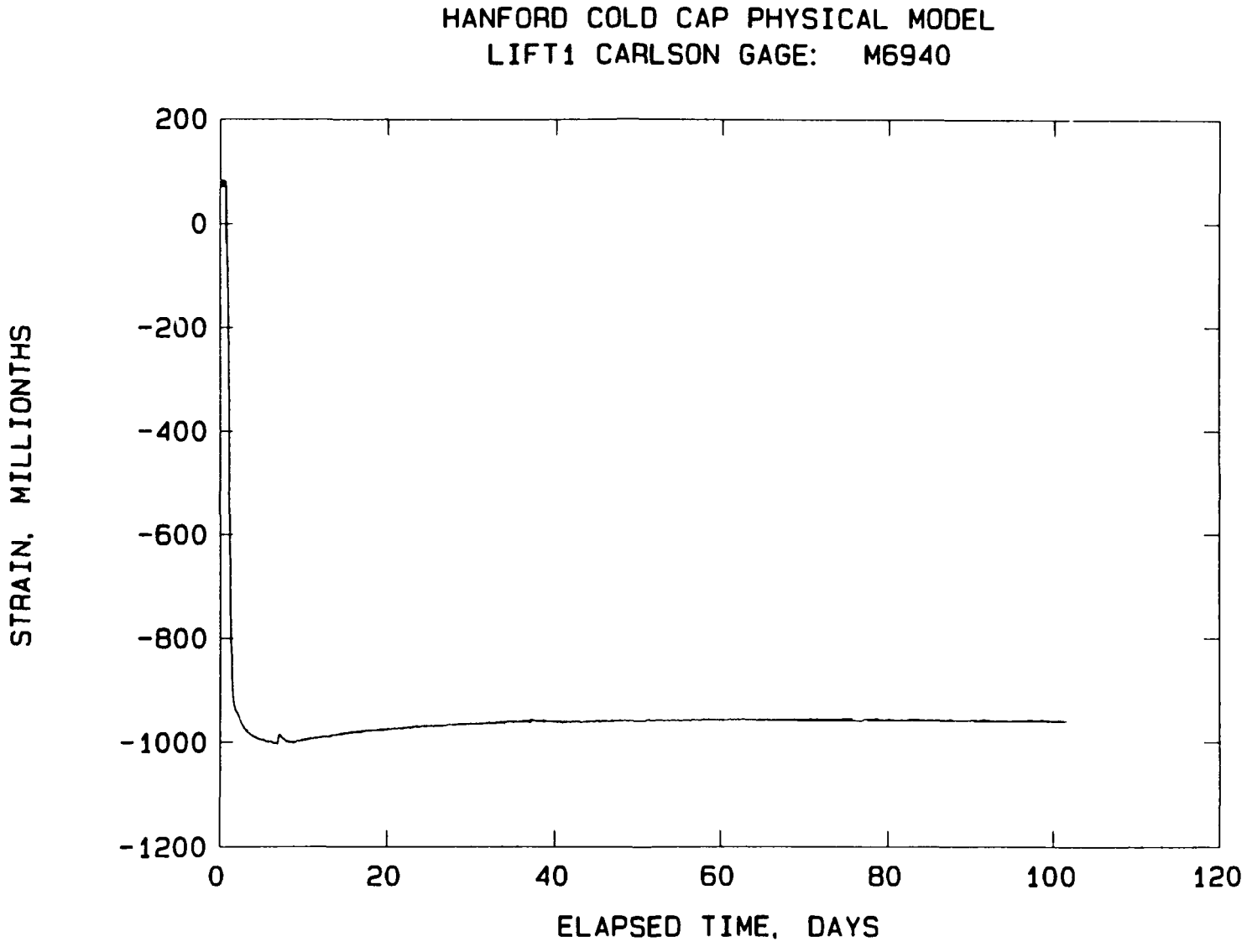
HANFORD COLD CAP PHYSICAL MODEL
LIFT1 CARLSON GAGE: M6940
200
0
-200
-400
-600
-800
-1000
-1200
STRAIN, MILLIONTHS
0
20
40
60
80
100
120
ELAPSED TIME, DAYS

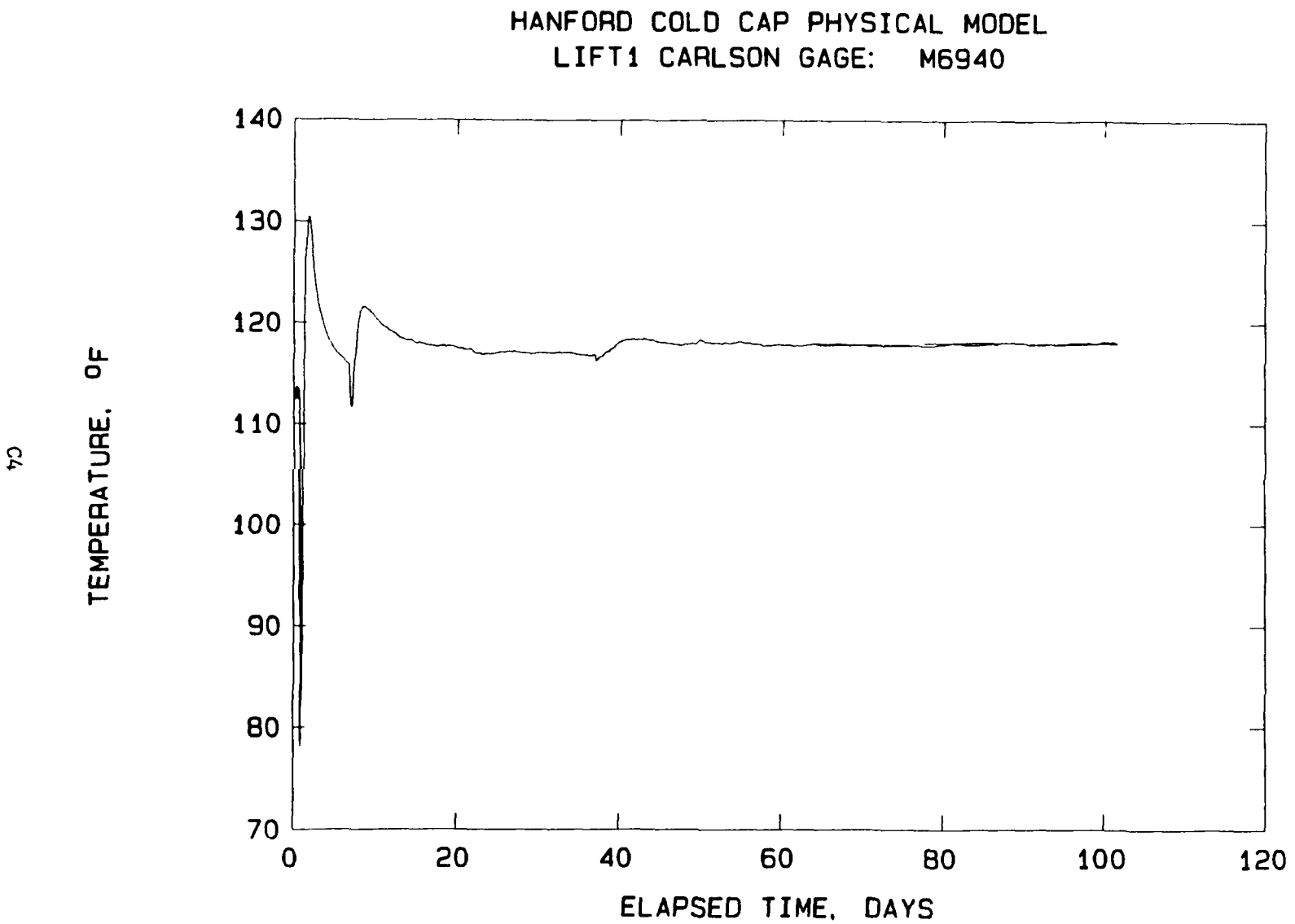
HANFORD COLD CAP PHYSICAL MODEL
LIFT1 CARLSON GAGE: M6940
TEMPERATURE, °F
140
130
120
110
100
90
80
70
0
20
40
60
80
100
120
ELAPSED TIME, DAYS

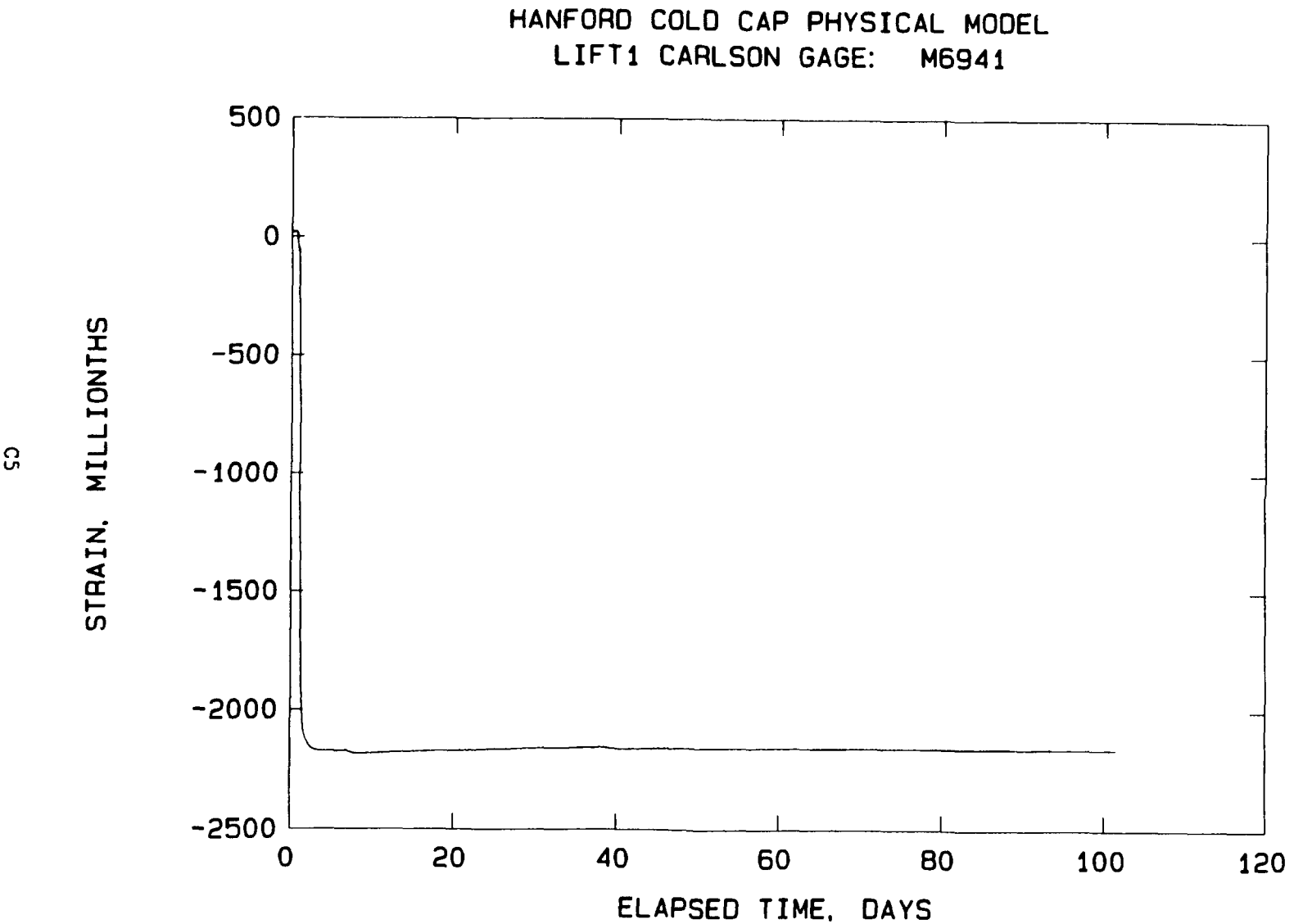
HANFORD COLD CAP PHYSICAL MODEL
LIFT1 CARLSON GAGE: M6941
STRAIN, MILLIONTHS
500
0
-500
-1000
-1500
-2000
-2500
0
20
40
60
80
100
120
ELAPSED TIME, DAYS

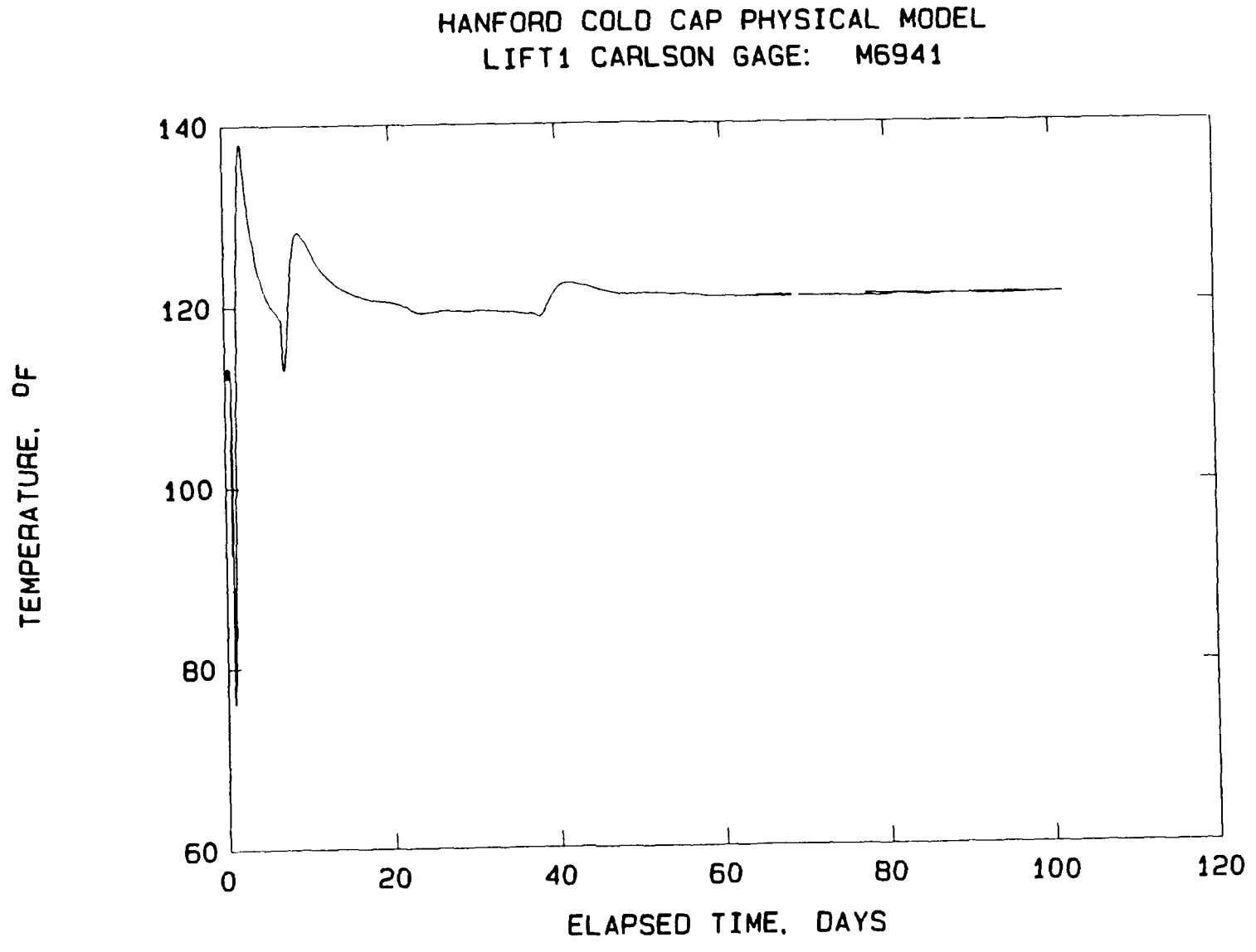
HANFORD COLD CAP PHYSICAL MODEL
LIFT1 CARLSON GAGE: M6941
TEMPERATURE, °F
140
120
100
80
60
0
20
40
60
80
100
120
ELAPSED TIME, DAYS

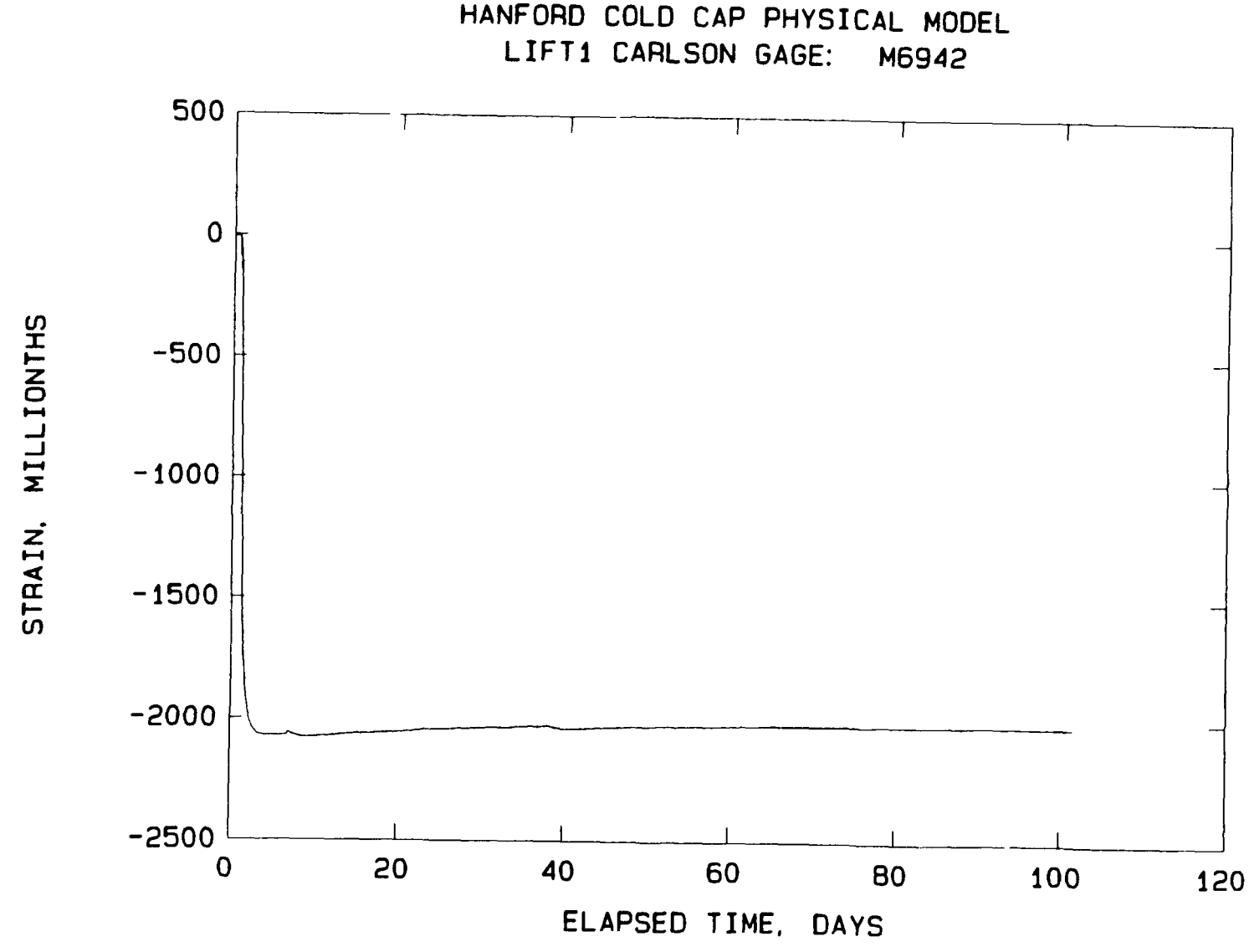
HANFORD COLD CAP PHYSICAL MODEL
LIFT1 CARLSON GAGE: M6942
STRAIN, MILLIONTHS
500
0
-500
-1000
-1500
-2000
-2500
0
20
40
60
80
100
120
ELAPSED TIME, DAYS

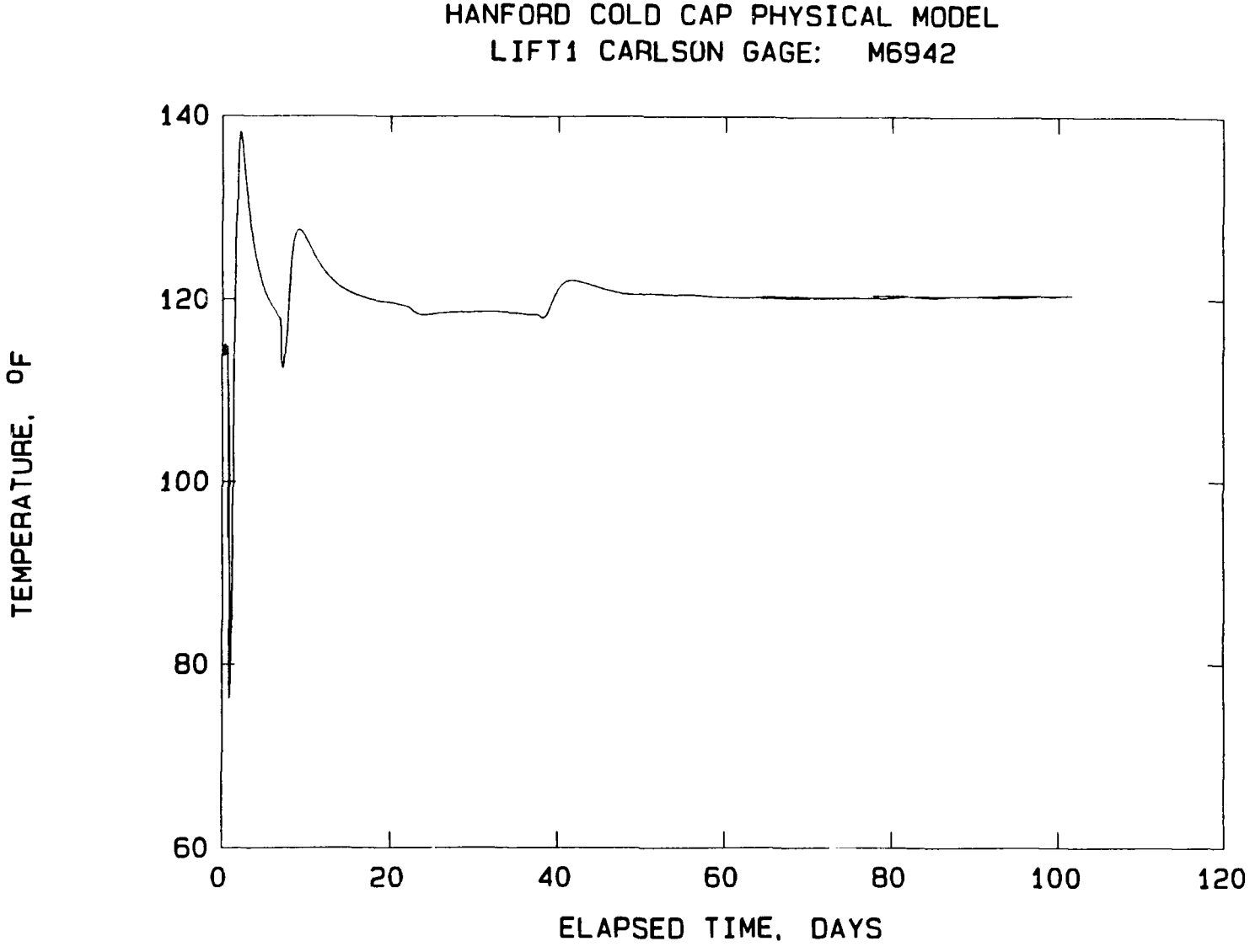
HANFORD COLD CAP PHYSICAL MODEL
LIFT1 CARLSON GAGE: M6942
TEMPERATURE, °F
140
120
100
80
60
0
20
40
60
80
100
120
ELAPSED TIME, DAYS

C8

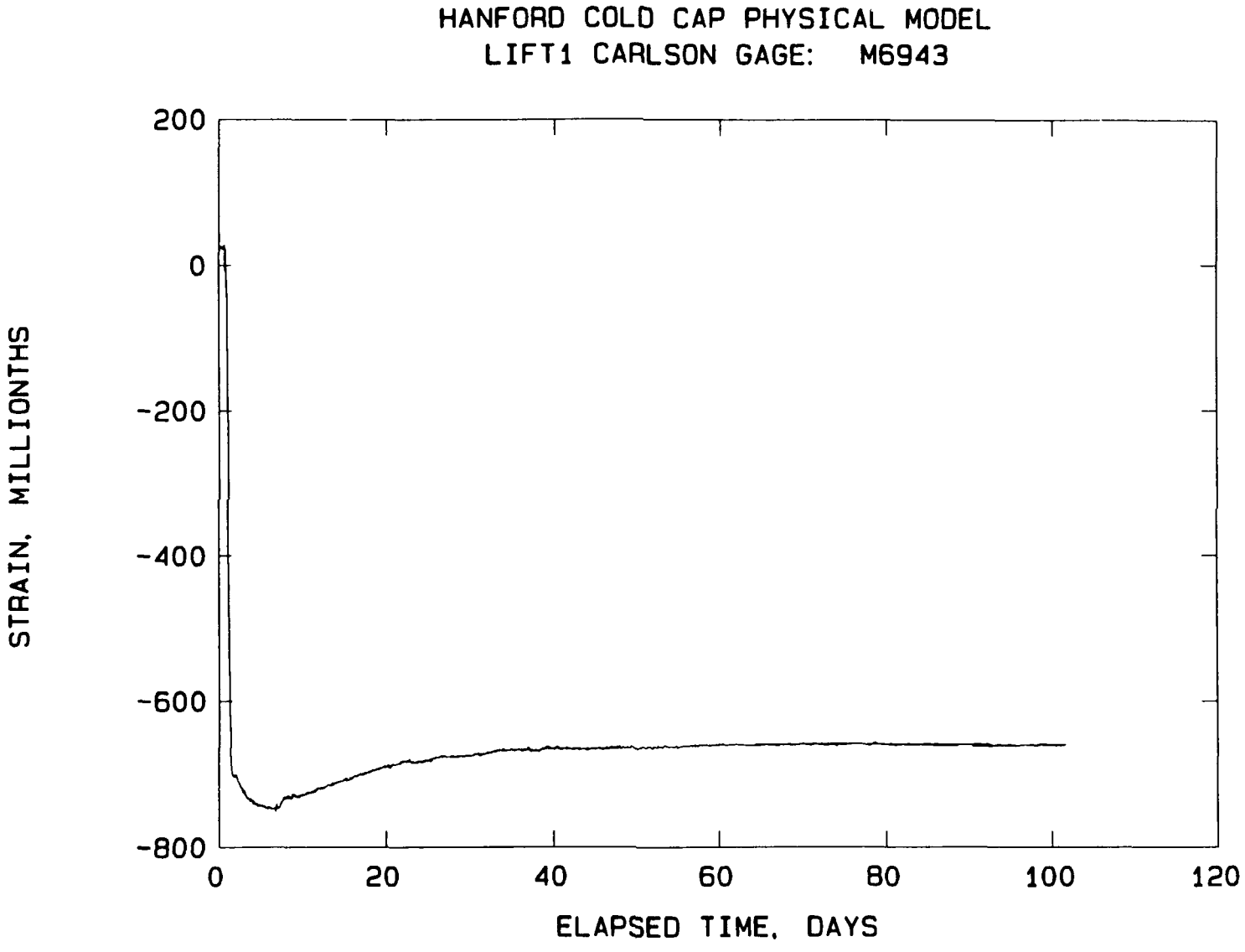
HANFORD COLD CAP PHYSICAL MODEL
LIFT1 CARLSON GAGE: M6943
STRAIN, MILLIONTHS
200
0
-200
-400
-600
-800
0
20
40
60
80
100
120
ELAPSED TIME, DAYS

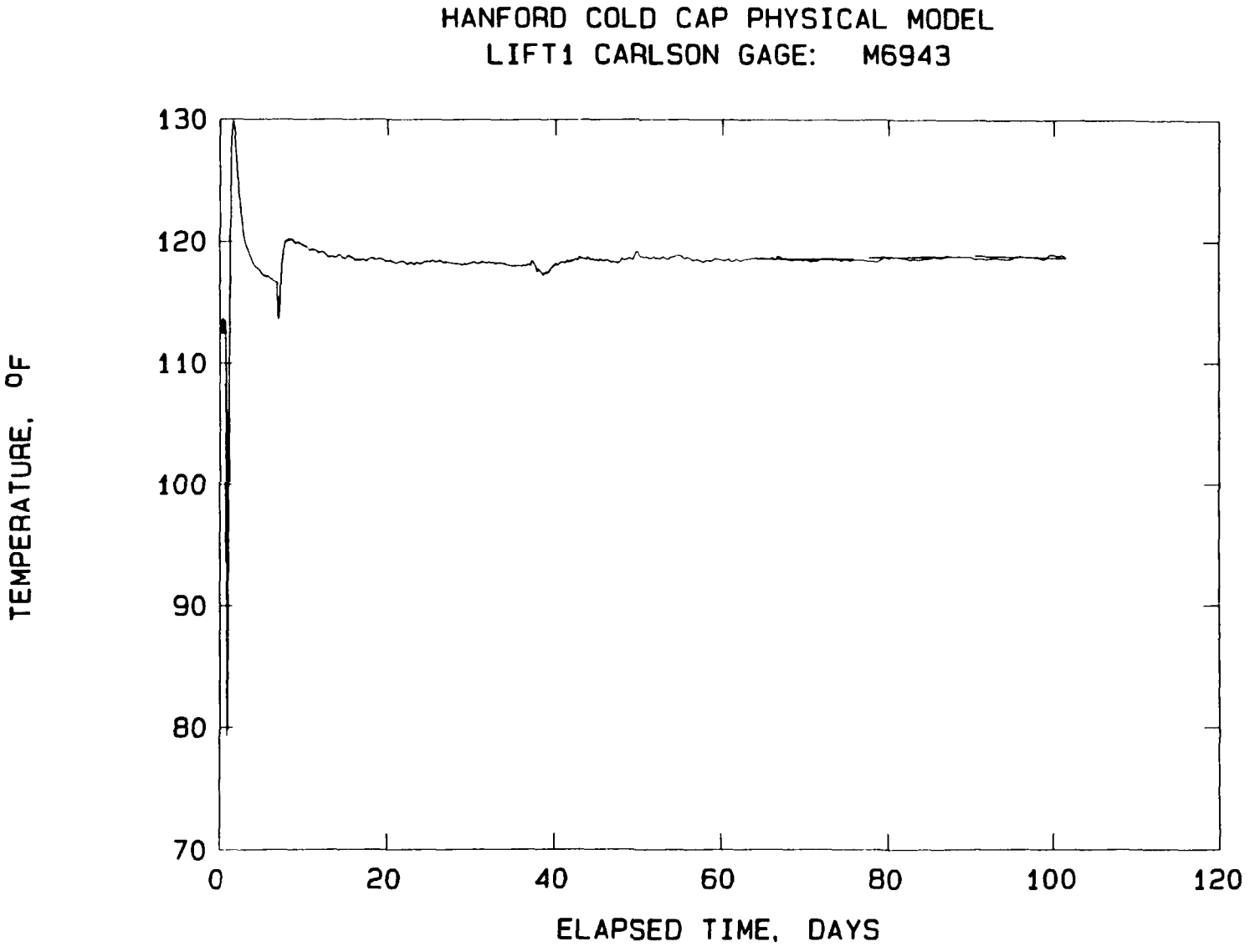
HANFORD COLD CAP PHYSICAL MODEL
LIFT1 CARLSON GAGE: M6943
TEMPERATURE, °F
130
120
110
100
90
80
70
0
20
40
60
80
100
120
ELAPSED TIME, DAYS

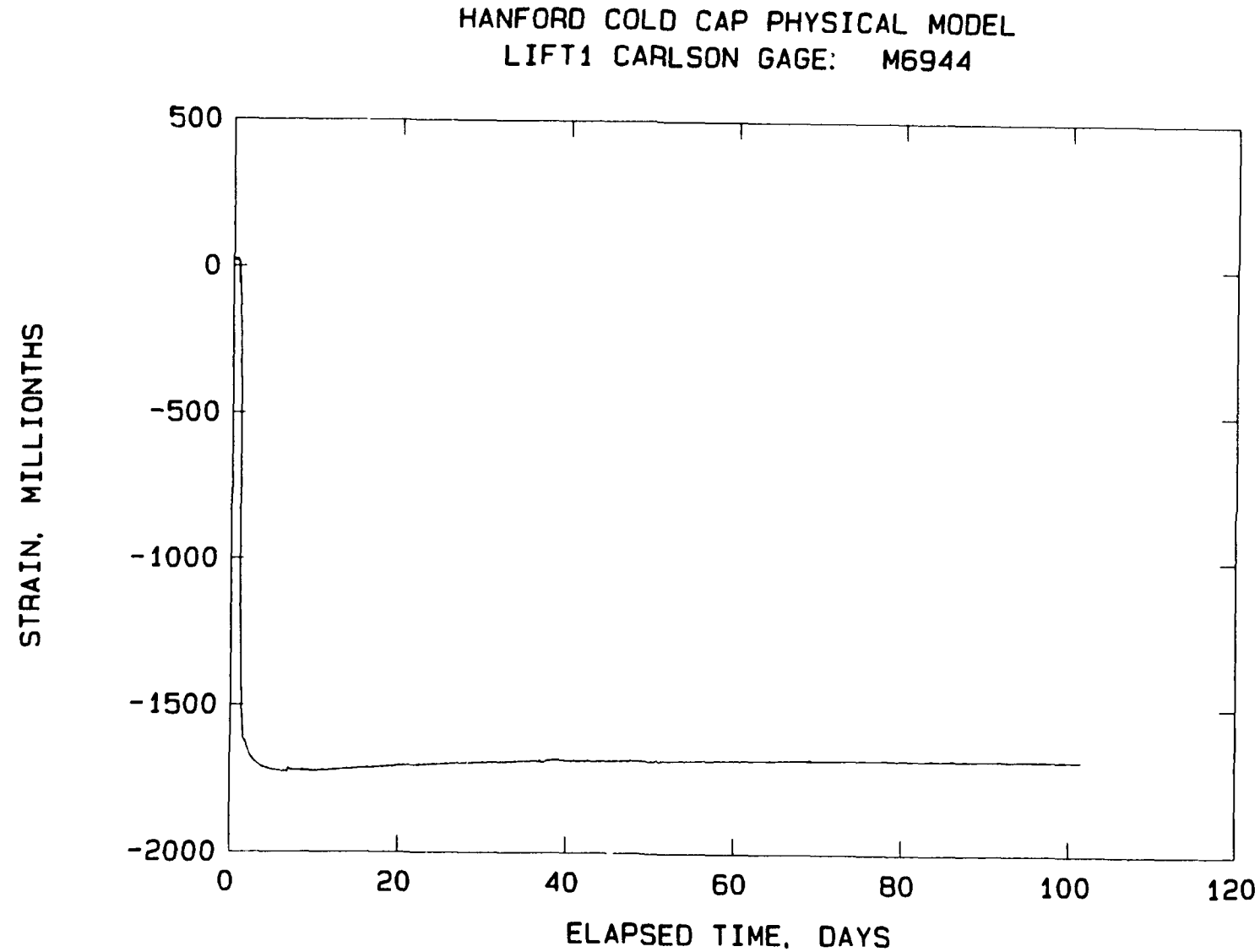
HANFORD COLD CAP PHYSICAL MODEL
LIFT1 CARLSON GAGE: M6944
500
0
-500
-1000
-1500
-2000
STRAIN, MILLIONTHS
0
20
40
60
80
100
120
ELAPSED TIME, DAYS

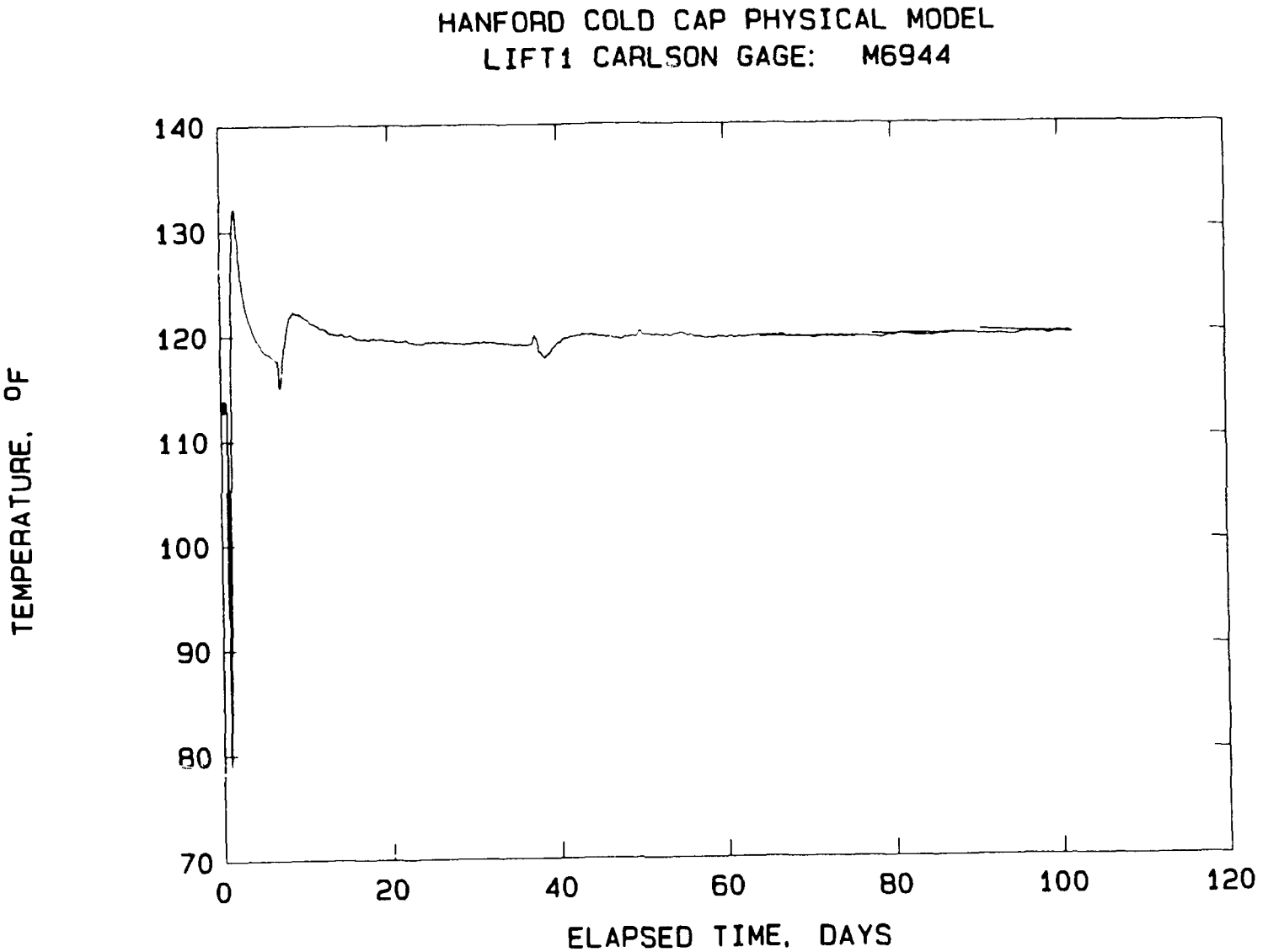
HANFORD COLD CAP PHYSICAL MODEL
LIFT1 CARLSON GAGE: M6944
TEMPERATURE, °F
140
130
120
110
100
90
80
70
0
20
40
60
80
100
120
ELAPSED TIME, DAYS

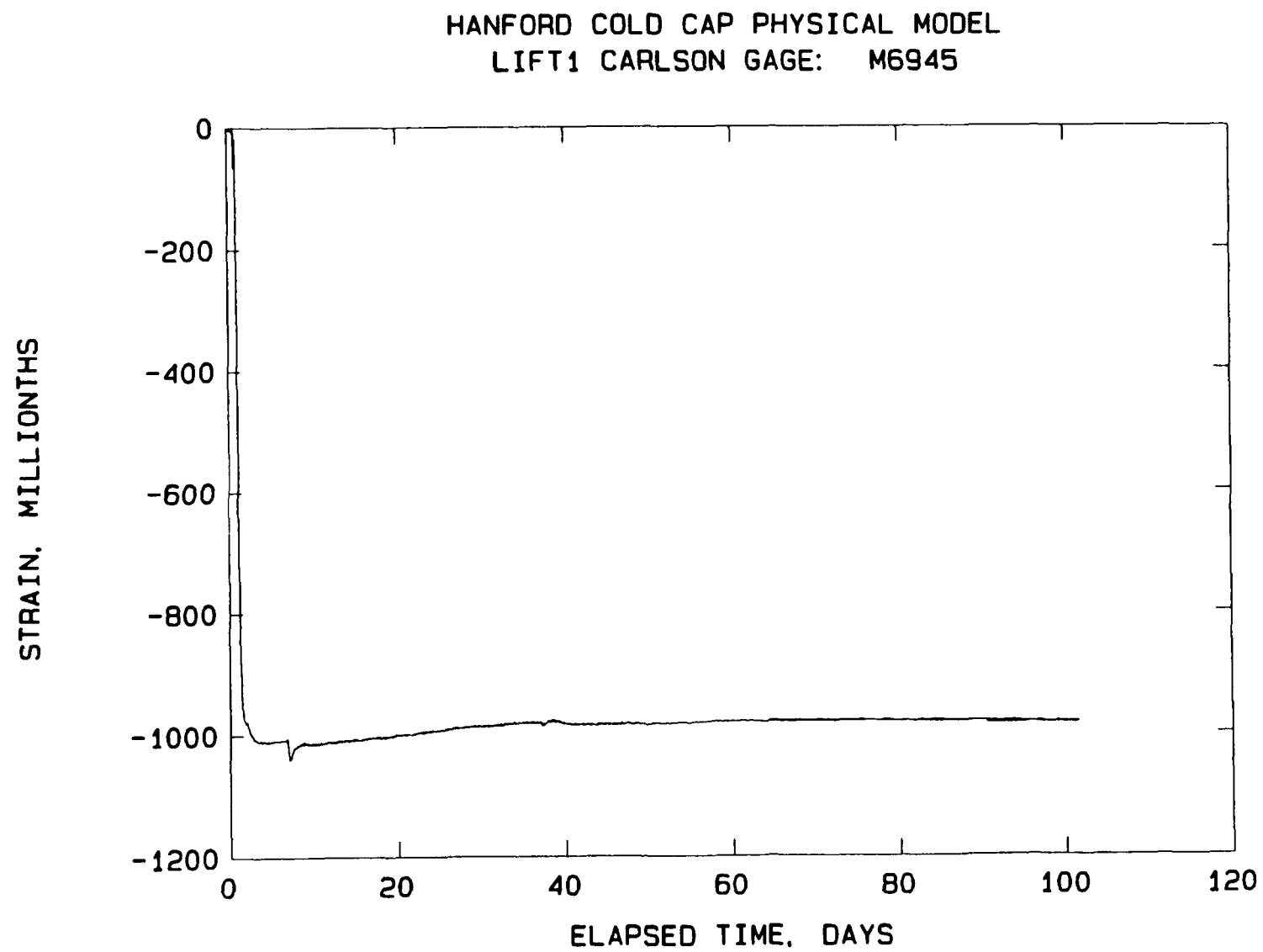
HANFORD COLD CAP PHYSICAL MODEL
LIFT1 CARLSON GAGE: M6945
STRAIN, MILLIONTHS
0
-200
-400
-600
-800
-1000
-1200
0
20
40
60
80
100
120
ELAPSED TIME, DAYS

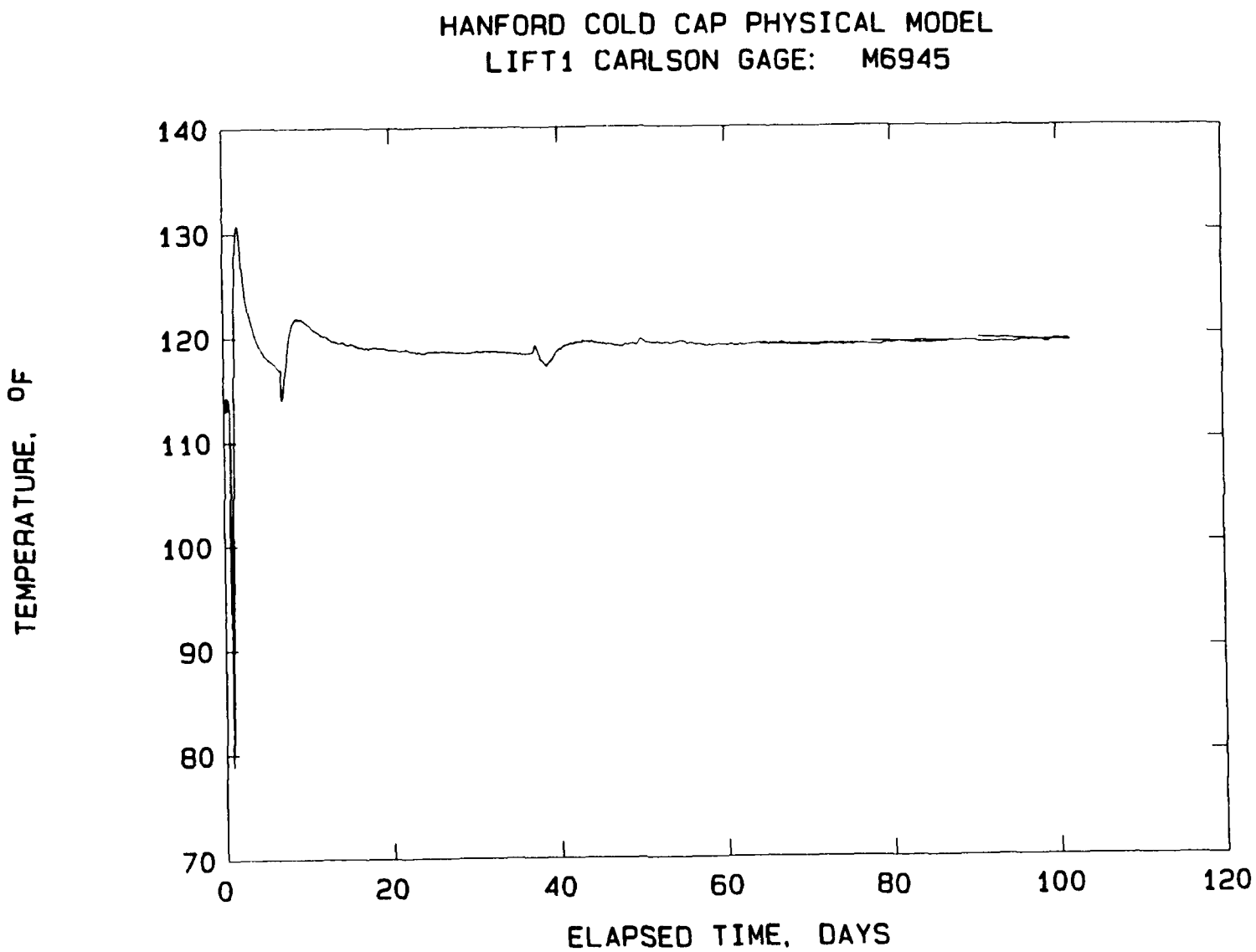
HANFORD COLD CAP PHYSICAL MODEL
LIFT1 CARLSON GAGE: M6945
TEMPERATURE, °F
140
130
120
110
100
90
80
70
0
20
40
60
80
100
120
ELAPSED TIME, DAYS

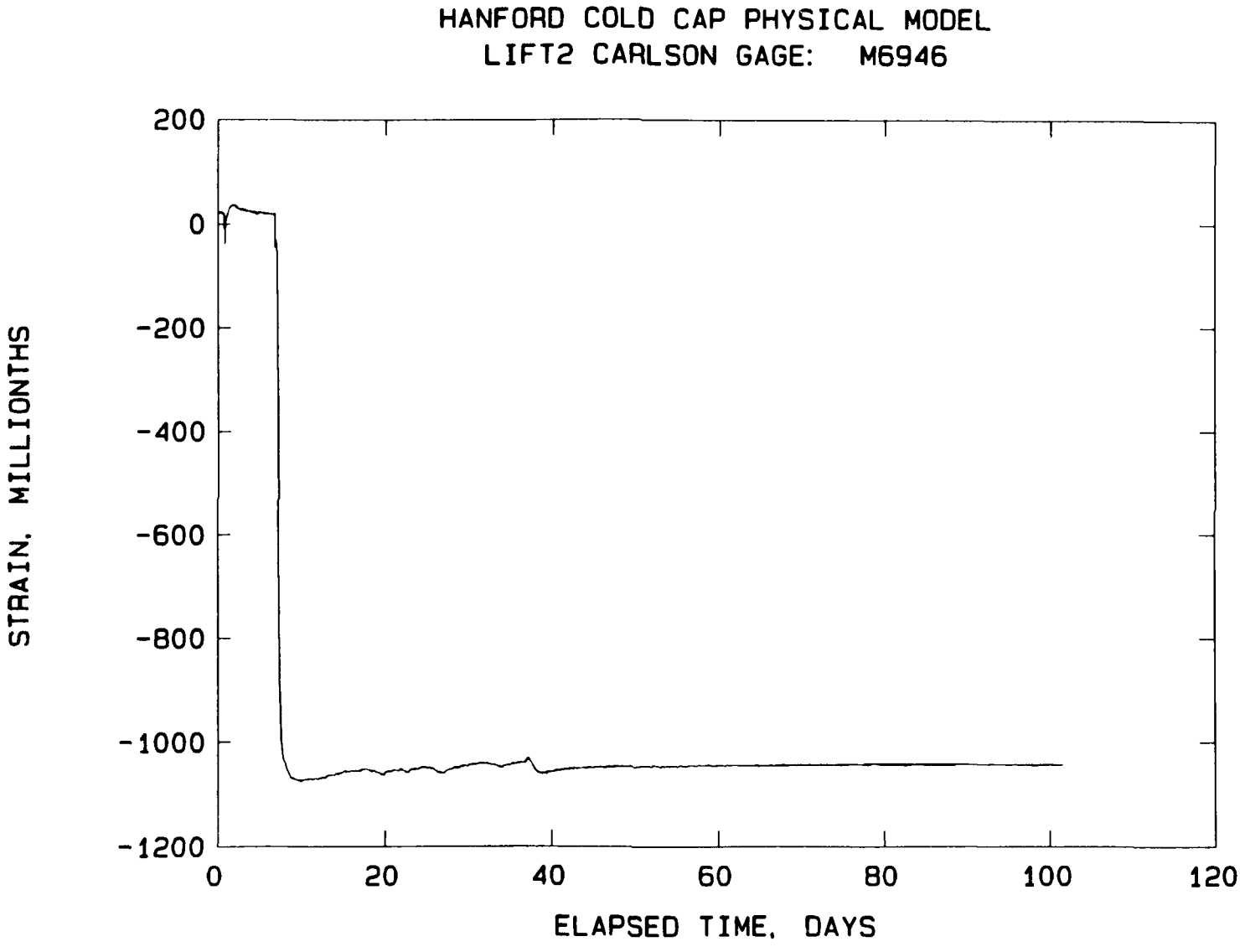
HANFORD COLD CAP PHYSICAL MODEL
LIFT2 CARLSON GAGE: M6946
STRAIN, MILLIONTHS
200
0
-200
-400
-600
-800
-1000
-1200
0
20
40
60
80
100
120
ELAPSED TIME, DAYS

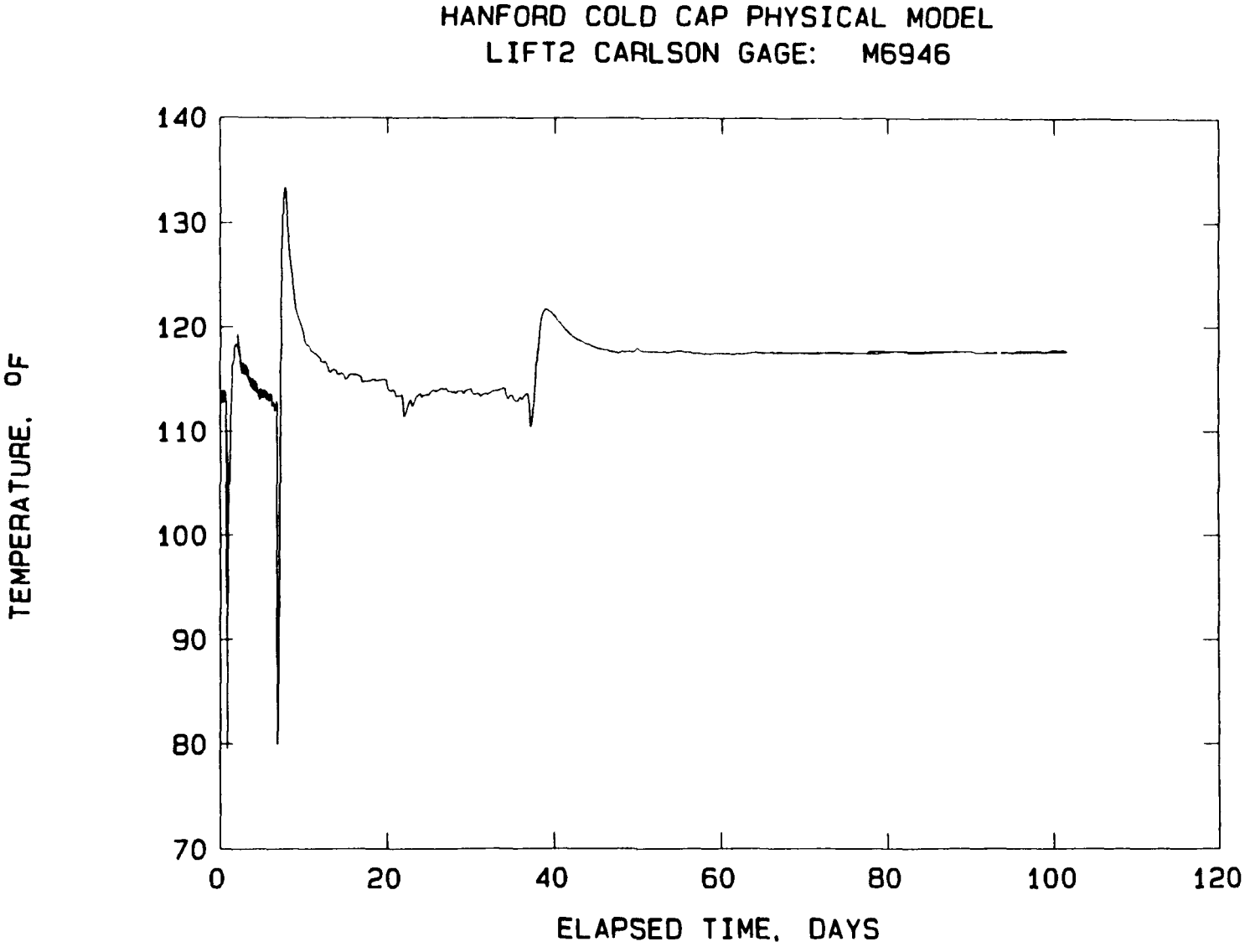
HANFORD COLD CAP PHYSICAL MODEL
LIFT2 CARLSON GAGE: M6946
TEMPERATURE, °F
140
130
120
110
100
90
80
70
0
20
40
60
80
100
120
ELAPSED TIME, DAYS

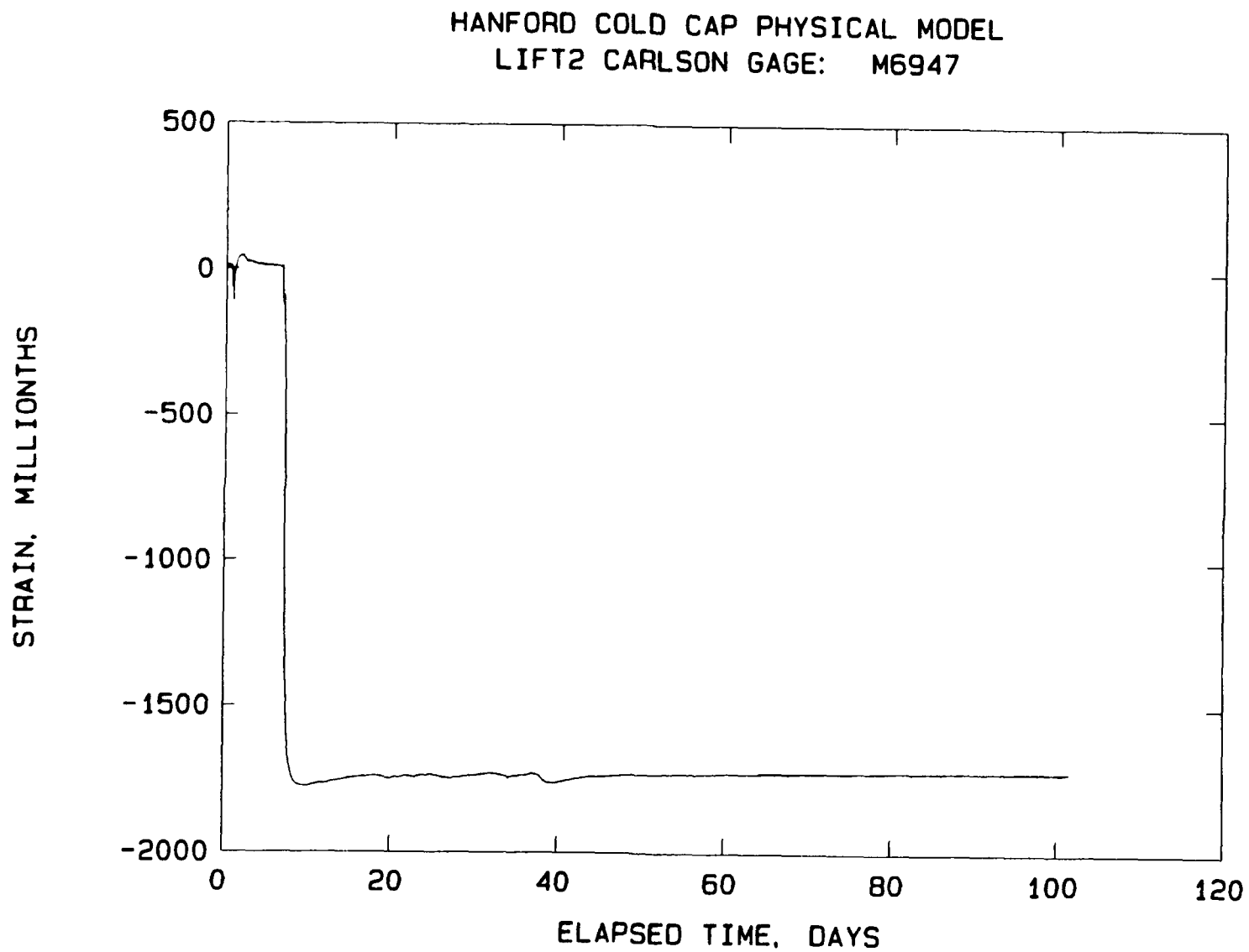
HANFORD COLD CAP PHYSICAL MODEL
LIFT2 CARLSON GAGE: M6947
STRAIN, MILLIONTHS
500
0
-500
-1000
-1500
-2000
0
20
40
60
80
100
120
ELAPSED TIME, DAYS

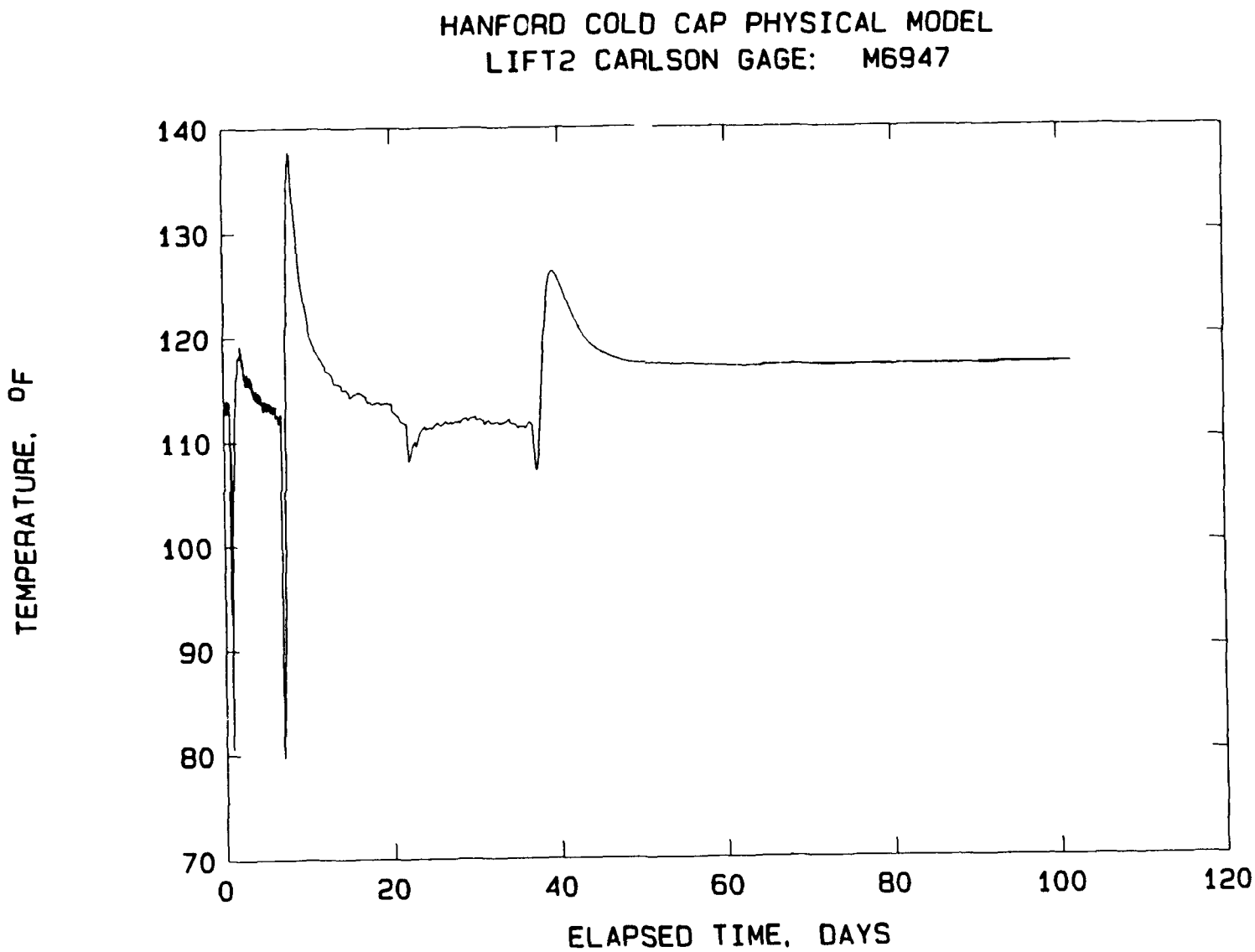
HANFORD COLD CAP PHYSICAL MODEL
LIFT2 CARLSON GAGE: M6947
TEMPERATURE, °F
140
130
120
110
100
90
80
70
0
20
40
60
80
100
120
ELAPSED TIME, DAYS

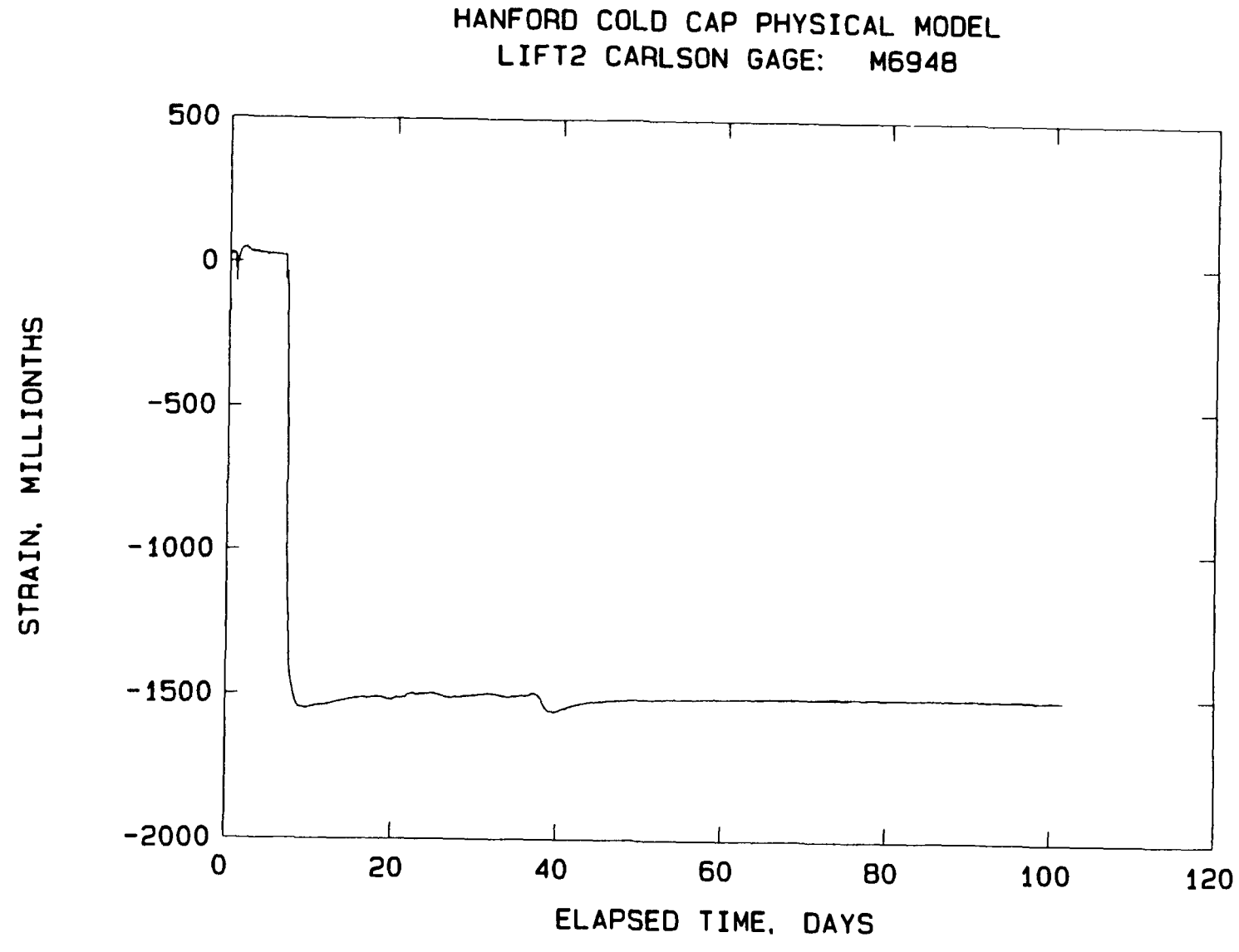
HANFORD COLD CAP PHYSICAL MODEL
LIFT2 CARLSON GAGE: M6948
STRAIN, MILLIONTHS
500
0
-500
-1000
-1500
-2000
0
20
40
60
80
100
120
ELAPSED TIME, DAYS

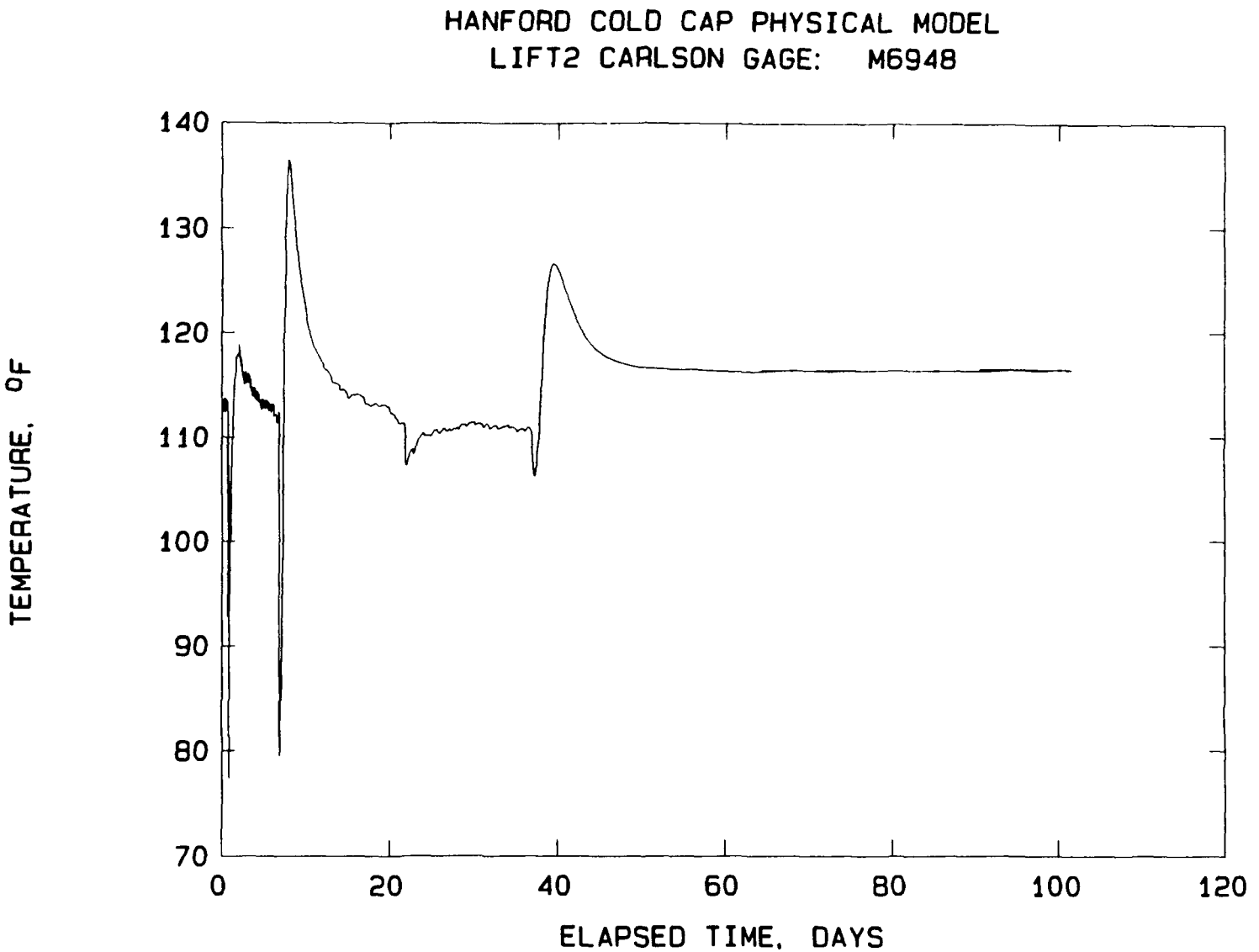
HANFORD COLD CAP PHYSICAL MODEL
LIFT2 CARLSON GAGE: M6948
TEMPERATURE, °F
140
130
120
110
100
90
80
70
0
20
40
60
80
100
120
ELAPSED TIME, DAYS

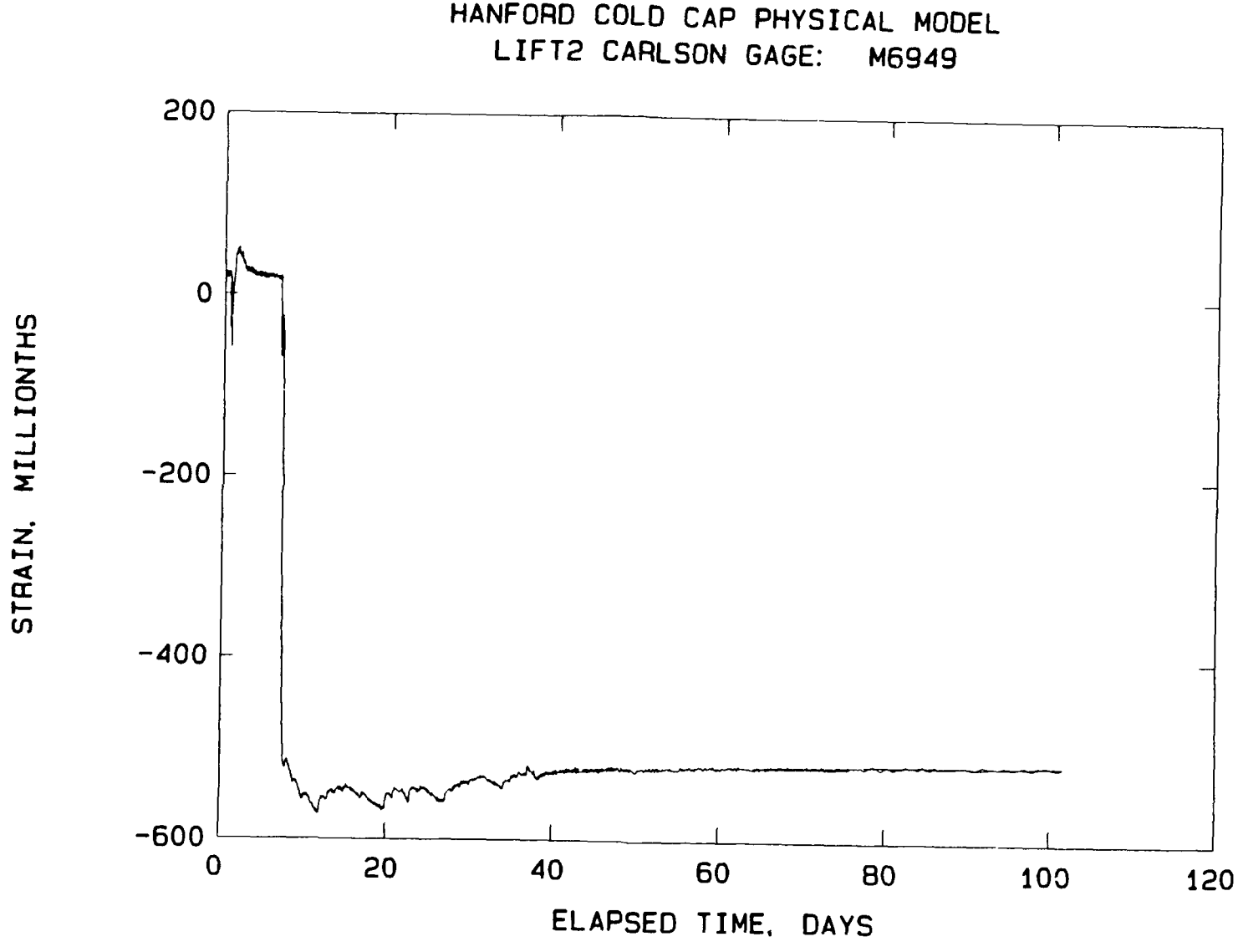
HANFORD COLD CAP PHYSICAL MODEL
LIFT2 CARLSON GAGE: M6949
200
0
-200
-400
-600
STRAIN, MILLIONTHS
0
20
40
60
80
100
120
ELAPSED TIME, DAYS

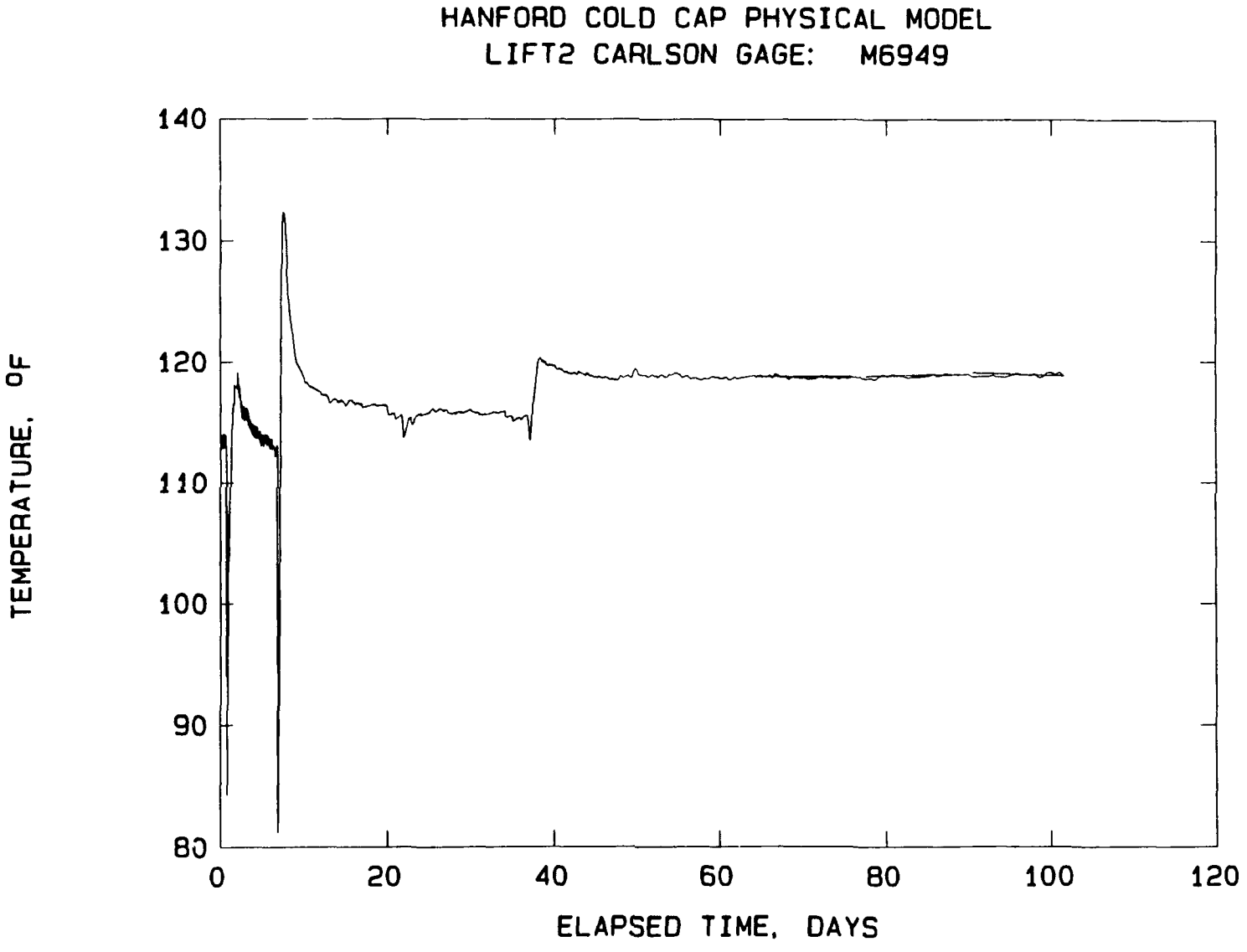
HANFORD COLD CAP PHYSICAL MODEL
LIFT2 CARLSON GAGE: M6949
TEMPERATURE, °F
140
130
120
110
100
90
80
0
20
40
60
80
100
120
ELAPSED TIME, DAYS

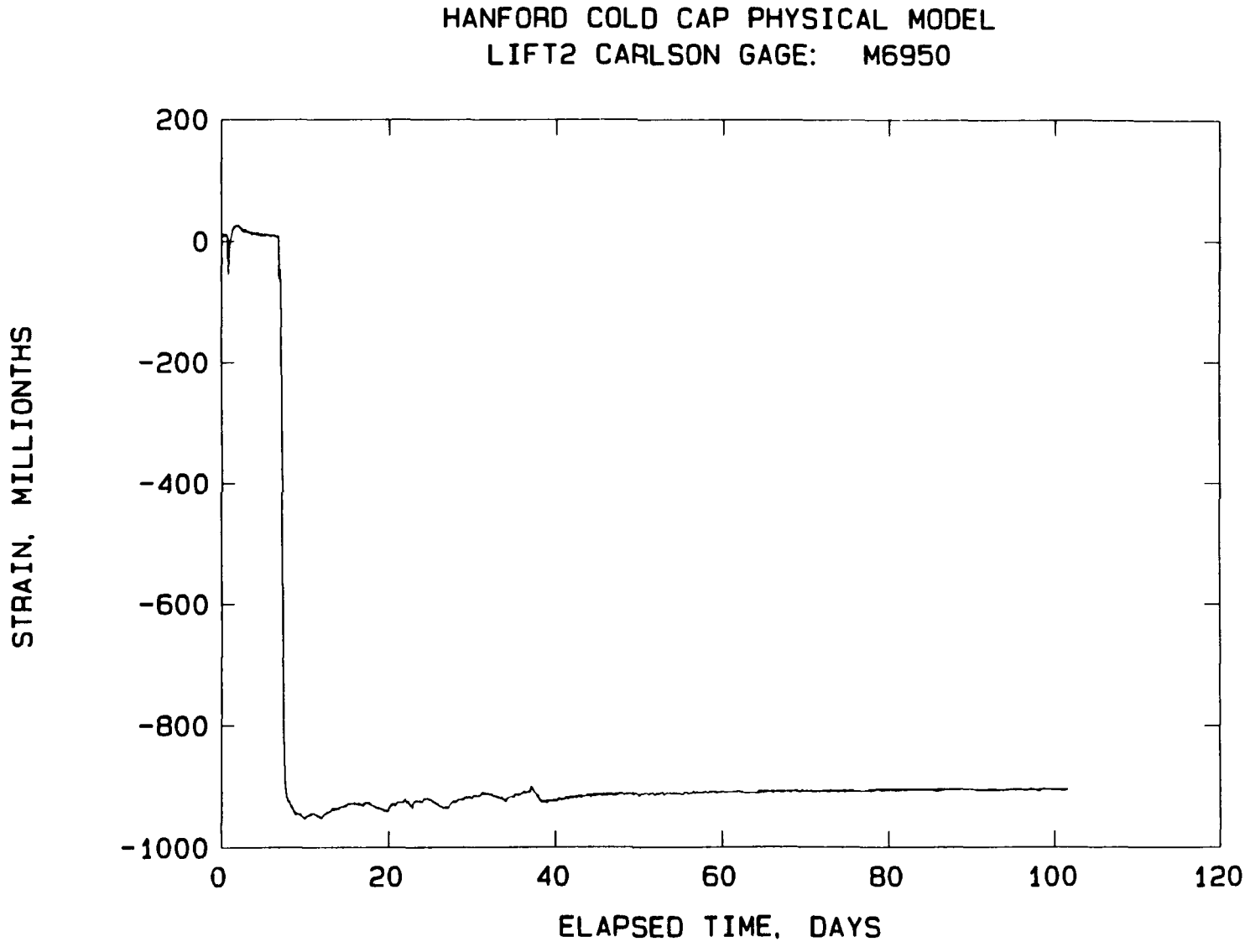
HANFORD COLD CAP PHYSICAL MODEL
LIFT2 CARLSON GAGE: M6950
STRAIN, MILLIONTHS
200
0
-200
-400
-600
-800
-1000
0
20
40
60
80
100
120
ELAPSED TIME, DAYS

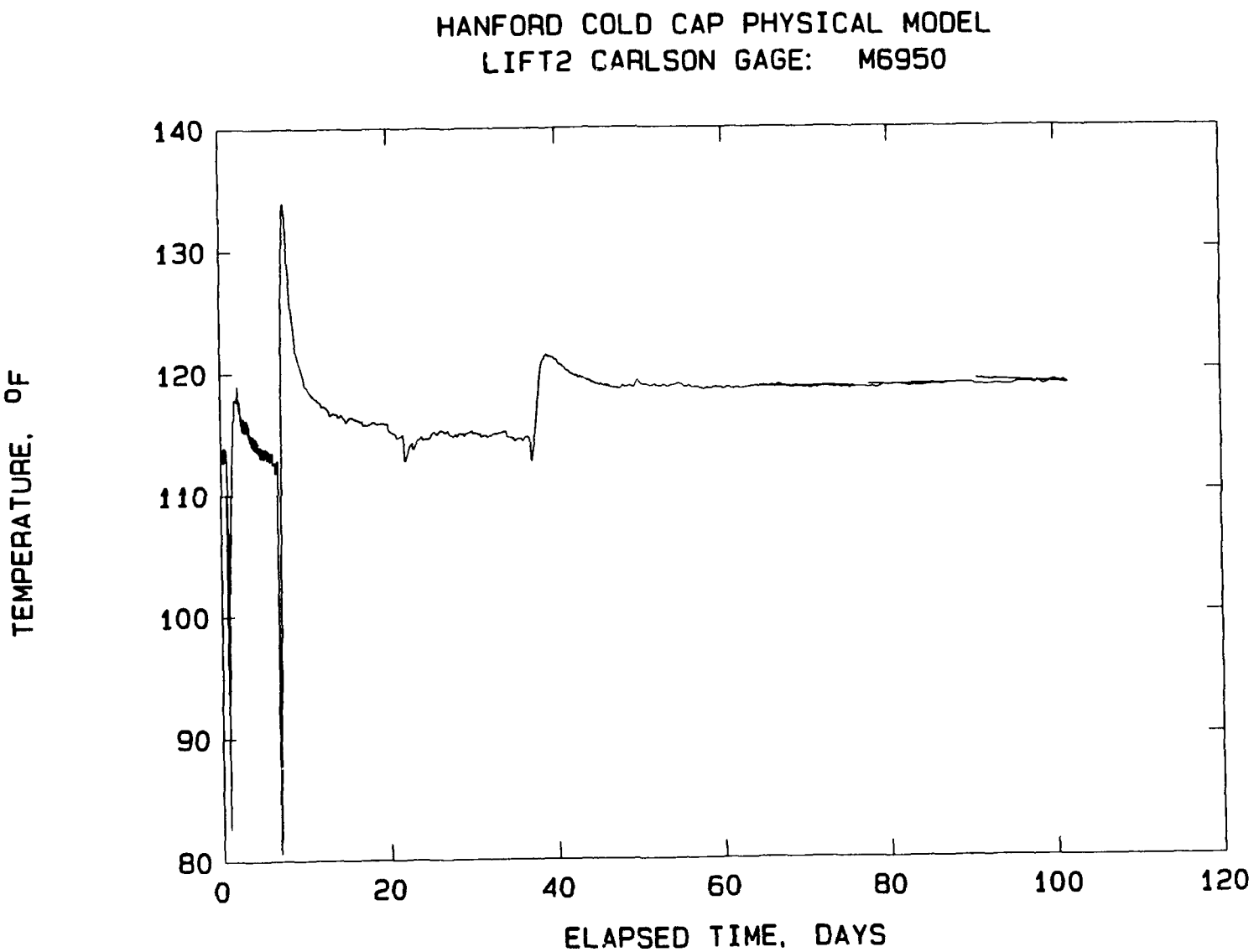
HANFORD COLD CAP PHYSICAL MODEL
LIFT2 CARLSON GAGE: M6950
TEMPERATURE, °F
140
130
120
110
100
90
80
0
20
40
60
80
100
120
ELAPSED TIME, DAYS

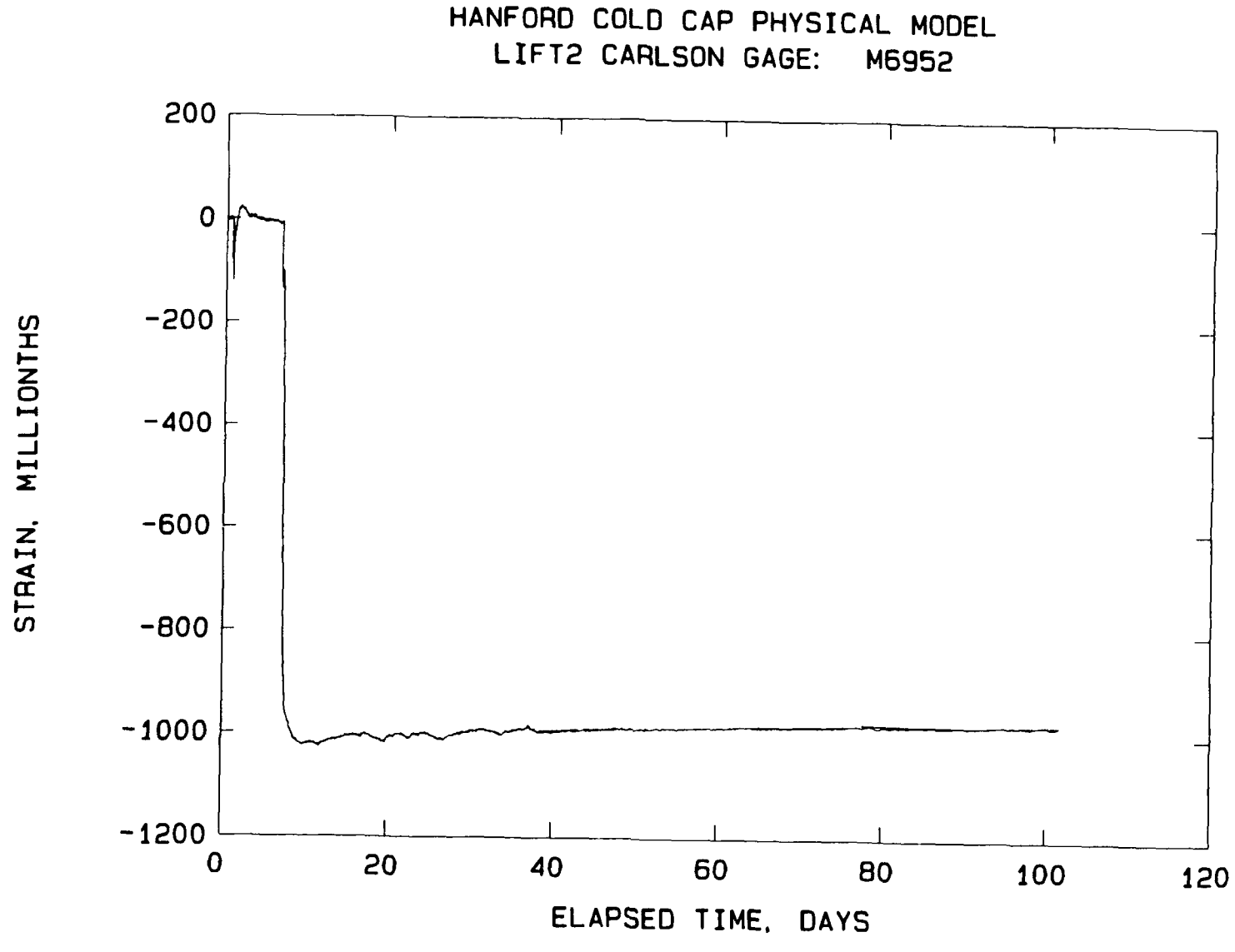
HANFORD COLD CAP PHYSICAL MODEL
LIFT2 CARLSON GAGE: M6952
STRAIN, MILLIONTHS
200
0
-200
-400
-600
-800
-1000
-1200
0
20
40
60
80
100
120
ELAPSED TIME, DAYS

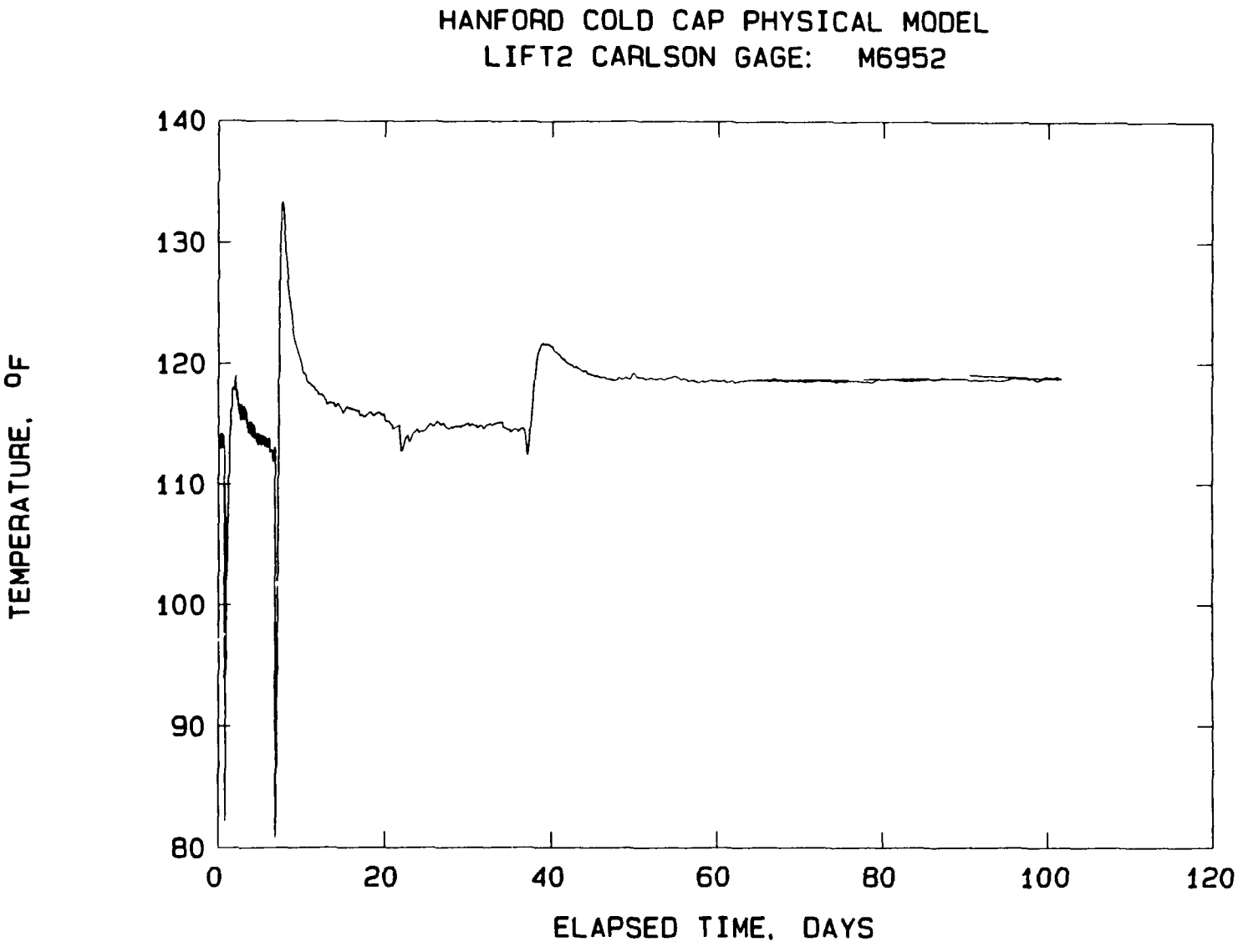
HANFORD COLD CAP PHYSICAL MODEL
LIFT2 CARLSON GAGE: M6952
TEMPERATURE, °F
140
130
120
110
100
90
80
0
20
40
60
80
100
120
ELAPSED TIME, DAYS

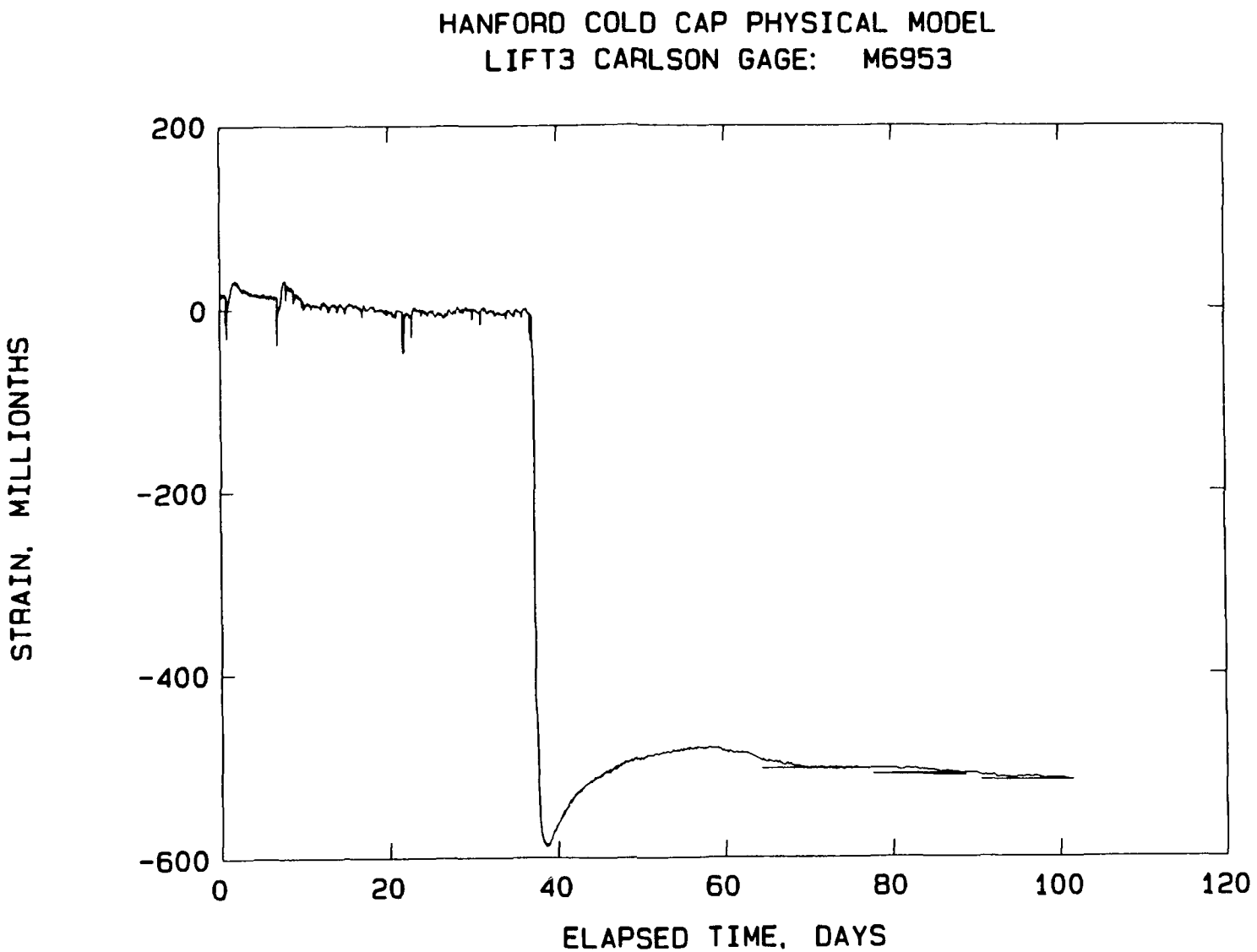
HANFORD COLD CAP PHYSICAL MODEL
LIFT3 CARLSON GAGE: M6953
STRAIN, MILLIONTHS
200
0
-200
-400
-600
0
20
40
60
80
100
120
ELAPSED TIME, DAYS

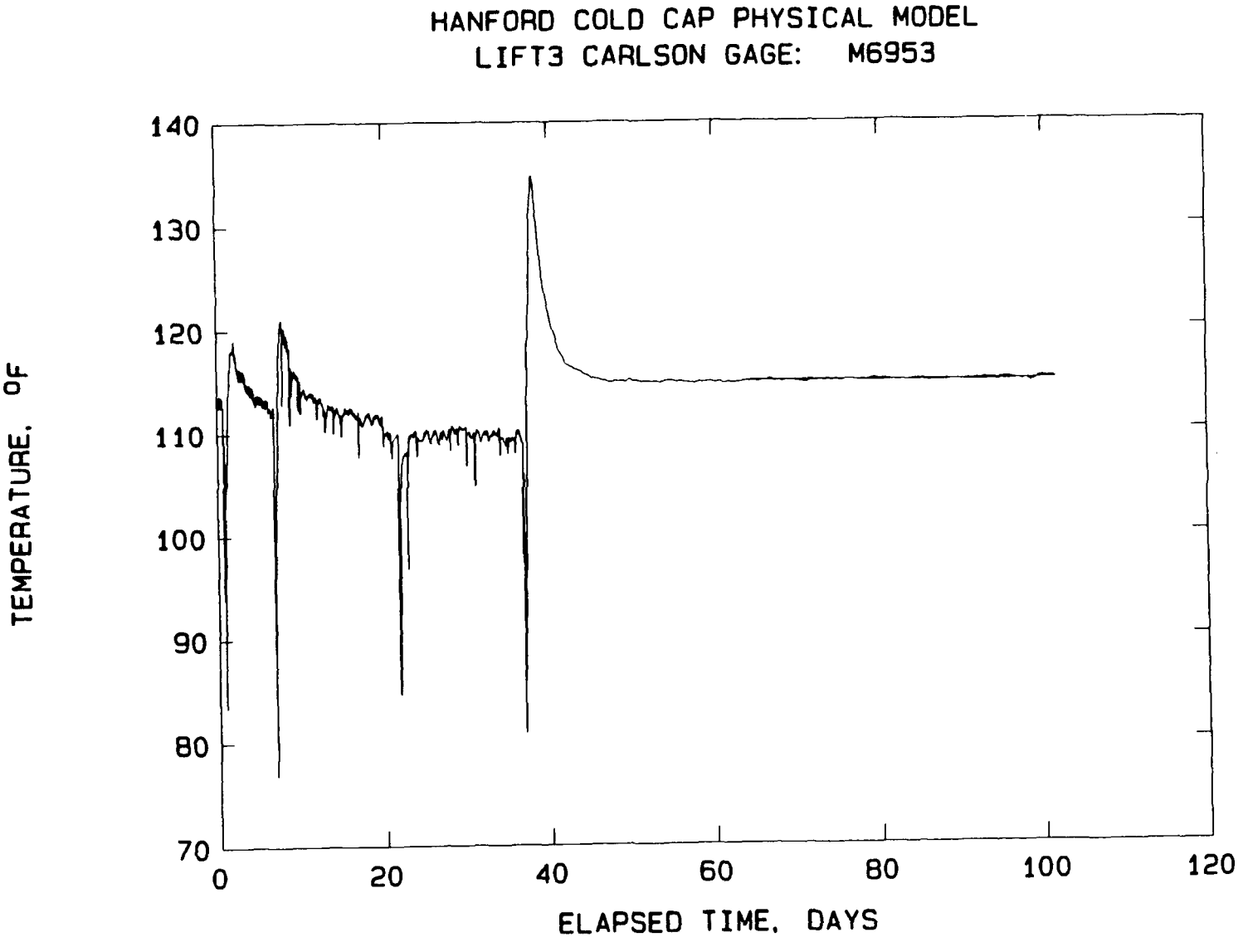
HANFORD COLD CAP PHYSICAL MODEL
LIFT3 CARLSON GAGE: M6953
TEMPERATURE, °F
140
130
120
110
100
90
80
70
0
20
40
60
80
100
120
ELAPSED TIME, DAYS

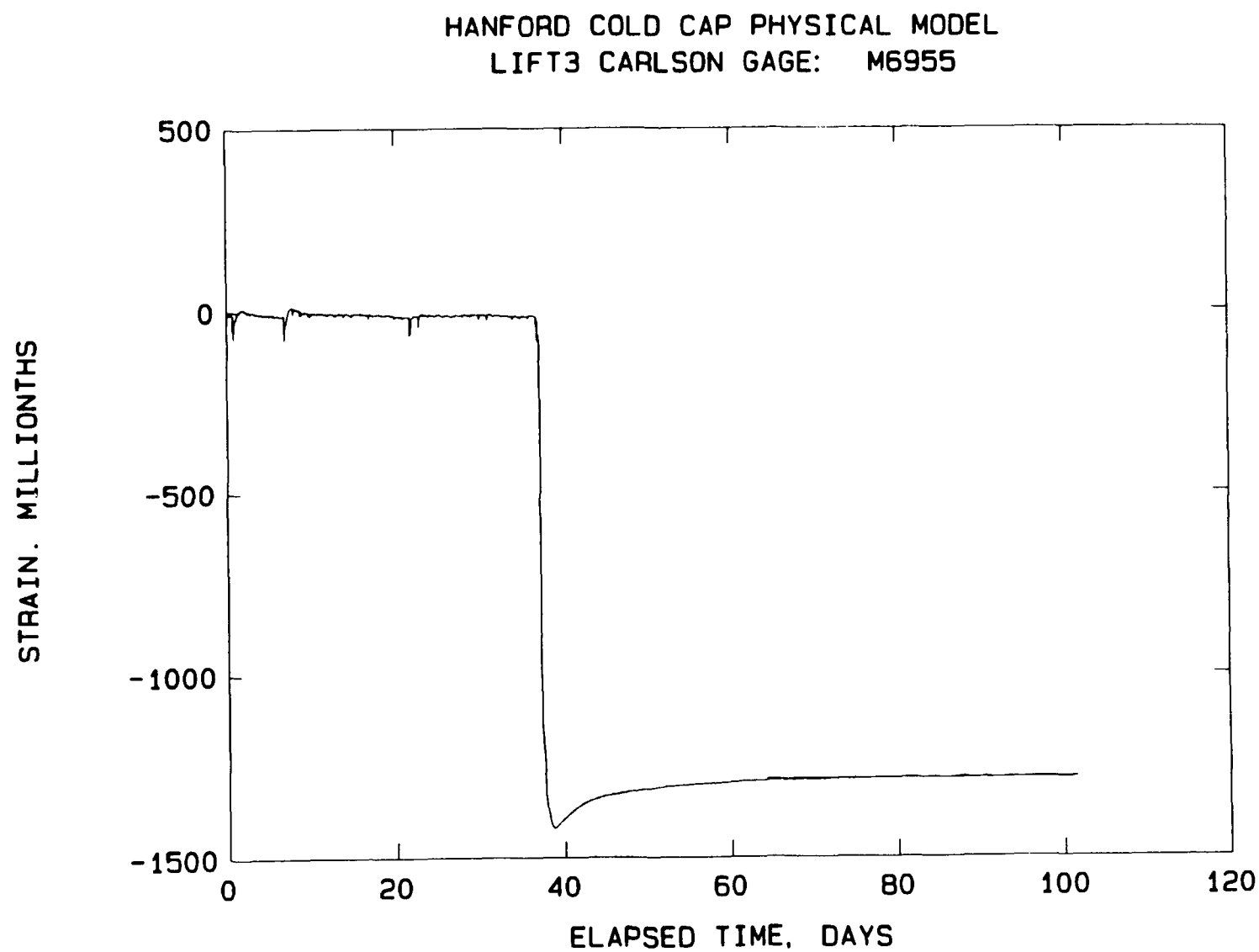
HANFORD COLD CAP PHYSICAL MODEL
LIFT3 CARLSON GAGE: M6955
STRAIN. MILLIONTHS
500
0
-500
-1000
-1500
0
20
40
60
80
100
120
ELAPSED TIME, DAYS

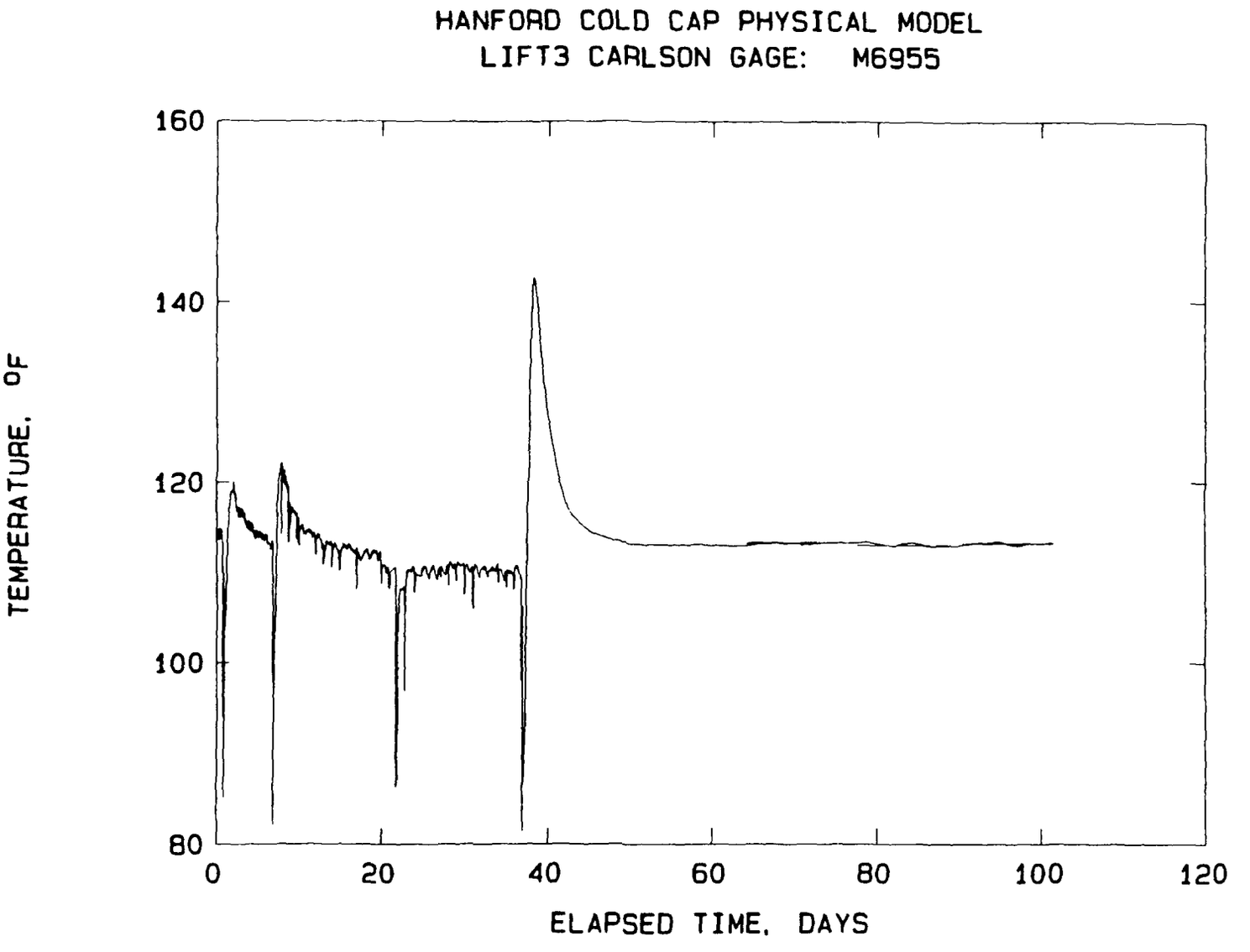
HANFORD COLD CAP PHYSICAL MODEL
LIFT3 CARLSON GAGE: M6955
TEMPERATURE, °F
160
140
120
100
80
0
20
40
60
80
100
120
ELAPSED TIME, DAYS

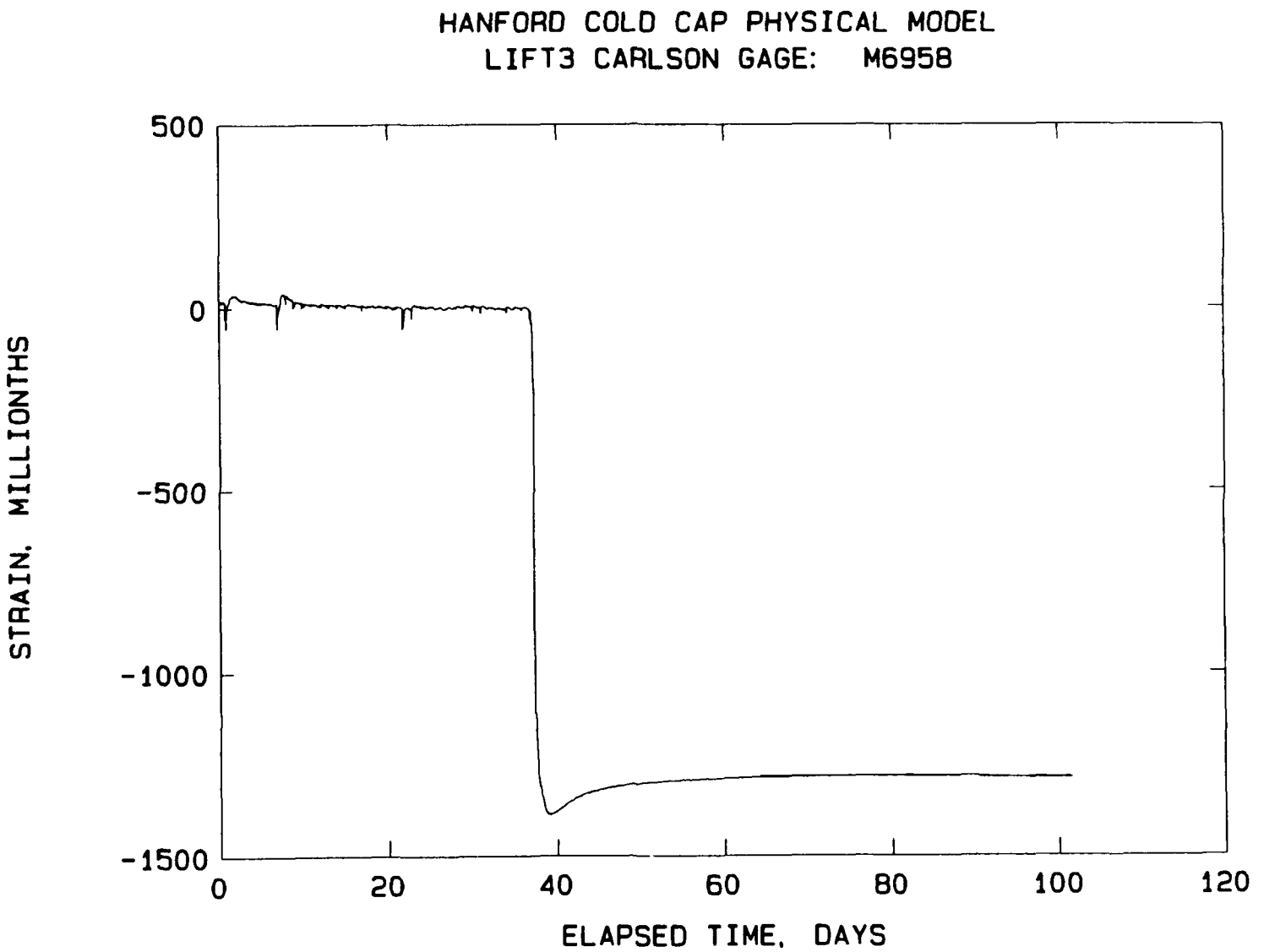
HANFORD COLD CAP PHYSICAL MODEL
LIFT3 CARLSON GAGE: M6958
500
0
-500
-1000
-1500
STRAIN, MILLIONTHS
0
20
40
60
80
100
120
ELAPSED TIME, DAYS

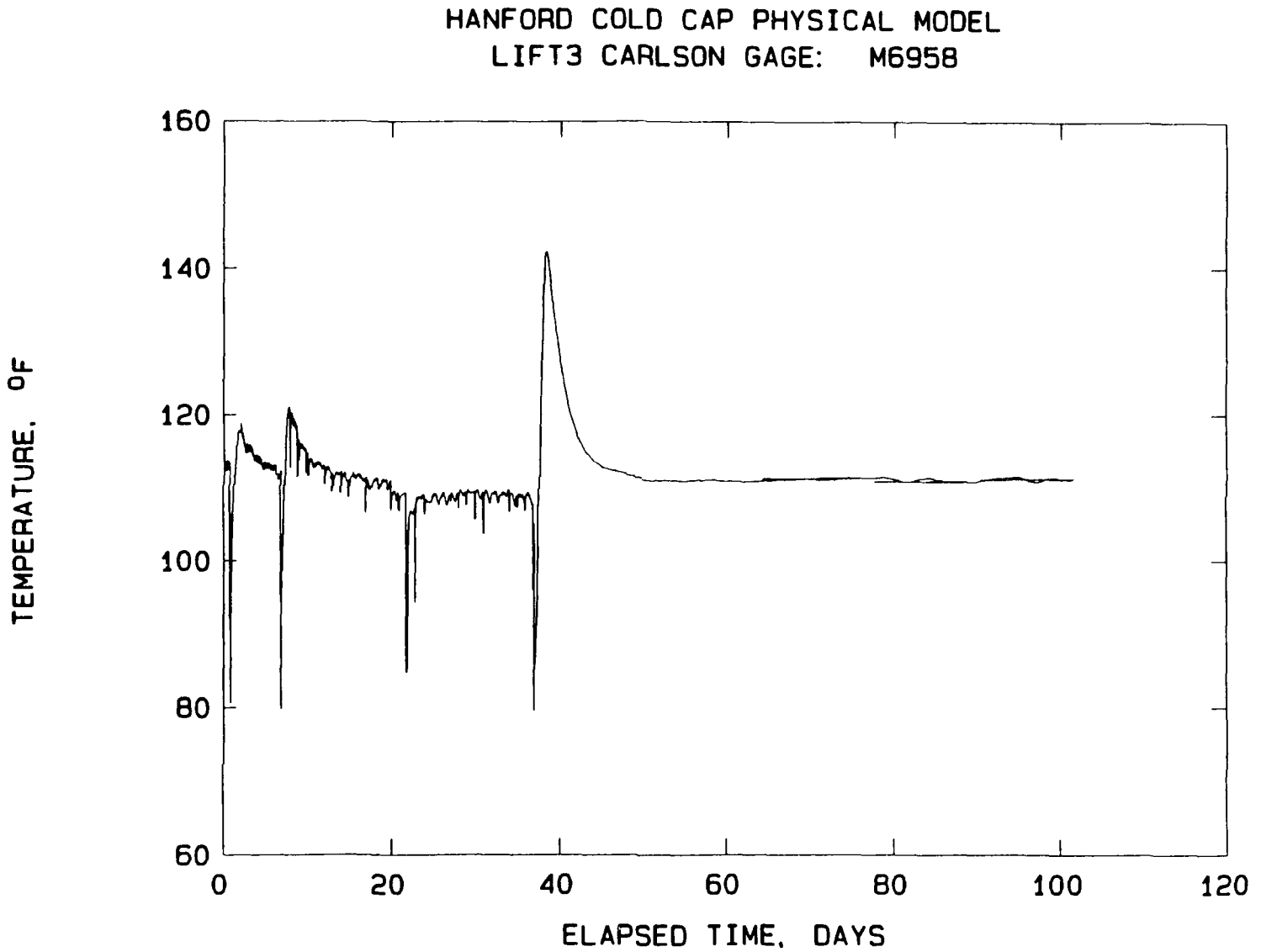
HANFORD COLD CAP PHYSICAL MODEL
LIFT3 CARLSON GAGE: M6958
TEMPERATURE, °F
160
140
120
100
80
60
0
20
40
60
80
100
120
ELAPSED TIME, DAYS

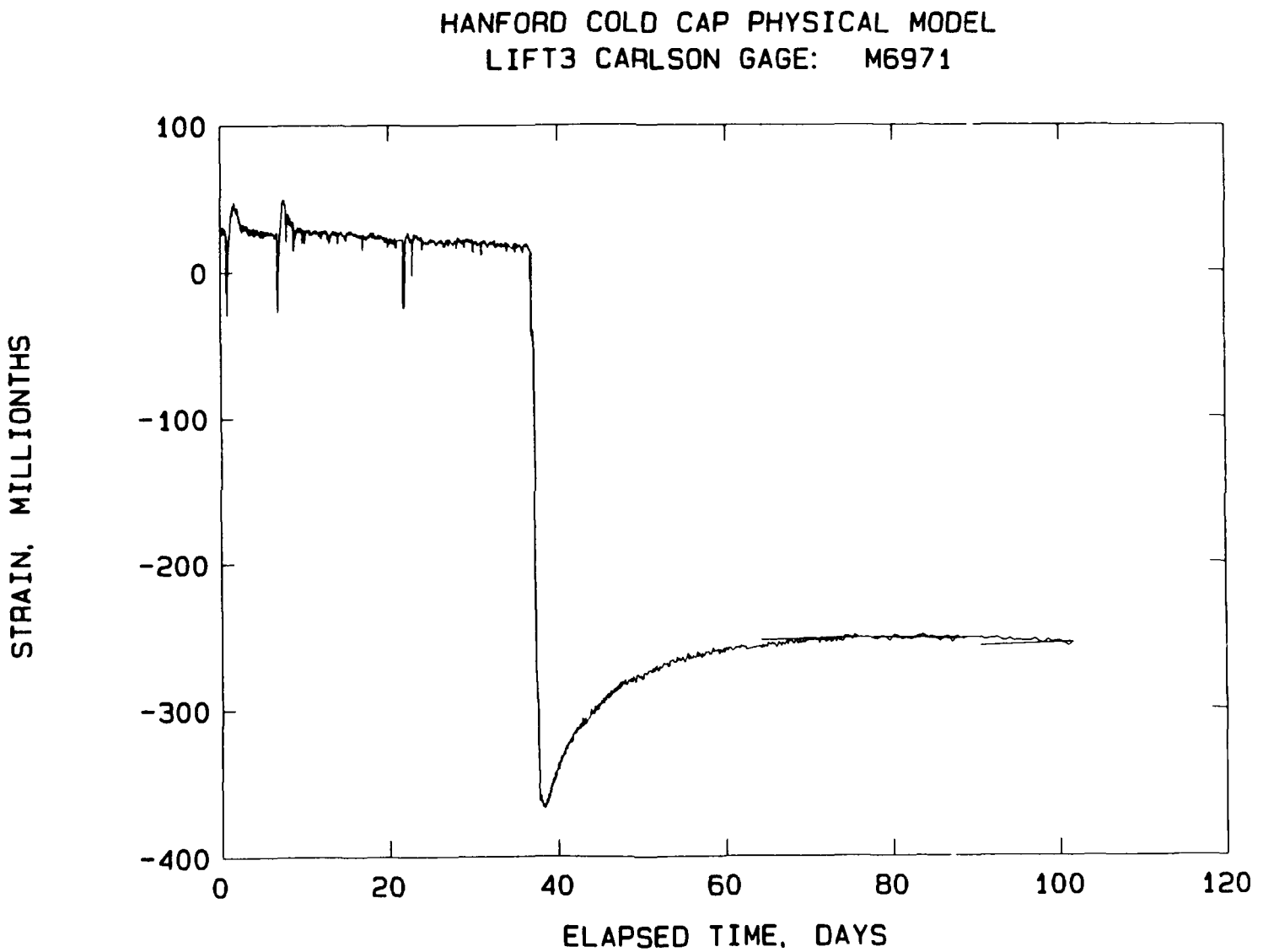
HANFORD COLD CAP PHYSICAL MODEL
LIFT3 CARLSON GAGE: M6971
STRAIN, MILLIONTHS
100
0
-100
-200
-300
-400
0
20
40
60
80
100
120
ELAPSED TIME, DAYS

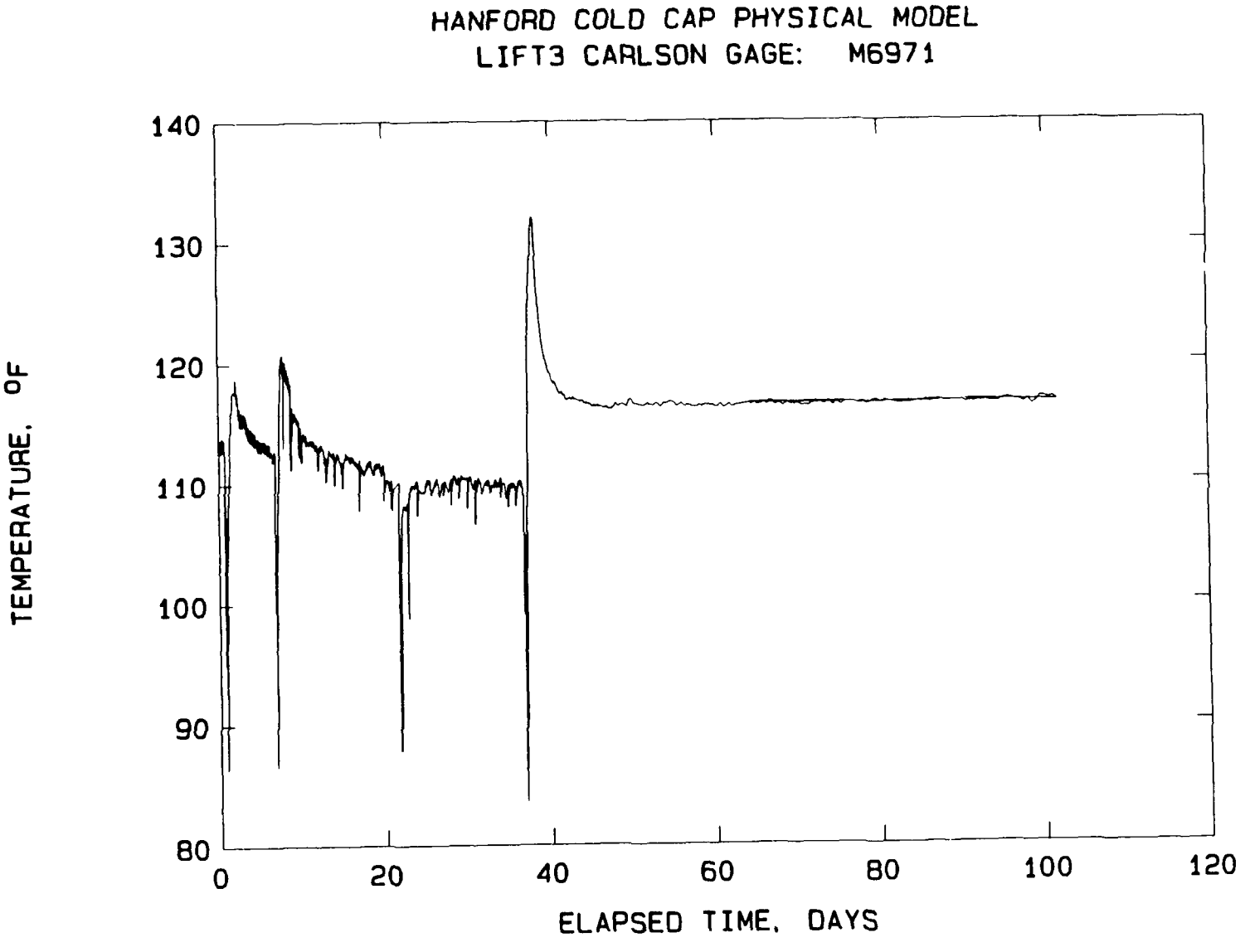
HANFORD COLD CAP PHYSICAL MODEL
LIFT3 CARLSON GAGE: M6971
TEMPERATURE, °F
140
130
120
110
100
90
80
0
20
40
60
80
100
120
ELAPSED TIME, DAYS

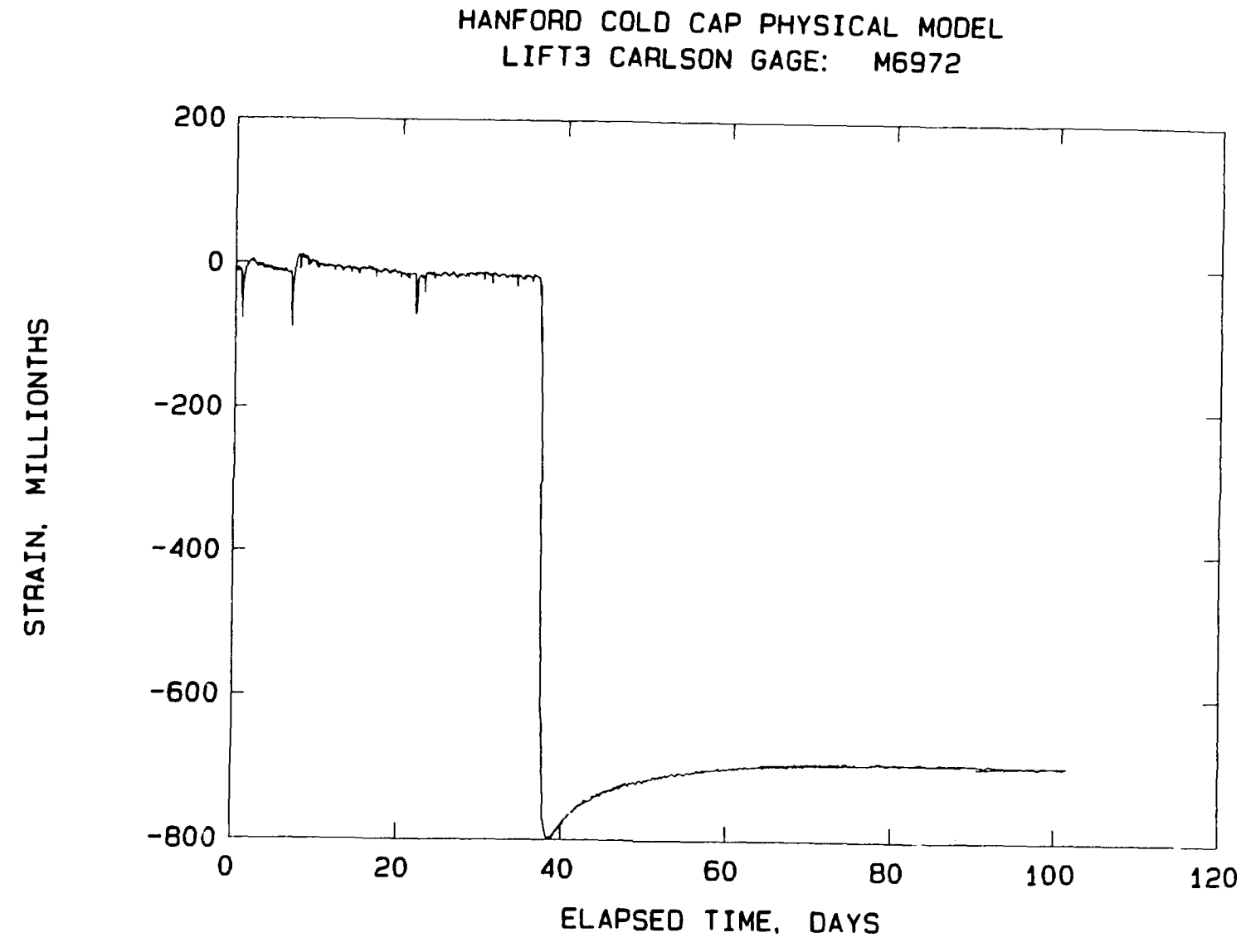
HANFORD COLD CAP PHYSICAL MODEL
LIFT3 CARLSON GAGE: M6972
200
0
-200
-400
-600
-800
0
20
40
60
80
100
120
STRAIN, MILLIONTHS
ELAPSED TIME, DAYS

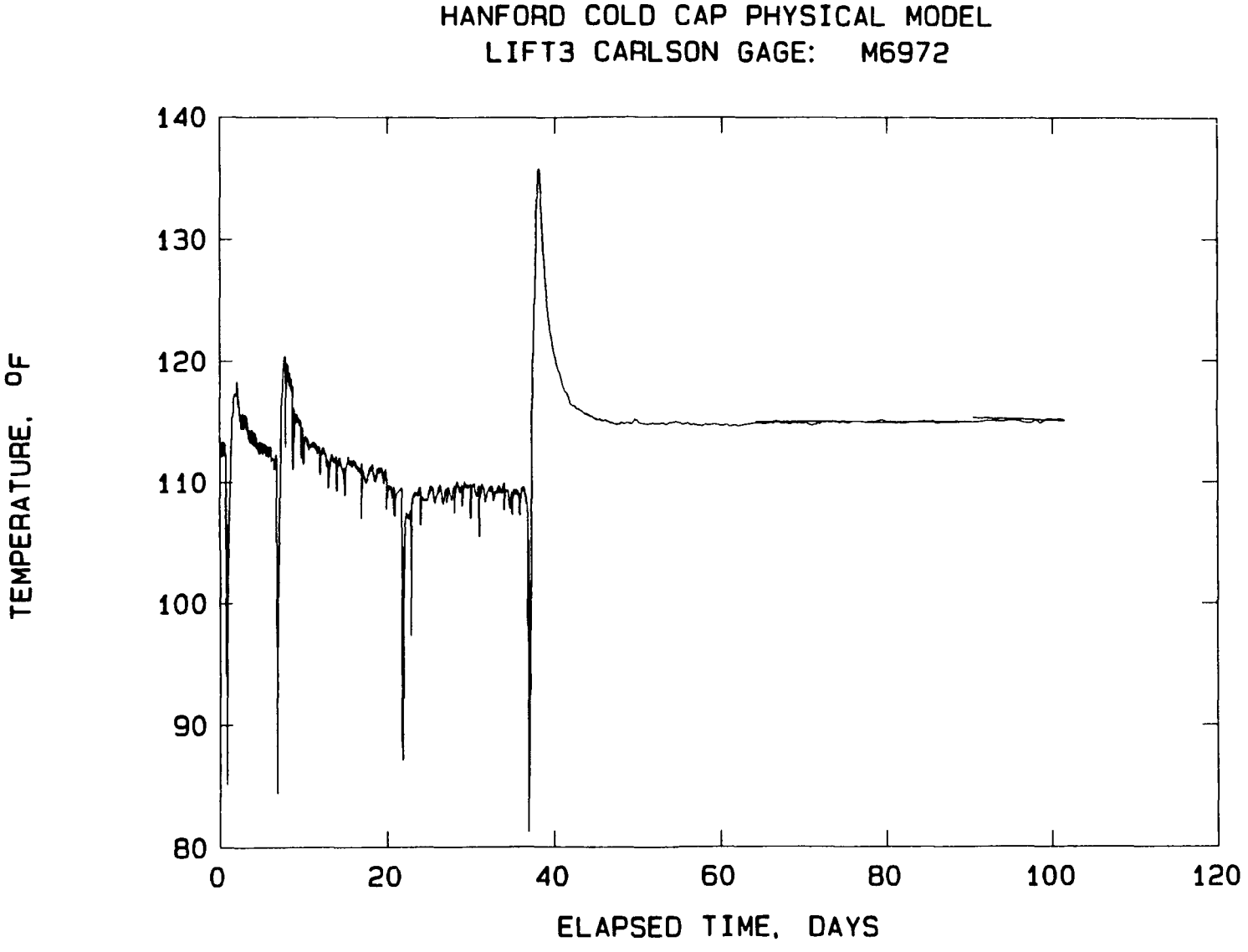
HANFORD COLD CAP PHYSICAL MODEL
LIFT3 CARLSON GAGE: M6972
TEMPERATURE, °F
140
130
120
110
100
90
80
0
20
40
60
80
100
120
ELAPSED TIME, DAYS

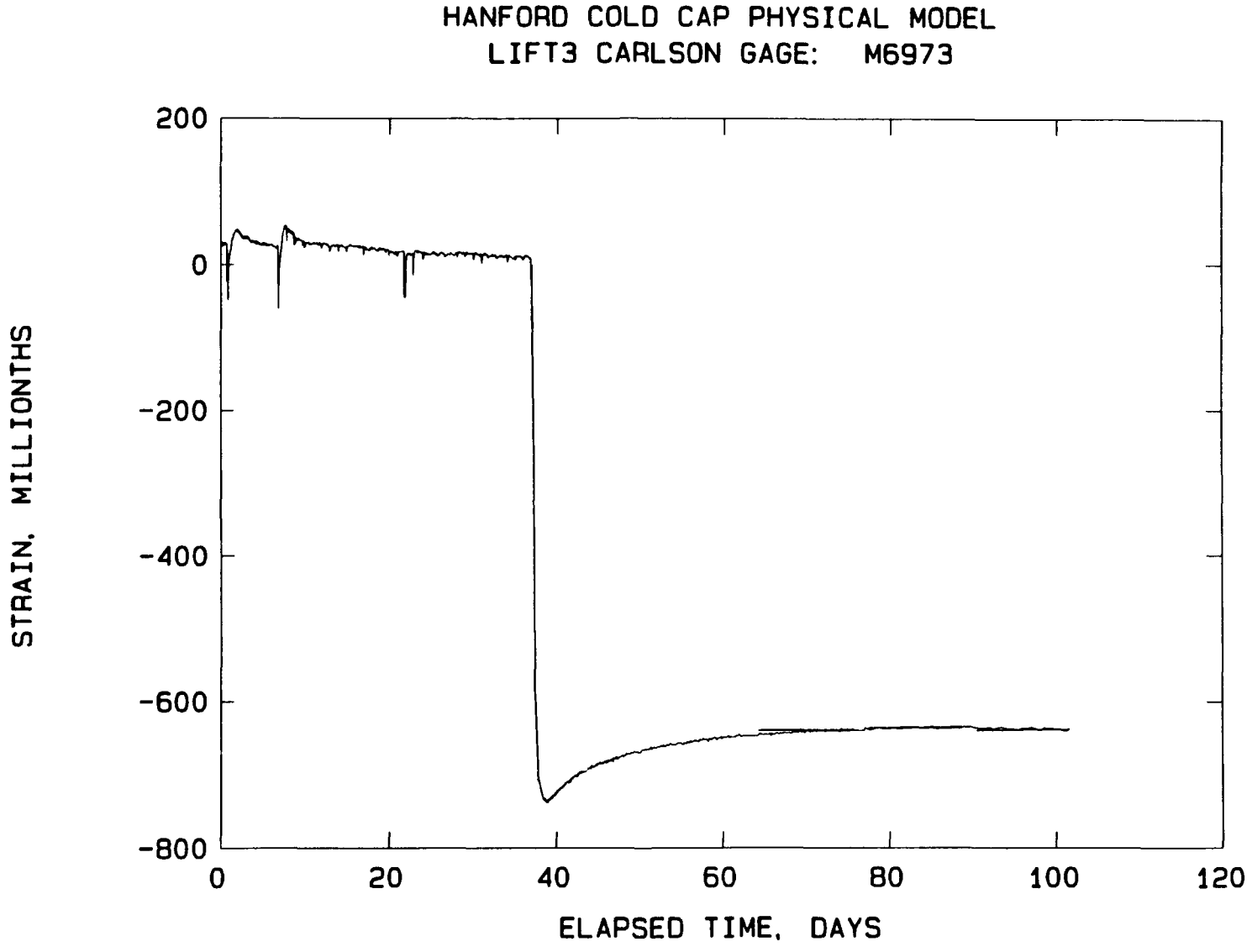
HANFORD COLD CAP PHYSICAL MODEL
LIFT3 CARLSON GAGE: M6973
STRAIN, MILLIONTHS
200
0
-200
-400
-600
-800
0
20
40
60
80
100
120
ELAPSED TIME, DAYS

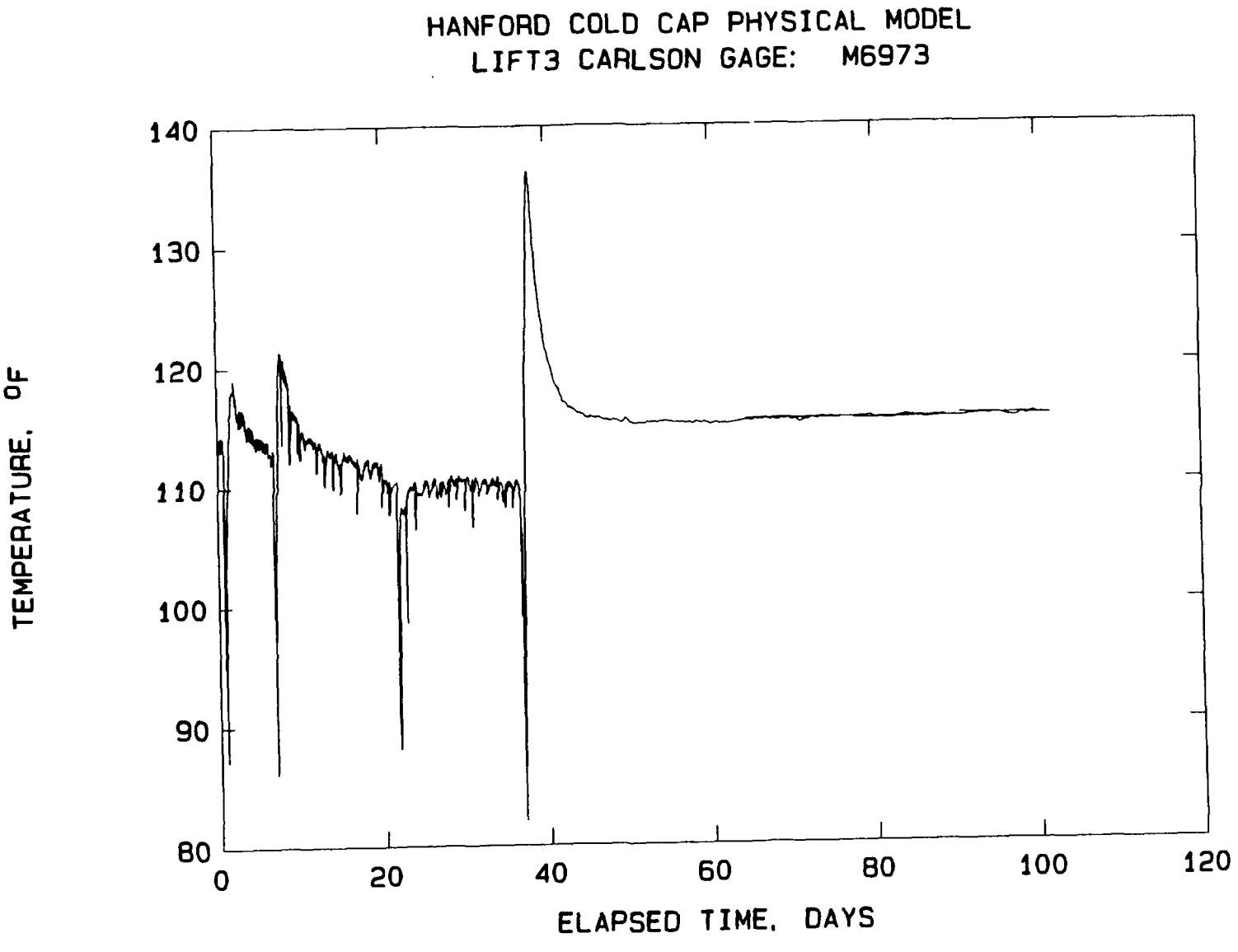
HANFORD COLD CAP PHYSICAL MODEL
LIFT3 CARLSON GAGE: M6973
TEMPERATURE, °F
140
130
120
110
100
90
80
0
20
40
60
80
100
120
ELAPSED TIME, DAYS